Towards MIP "Nano-monolith"
Composite Membranes for Enantioselective Separations

(Herstellung und Charakterisierung von MIP "Nano-Monolith"
Komposit-Membranen für enantioselektive Trennungen)

by

Abdus Salam

Thesis submitted to the Department of Chemistry,
Universität Duisburg-Essen, in partial fulfillment of
the requirements of the degree of
Dr. rer. nat.

Approved by the examining committee on June 11, 2008:

Chair : Prof. Dr. Thomas Schrader
Advisor : Prof. Dr. Mathias Ulbricht
Reviewer : Prof. Dr. Christian Mayer

Essen, 2008

ABSTRACT

A molecular imprinting procedure based on hydrogen bonding interactions between the template butoxycarbonyl-D-phenylalanine (Boc-D-PhA) and the functional monomer methacrylic acid (MAA) was used to synthesize a porous molecularly imprinted polymer (MIP) in the pores of polypropylene (PP) microfiltration and poly(ethylene terephthalate) (PET) track-etched membranes for the separation of enantiomeric mixture (Boc-DL-PhA) in solution via permselective transport through these composite membranes under diffusion (dialysis) and electrodialysis conditions. Bulk porous MIP and non-imprinted polymer (NIP; for control experiments) monoliths were synthesized to optimize the synthesis conditions and their pore morphology. Pre-modification of the entire pore surface of the PET track etched and PP microfiltration membrane by UV-initiated grafting with polyethylene glycol (400) monomethacrylate (PEGMA) was done using an already established method including the adsorption of the photoinitiator, benzophenone (BP). Subsequently these membranes were functionalized by filling the pores with porous MIP and NIP monoliths from MAA and ethyleneglycol dimethacrylate (EDMA) (*poly(MAA-co-EDMA)*) and compared with the membranes which had been functionalized without pre-modification step.

Characterization had been done mainly by degree of grafting (DG), scanning electron microscopy (SEM), gas adsorption isotherm method (BET), and adsorption experiments in combination with chiral high performance liquid chromatography. Diffusion (dialysis) and electrodialysis experiments were conducted using these enantioselective membranes to separate Boc-DL-PhA racemic mixture. In case of bulk monoliths, MIP *poly(MAA-co-EDMA)* monoliths have shown higher binding capacity and enantioselectivity for the imprint molecule (Boc-D-PhA) in the racemic mixture of Boc-D/L-PhA in acetonitrile (AN) as solvent. However, the

enantioselectivity was slightly decreased with the increase in the equilibration time. The MIP *poly(MAA-co-EDMA)* monolith PP and PET composite membranes have shown higher binding capacity than their respective NIP composite membranes. The pre-modified MIP composite membranes have shown better enantioselectivity than the unmodified MIP composite PP membranes.

The effect of pre-modification on the interaction of macroporous substrates (membranes) with mainly micro- and mesoporous polymer monoliths has also been studied. DG values after composite membrane preparation under identical conditions were not influenced by the pre-modification. However, from SEM images it was very clearly seen that the pre-modification step prevents the formation of voids at the monolith-membrane pore interface. Larger specific surface area and pore volume values for composite membranes prepared after pre-modification fully support the SEM results. Especially large differences in pore structure between the two different composite membranes were found in the mesopore range. Hence, with the pre-modification step, it is possible to prepare porous composite membranes where the trans-membrane transport is exclusively controlled by the pore and surface structure of a functional polymeric monolith, for example made from a molecularly imprinted polymer (MIP).

The effective diffusion rate of PEGs or a racemic mixture of template (Boc-D-PhA) and its counterpart (Boc-L-PhA) through the composite membranes was a function of imprinting and degree of pre-modification. The MIP *poly(MAA-co-EDMA)* monolith PET composite membranes pre-modified with 25 g/L of *PEGMA* had shown larger effective diffusion coefficient values than the NIP *poly(MAA-co-EDMA)* monolith PET composite membranes and the further increase in the DG values of pre-modification resulted in a significant decrease in effective diffusion coefficient values. The larger values of effective diffusion coefficient for the diffusion of PEGs

in water and racemic mixture in AN through MIP composite membranes indicated that the imprinting leads to connected pores within the composite structure which are responsible for this increased flux. In contrast, during the diffusion of single enantiomer in AN/H_2O system, these membranes behaved like a "gate": only for the amino acid used as template, no flux was detected while the other enantiomer diffused through the membrane. This effect is presumably due to an increase of membrane swelling as a consequence of binding of the template to imprinted sites which resulted in the blocking of the pathways for the transport of the molecules.

The process of electrodialysis had facilitated the transport of template molecules (Boc-D-PhA) through the *poly(MAA-co-EDMA)* PET composite membranes pre-modified with *poly(PEGMA)*, while there was no significant transport of the template molecules through these composite membranes during the diffusion process. However, both MIP and NIP composite membranes did not show any enantioselective transport during the process of diffusion or electrodialysis when using racemates. The nature of the solvent and its pH are very much important for the binding and selective transport of molecules through the imprinted polymer materials. The influence of solute concentration onto enantioselectivity (high for low concentrations) and onto flux through the membrane (high for high concentrations) are contradictory with respect to enantio-selective transport in the diffusion experiments performed in AN. And electrodialysis was only possible in an aqueous solvent where enantio-selectivity was not detectable.

This thesis is dedicated
with love to my wife (Sabeeha) and my
children (Zujaija, Zunairah and Abdul Waseh) for
their love, prays and patience during the course of
my Ph.D. studies

PREFACE

With the name of almighty Allah who is the most beneficent and merciful.

The work on this project was done during the period from January 2005 to February 2008 to fulfill the requirements for doctoral program (Dr. rer. net) at the Institute of Technical Chemistry (Lehrstuhl für Technische Chemie II), Department of Chemistry, Universität Duisburg-Essen, under the supervision of Prof. Dr. Mathias Ulbricht. The main objective of this work was to synthesize the MIP "nano-monolith" composite membranes via in situ UV-initiated polymerization for enantioselective separations.

This thesis comprises of five chapters. Chapter 1 gives the background, objective and state of the research work. Chapter 2 discusses briefly the fundamentals for the synthesis and characterization of polymer monoliths, molecularly imprinted polymer (MIP) monoliths and molecularly imprinted membranes (MIM). Further, recent developments in surface modification of the membranes are discussed. Materials, methods and techniques used during experimental work are covered in Chapter 3. All the results and discussion on the phenomena behind the obtained results and their correlation are presented in Chapter 4. In this chapter, results are classified into four main parts, i.e. (i) preparations and pore characterizations, (ii) equilibrium binding and enantioselectivity, (iii) transport experiments (diffusion and electrodialysis), and (iv) correlations between syntheses, pore-structure, binding and transport properties. Chapter 5 presents the conclusion of this work.

Upon finishing this work I would like to pay my special thanks to all who have supported, guided and assisted me during the work on this project. Above all, I would like to pay my gratitude to Prof. Dr. Mathias Ulbricht for his kind supervision and for providing an excellent working environment. Because of the financial support provided by him, I was able to live in Germany along with my family. His trade mark cool mindedness and appreciation was instrumental during the course of this work. His encouragement and guidance was the key to broaden my horizon and to think critically about the problems during this research work. His kind support in other parts of life is also, highly acknowledged.

I am grateful to all members of our research group at Lehrstuhl für Technische Chemie II, Universität Duisburg-Essen, namely, Heru, Dongming, Mehmet, Christian, Marcel, Halim,

Claudia, Danuta, Haofei, Alex, Falk, Monica, Nadia, Eva, Jun, Rafael, Dr. Illing, Polina, Yu, Su-Hyoun, Frank, Michael, Uwe, Melvy, Dimitrios, Frau Steffens and Frau Nordmann for providing nice company and excellent working environment. In particular, I would like to pay my thanks to Inge for her nice cooperation during my studies, Dr. Diesing for providing guidance on electrodialysis, Smail Boukercha for SEM visualization and Dieter Jacobi for his contribution in GPC analysis.

Finally, this thesis would not have been possible without the contribution from my parents and my friend Saleem. I would love to pay my special gratitude to my parents for their endless love and prays during my studies. I am grateful to Saleem for his motivation, care and providing guidance since my first day in Germany.

CONTENTS

LIST OF TABLES

LIST OF FIGURES

Chapter 1

INTRODUCTION

1.1. Background

Many important molecules required for life exist in two forms. These two forms are non-superimposable mirror images of each other, i.e.: they are related like our left and right hands. Hence this property is called chirality, from the Greek word for hand. The two forms are called enantiomers (from the Greek word for opposite) or optical isomers, because they rotate plane-polarized light either to the right or to the left.

Nowadays the need to obtain pure isomers not only in pharmaceutical industry, but also in agrochemical industry and food additive industry is becoming more and more important [1,2]. Although there are various enantiomeric separation techniques, for example, liquid chromatography, gas chromatography, capillary electrophoresis, crystallization, and liquid-liquid extraction and so on [3], however, each process showed its limitations. The main advantages of membrane technology as compared with other unit operations in (bio)chemical engineering are related to this unique separation principle, i.e. the transport selectivity of the membrane. Separations with membranes do not require additives, and they can be performed isothermally at low temperatures and –compared to other thermal separation processes– at low energy consumption. Also, upscaling and downscaling of membrane processes as well as their integration into other separation or reaction processes are easy [4].

Many different types of membranes have been prepared till the date, but, for example, the supported liquid membranes containing chiral selectors suffer from instability and, consequently, it is easy to pollute the separated product [5]. Molecular imprinting developed by Wulff et al. [6],

is a technique that has been used to make a polymeric matrix with a selective affinity to certain molecules, and some researchers have tried to use this technique to make a permselective membrane useful for the optical resolution of chiral compounds. Recently, several different types of molecularly imprinted polymer (MIP) composites in membrane shape have been prepared for the molecular recognition in separation system [7-16]. However, irrespective the proof of feasibility in some special cases (cf. [10,14]), the envisioned application of MIP membranes for enantio-separation have not yet been realized.

1.2. Objective of the Research

Main objective of this research work is to synthesize MIP "nano-monolith" composite membranes by in situ polymerization in the pores of membranes to create recognition sites in the pores for selective ("fixed carrier") transport of molecules of interest, i.e.:

(i) Pore-filling of membrane with MIP monoliths of suited pore structure (no large macropores and high specific surface area) and high binding selectivity for templates such as amino acids,

(ii) Separation of enantiomeric mixtures in solution via permselective transport through the composite membranes under diffusion (dialysis) and electrodialysis conditions.

1.3. Scope of the Research

After establishing the synthesis conditions and their pore morphology, the MIP and non-imprinted polymer (NIP; for control experiments) monoliths were synthesized by in situ UV-polymerization of the polymerization mixture (cf. Table 3.2, Chapter 3). Pre-modification of the entire pore surface of polypropylene (PP) microfiltration membranes and poly(ethylene

terephthalate) (PET) track-etched membranes by UV-initiated grafting with polyethylene glycol (400) monomethacrylate (PEGMA) was performed using already established methods including coating the photoinitiator, benzophenone (BP). Subsequently these membranes were functionalized by filling the pores with MIP and NIP monoliths from methacrylic acid (MAA) and ethyleneglycol dimethacrylate (EDMA) (*poly(MAA-co-EDMA)*) and compared with the membranes which had been functionalized without pre-modification step.

Characterization had been done mainly by degree of grafting (DG), scanning electron microscopy (SEM), and gas adsorption isotherm method and adsorption experiments in combination with chiral high performance liquid chromatography. Diffusion (dialysis) and electrodialysis experiments were conducted using these enantioselective membranes to separate Boc-DL-PhA racemic mixture.

Chapter 2

THEORY

2.1. Polymer Monoliths

Monoliths are separation media in a format that can be compared to the single, large ‘‘particle’’ that does not contain inter-particular voids, typical of packed beds. In contrast to common crosslinked polymers that must be swollen in a solvent to achieve porosity, these rigid polymer materials possess a permanent pore structure even in the dry state, which permits liquids to flow through the polymer matrix. Because of this feature, polymeric monoliths have a variety of applications, such as in ion exchange catalysis, adsorption and chromatographic separations [17]. In the late 1960s, these polymers were first prepared as macroporous beads through a suspension polymerization technique [18-20]. In 1992, Svec and Fréchet presented a new procedure to synthesize macroporous polymer monoliths for applications such as capillary electrochromatography and HPLC [21]. The rigid and porous polymer monolith can be synthesized by *in situ* crosslinking polymerizations using high contents of crosslinker monomers in the reaction mixture in a mold of any shape [22,23]. Hjertén and others extended their extensive research to synthesize the monoliths for continuous bed applications [24-28]. The development of macroporous polymers in the monolith format has provided its own unique challenges. The procedure for the synthesis of polymer monoliths was quite different from the procedure which was previously used to obtain macroporous polymer beads and the resulting pore size distributions were also quite different even when prepared from identical polymerization mixture [29,30].

The pore size distribution within a monolith has a direct effect on the performance of the material. Large macropores are required for the mobile phase to flow through the monolith at low pressures, while mesopores (2-50 nm) and micropores (< 2 nm) afford a high surface area for increased capacity (cf. Figure 2.1). Optimization of pore size distribution within the polymer monolith is required for different applications. Pore sizes ranging from a few to tens of microns have shown to be suitable for micromonoliths used in microfluidic applications [31].

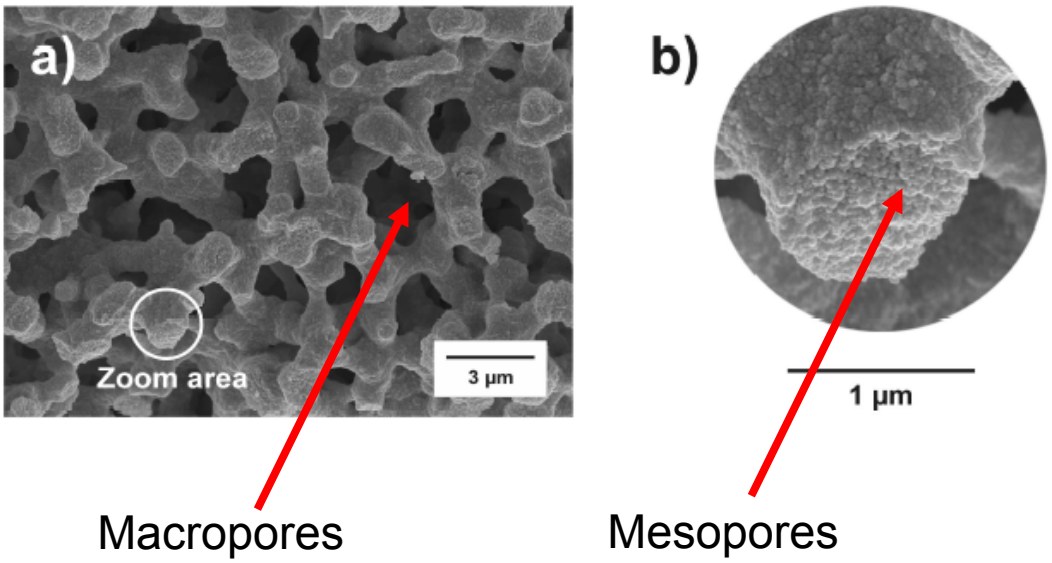

Figure 2.1. A typical acrylate-based porous material with (a) macropores and (b) mesopores (taken from Sebastiaan Eeltink, Agilent Technologies, Germany).

Fréchet, Svec and coworkers determined different factors affecting the porosity of a monolith [21,29-33]. In order to discuss these factors, it is necessary to understand the actual mechanism for pore formation during the polymerization process. In this mechanism, a polymerization mixture composed of monomers, crosslinkers, an initiator and a porogenic solvent undergoes polymerization process which begins as the initiator decomposes through

either thermal or photolytic degradation. The polymer chains that are formed during the propagation precipitate out of solution and form insoluble gel-like nuclei either due to their extensive crosslinking or because of porogen present becomes a poor solvent for the growing polymer chains. These nuclei tend to grow during the process of polymerization and become crosslinked to other nuclei via branched or crosslinking polymer chains. In this manner, clusters (globules) are formed. These clusters eventually contact one another to make a matrix composed of crosslinked globules and voids. At the end of polymerization, the voids between the globules are filled with the porogen [34]. This mechanism does not provide any information about the sizes of these pores. Key variables which tune the pore size and pore size distribution within the monolith are temperature/irradiation power, pore forming solvent (porogen), and content of crosslinker monomer [30,33,35].

The choice of a porogen is the mostly used tool for the control of porous properties without changing the chemical composition of the final monolith [17]. In general, larger pores are obtained in a poorer solvent due to an earlier onset of phase separation. The study by Santora et al. [35] provides a good illustration of this point. For the nonpolar system divinylbenzene/styrene, the nonpolar porogen n-hexane generated a smaller average pore size, smaller globules, and higher surface area. The polar porogen methanol, on the other hand gave a larger average pore size, larger globules and thus lower surface area. In the more polar EDMA/MMA system, the role of n-hexane and methanol was reversed. The porogenic solvent controls the porous properties of the monolith through the solvation of the polymer chain in the reaction medium during the early stage of the polymerization [33,35].

In the conventional polymer materials, pores are formed after removal of the porogenic solvent that previously occupied the pore volume during the crosslinking polymerization and

phase separation processes. Typically, the volume fraction of the monomers is approximately 40-60%. The obtained polymer block is composed of densely fused, interlinked microgels that display high mechanical strength and therefore are able to withstand high pressure and chemical treatment without loss of porosity. The microgels are believed to form during the early stages of every polymerization reaction leading to crosslinked polymer networks [36].

The pore size distribution of the molded monoliths is quite different from those observed for "classical" microporous beads. Several approaches have been used to obtain polymer particles with a controlled size and shape distribution. Suspension polymerization has been often utilized to obtain monodispersed particles of several microns diameters [29,37,38]. According to Svec and Fréchet, the "bulk" polymerization in the presence of porogen results in macroporous materials containing very large pores with sizes those even exceed 1000 nm, at least 1 order of magnitude larger than the macropores of beads prepared by suspension polymerization [29]. The overall morphology of globules and cluster based monolith was similar to that found for beads [39]. However, the size of clusters and the irregular voids between them was much larger in the monoliths. The mechanism of pore formation during the polymerization in a mold seems to be affected by the absence of both the interfacial tension between the aqueous and organic phases and the dynamic forces that are typical for the suspension polymerization process [29].

The current rapid developments of microfabricated analytical devices are fueled by the need of significant improvements in speed, sample throughput, cost and handling of analyses. A variety of applications involving, for example, sensors, chemical synthesis or biological analysis have already been demonstrated using the microfluidic chip format [40]. Following the trend of miniaturization towards more complex micro total analysis system (TASs), the so-called "Lab-on-a-chip" systems, polymer monoliths in micro-channels (with diameters of the order of 50 μm)

have also been prepared successfully, for example for the electrochromatographic separation of peptides [41] (cf. Figure 2.2), or for the trypsin digestion of the proteins before mass spectrometry analysis [42].

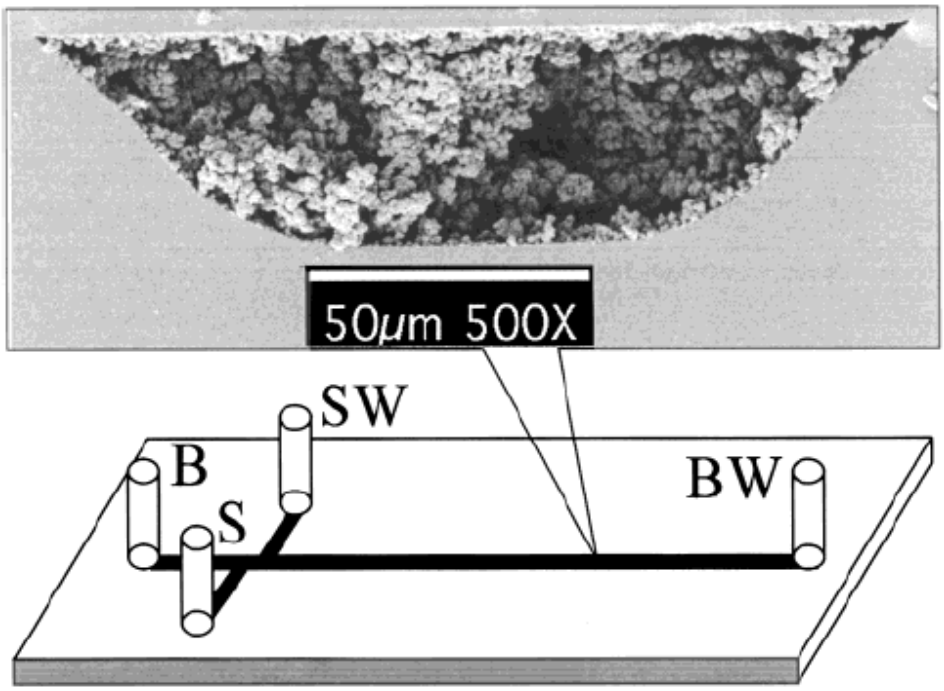

Figure 2.2. Schematic of the microchip used for electrochromatography. B, S, BW, and SW denote reservoirs containing buffer, sample, buffer waste, and sample waste, respectively. The inset shows a scanning electron micrograph of a channel cross-section filled with acrylate polymer monolith prepared via photoinitiated *in situ* polymerization [41].

2.2. Molecularly Imprinted Polymer Monoliths

Molecular imprinting by *in situ* polymerization is an easy and effective technique to prepare polymers with selective molecular-recognition properties. Molecularly imprinted polymers (MIPs) with specific binding sites can be prepared by *in situ* copolymerization of a functional monomer with a cross-linker in the presence of a template and subsequent template

extraction (cf. Figure 2.3). In the field of analytical chemistry, such MIPs have found applications in solid-phase extraction, ligand binding assays, sensors and chromatography, where MIP materials offer attractive properties such as pre-determined selectivity, robustness and resistance to mechanical and chemical stress [43]. The formation of complex between template and functional monomer prior to polymerization is necessary for the high enantioselectivity and binding capacity [44].

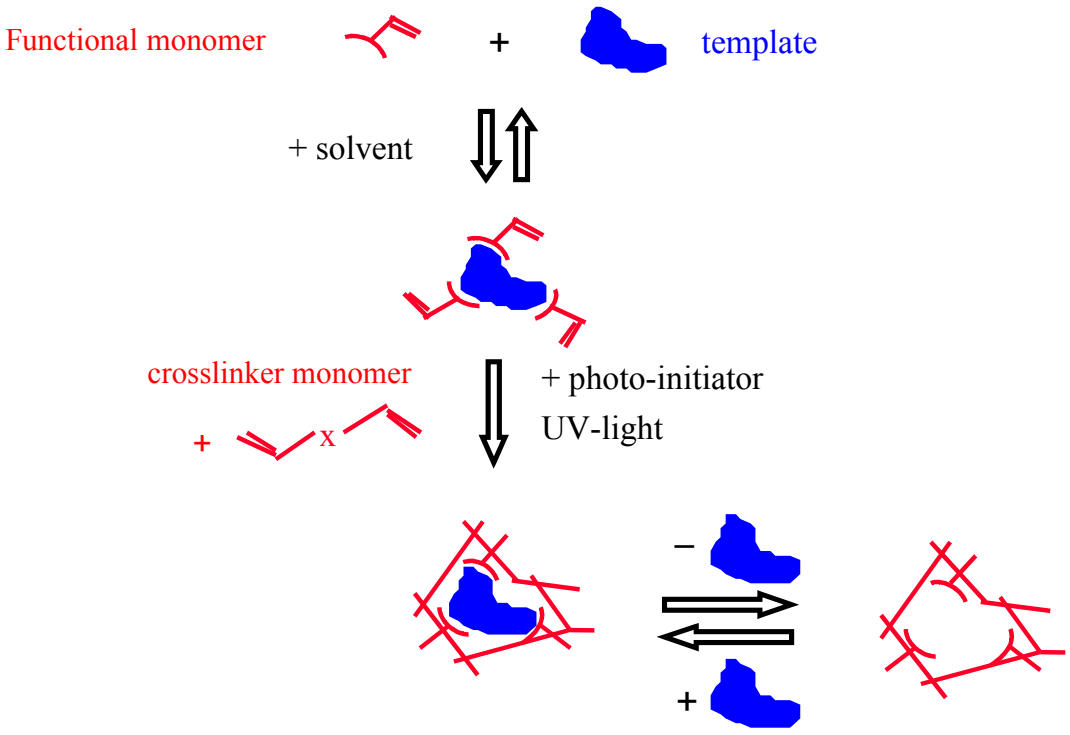

Figure 2.3. Molecular imprinting by in situ UV- initiated polymerization.

In molecular imprinting, monomer-template interactions can be covalent [6] or noncovalent [45]. The covalent imprinting approach is claimed to yield more uniform imprinted sites than the noncovalent approach because the monomer and template are held together by a chemical bond

during polymerization. However, requirements for the molecular template and the polymer system are much more stringent in the case of covalent imprinting and require the synthesis of special template derivatives for each polymer system whereas non-covalent imprinting can generally be used for all miscible molecular templates and monomer systems. During the noncovalent imprinting, weak intermolecular interactions are used to self assemble the monomer(s) around the template molecule. Typical interactions include metal-ligand complexation, hydrogen bonding and ionic, π-π, dipole, and hydrophobic interactions. Noncovalent imprinting is more flexible and simpler to implement than covalent imprinting; thus, it has become the more popular method for synthesizing MIPs.

Most MIPs prepared via the noncovalent imprinting method are synthesized and evaluated in nonpolar solvents. It has been shown that the hydrogen bonding plays a significant role in the recognition processes of such MIP system [46], in addition to the shape recognition [47].

The structure of the polymeric matrix is crucial in the imprinting process. As the specific structure of the cavity is not determined by the low molecular weight molecules, but by the fixed arrangement of the polymer chains, the optimization of the polymer structure is extremely important. The polymer should have the properties like stiffness of the polymer structure, high flexibility, and good accessibility, mechanical and thermal stability to attain the high imprinting efficiency [6]. The macroporous imprinted polymers with permanent pore structure, relatively large inner surface area (50-600 m^2/g) and large pores (about 10-60 nm) ensures that the specific microcavities formed by the imprinting process (about 0.5-1.5 nm in diameter) are readily accessible, and smaller molecules can diffuse freely inside the pores. If high levels of cross-linking agent are used, the cavities retain their shape quite well after removal of the templates [6]. The ratio of porogen to monomer should be approximately 1:1 (mL:g). The type of porogen

has a strong influence on the morphology of the polymer, but the effect on the selectivity of the cavities formed is small [48-50]. The decisive factor for high selectivity is the type and the quantity of the cross-linking agent used in the production of macroporous polymers [6].

The highly crosslinked polymer nanoparticle (microgels) are another class of imprinted materials which are the excellent candidate for use as e.g. controlled release devices [51] and as support for reagents and catalysts [52,53] because of facilitated accessibility of the binding site due to the submicron size of the microgels. Also, with decreasing size of imprinted particles their specific surface is intrinsically increasing. The synthesis of an imprinted microgel would yield a material in which the cavity is built in a polymer particle with dimensions comparable to those of an enzyme. If the cavity selectively binds a molecule or catalyses a specific reaction, then this can be best described as an artificial antibody or enzyme [36]. In order to know whether these "cavities" are still present on discrete polymer particles down to the submicrometer size, Mosbach and his coworkers, concluded that the specific binding sites are distributed on the microgel particles in the conventional imprinted polymer monolith and that these binding sites are kept intact when the fused microgels are dissected by large excess of solvent [54]. Although the obtained selectivities are still low compared to the results achieved with insoluble crosslinked polymers, the success of this approach represents an important step towards the development of "artificial enzymes" [36].

Molecular imprinting has become increasingly popular in recent years and MIPs have proven suitable for advance separation techniques [55,56], sensor applications [57,58], artificial anti bodies [59], catalysts [60,61], and drug assay tools [62]. Recently, there has been interest in shrinking imprinted polymers into micromonoliths that may be later integrated into miniaturized systems capable of performing on-chip chromatographical separations and sensing. Advantages

in speed, portability, sample/reagent consumption, and efficiency may be gained through the application of such miniature systems. The open channel microfluidic chips are not suitable for applications like solid-phase extraction, separation or catalysis where a solid phase inside a channel is desirable. One solution is to coat the inside of the channel with the thin coating of the solid phase. The low surface-to-volume ratios provided by the thin coatings, resulted in the low loading capacities [63]. Monoliths provide an alternate design with benefits that include ease of fabrication and higher loading capacities [34]. Recently, some efforts have been made to prepare monolithic MIPs in molds, e.g. capillaries, with characteristic dimensions in the μm-scale using the technique of micromolding in capillaries [64] and for three-dimensional microstructures using a technique of micro stereolithography [65].

2.3. Surface Modification of Membranes

In this section, a recent comprehensive feature review by Ulbricht [66] is used as the main reference. A membrane surface modification is aimed either to minimize undesired (secondary) interactions (adsorption or adhesion), which reduce the performance (membrane fouling), or to introduce additional interactions (affinity, responsive or catalytic properties) for improving the selectivity or creating an entirely novel separation function [66]. A key feature of a successful (i.e. “tailored”) surface functionalization is a synergy between the useful properties of the base membrane and the novel functional (layer).

Overall, the excitation with UV irradiation has the great advantage that the wavelength can be adjusted selectively to the reaction to be initiated, and, hence, undesired side reactions can be avoided or at least reduced very much [66]. Photoinitiation can be used without problems also in small pores. The UV technology can be integrated into continuous manufacturing processes

simply and cost–efficiently. Photo–initiated processes have their largest potential when surface–selective functionalizations of complex polymer morphologies shall be performed with minimal degradation of the base membrane, and when they are used to create macromolecular layers via "grafting–to" or "grafting–from". However, "Grafting-from" has proven to be the most effective and flexible method for tailored surface functionalization.

"Grafting–from" reaction. During "grafting–from" reaction, monomers are polymerized using an initiation at the surface. Until now, synthesis of macromolecular layers via "grafting–from" a polymer membrane surface is done by radical polymerization. Figure 2.4 shows the different ways for initiation during "grafting–from" reaction.

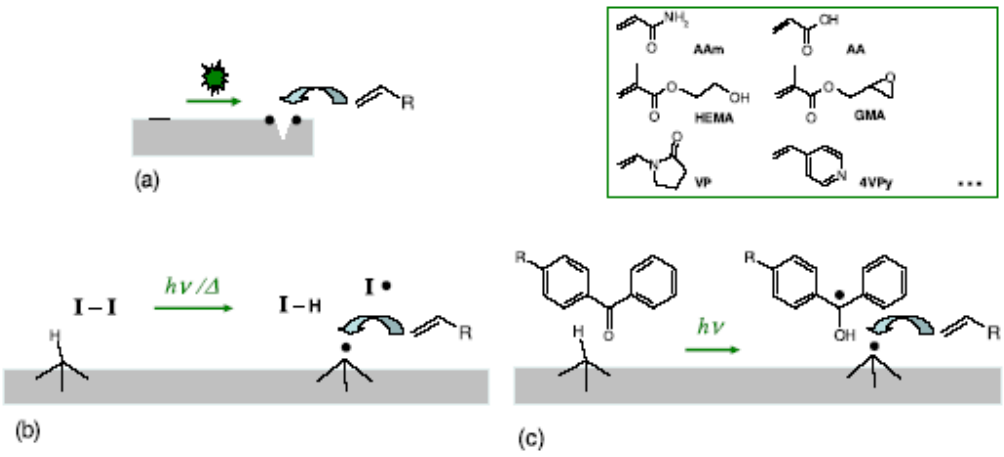

Figure 2.4. Initiation (formation of starter radicals) during heterogeneous radical graft copolymerization ("grafting–from") of functional monomers on membrane polymers: (a) degradation of the membrane polymer (main chain scission or cleavage of side groups), via physical excitation with radiation or plasma, (b) decomposition of an initiator in solution and radical transfer (here hydrogen abstraction); radicals in solution may initiate a homopolymerization as a side reaction or leading to grafting via radical recombination, (c) adsorption of a type II photoiniator (e.g., benzophenone derivative) on the surface and selective UV excitation [66].

The use of UV–assisted methods for a heterogeneous graft copolymerization, mainly with the intention to improve the 'decoupling' effects of the activation and the grafting reactions had been developed by Ulbricht *et al*. [67-73]. Additional photoinitiators, which can be selectively excited by certain UV energies, were used. An especially easy and effective two–step approach is based on (i) the adsorption of a 'type II' photoinitiator (e.g., benzophenone, BP) on the membrane surface and (ii) the subsequent UV initiated hydrogen abstraction reaction to yield polymer radicals on the surface of the membrane in the presence of monomer [70] (cf. Figure 2.4 (c)). Recently, another option to improve the surface selectivity by confining the initiator had been demonstrated: The photoinitiator BP had been 'entrapped' in the surface layer of polypropylene (PP) by using a solvent, which can swell the PP in the coating step (i). By selecting suited BP concentration and time the uptake in the surface layer of the PP can be adjusted, and after change to a more polar solvent such as water or alcohol a fraction of the BP is immobilized but can still initiate a graft copolymerization [73].

2.4. Molecularly Imprinted Membranes

A membrane is an interphase between two adjacent phases acting as a selective barrier, regulating the transport of substances between the two compartments. The main advantages of membrane technology as compared with other unit operations in (bio)chemical engineering are related to this unique separation principle, i.e. the transport selectivity of the membrane. Separations with membranes do not require additives, and they can be performed isothermally at low temperatures and –compared to other thermal separation processes– at low energy

consumption. Also, upscaling and downscaling of membrane processes as well as their integration into other separation or reaction processes are easy [66].

The template binding to MIP sites in a molecularly imprinted membrane (MIM) can be coupled with selective transport through the MIM thus enabling a membrane separation. The transport pathways in a polymer membrane can be either the free volume between polymer chains, the solvent fraction of a swollen polymer gel or connected pores in a solid polymer. Generally there are two separation mechanisms for MIM (cf. Figure 2.5) [4]:

(i) facilitated permeation driven by preferential sorption of the template due to affinity binding—slower transport of the other solutes,

(ii) retarded permeation due to affinity binding—faster transport of other solutes, until a saturation of MIP sites with template is reached.

The template binding can also change the barrier properties of the MIM e.g. via an altered membrane swelling (Figure 2.5). For tailoring and optimizing MIM function, it is critically important to control the affinity of MIP sites along with their density in the membrane and to create well-defined membrane pore morphology. With mainly meso- and microporous MIM, template binding to imprinted sites can either change the pore network thus altering membrane permeability in general (“gate effect”) or the permeation rate is controlled by the interaction with the micropore “walls”. In MIM with trans-membrane macropores, non-selective transport by diffusion or convection can only be compensated by binding to accessible imprinted sites, causing a retardation which can be used in membrane adsorbers [4].

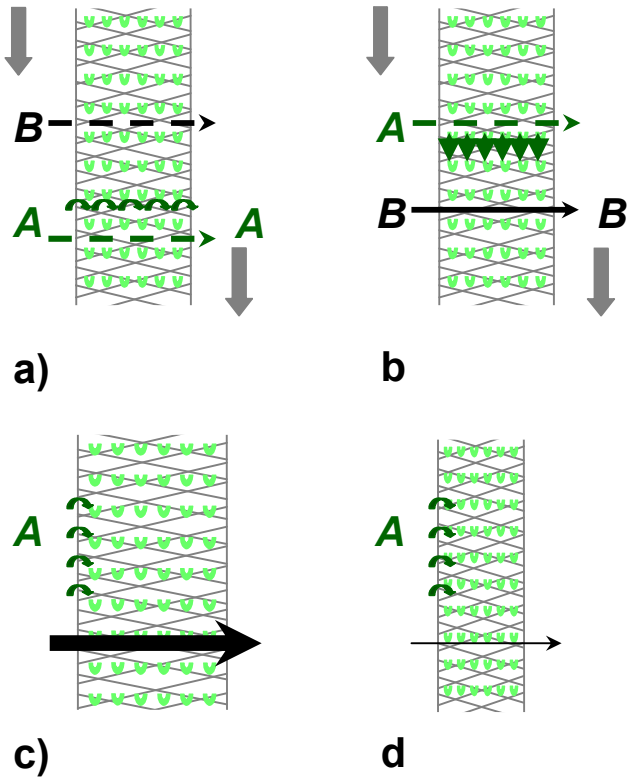

Figure 2.5. Separation mechanisms for MIM as a consequence of the binding selectivity obtained by imprinting for a substance A: (a) transport of A driven by a concentration gradient is facilitated via binding/desorption to neighborhood binding sites, while the non-specific transport of another substance B by diffusion is hindered by the micropore structure of the membrane („fixed carrier“ membrane), (b) transport of A is retarded either by binding or binding/desorption to MIP sites on the surface of trans-membrane pores, while another substance B which has no specific interactions with the membrane surface will be transported by diffusion or convection (membrane adsorber), (c) the MIM permeability is increased, e.g. due to an increase of membrane (barrier) swelling as a consequence of A binding to MIP sites, (d) the MIM permeability is decreased e.g. due to a decrease of membrane (barrier) swelling as a consequence of A binding to MIP sites [4].

A MIM is a membrane either composed of a MIP or containing a MIP. A high membrane performance depends on well-defined membrane morphology with respect to barrier pore size and layer topology, especially the thickness of the barrier layer. Preparation of MIM can be classified in three main strategies [4]:

(1) Sequential approach—preparation of membrane from previously synthesized "conventional" MIPs, i.e. particles.

(2) Simultaneous formation of MIP structure and membrane morphology,

(3) Sequential approach—preparation of MIPs on or in the support membranes with suited morphology.

For strategy (1), the only promising example in this category is the arrangement of the MIP nanoparticles as a filter cake between two microfiltration membranes; these flat-sheet filters had been evaluated with respect to their flow and binding, i.e. adsorber, properties [74,75].

Self-supported flat sheet membranes should be at least 10 μm thick in order to have the sufficient stability. Therefore, when using simultaneous MIM preparation, the control of film thickness, e.g. by solution casting or using mould, is essential. For strategy (2), two main routes towards MIM had been used, the "traditional" in situ crosslinking polymerization and the "alternative" polymer solution phase inversion, both in the presence of templates [4].

In situ crosslinking polymerization

First experiments with MIP membranes have been carried out by Piletsky et al. in 1990 [76]. In this study, the MIM were prepared by in situ crosslinking polymerization of acrylates monomers forming a film in the presence of adenosine monophosphate (AMP). The permselectivity between AMP and guanosine monophosphate (GMP) was investigated by

diffusion experiments. The AMP imprinted membranes discriminated the slight difference between AMP and GMP [77]. Flat sheet, free standing but brittle MIMs were prepared by in situ copolymerization of one of the "standard" monomer mixtures (MAA/EDMA) and 9-ethyladenine was adopted as print molecule [12]. Scanning electron microscopy (SEM) studies revealed a regular porous structure built up by 50-100 nm diameter closely packed polymer domains. These MIM were used for the selective permeation of adenosine from the adenosine-guanosine mixture. The 9-ethyladenine imprinted membrane permeated adenosine in preference to guanosine and its separation factor was determined to be 3.4, while the control membrane hardly showed any permselectivity [12]. A significant improvement had been achieved by using an oligourethane-acrylate macromonomer in in-situ imprinting polymerization mixtures in order to increase the flexibility and mechanical stability of the membranes; self-supported MIM with a thickness between 60 and 120 μm had been prepared [78]. In addition to increased flexibility and mechanical stability, the higher membrane permeabilities were obtained by using high molecular weight polyethylene glycol (PEG) as porogen in the polymerization mixture [79]. A self-supported MIM with a thickness of 60 μm and imprinted with atrazine were prepared by in situ UV-initiated copolymerization. The addition of high molecular weight PEG significantly increased the water flux through the atrazine–imprinted membranes and SEM studies also confirmed the formation of "large through-membrane" pores.

Polymer solution phase inversion

Polymer solution film casting and subsequent phase inversion, the main approach towards technical polymeric membranes, can also be applied for molecular imprinting. Instead of an in situ polymerization, the solidification of a polymer is applied for the synthesis of MIM [4].

Until today, there had been only relatively few attempts to adopt the molecular imprinting for the preparation of polymer membranes for chiral separation. This was mainly due to problems to directly apply the established imprinting methods for the preparation of mechanically stable films [66]. The group of Yoshikawa has done very comprehensive work to establish an alternative approach towards molecular imprinting: specifically synthesized polystyrene resins with chiral oligopeptide recognition groups in a blend with a matrix polymer acrylonitrile-styrene (PAN-co-St) had been used for the membrane formation via a evaporation induced phase separation (EIPS) process, by casting a polymer solution and subsequent evaporation of the solvent, and chiral amino acid derivatives had been used as the template [77,80-84]. Systematic variations of the peptides on the resin indicated that imprinting specificity was indeed influenced by structure, size and architecture of the recognition group [84]. The permeability was much higher for the MIM as compared with the blank membranes. In diffusion studies where a concentration difference was adopted as the driving force for permeation through the membrane, permeation of the template was retarded compared to its counterpart. This opposite behavior during permselectivity compared to adsorption selectivity was explained by retardation due to specific template binding to the “pore walls”. In order to selectively permeate the isomer which is preferentially incorporated into the membrane, electrodialysis was found to be the one way to attain such a membrane transport system which showed the possibility that permselectivity directly reflects its adsorption selectivity. Hence, the same membranes which were previously used for diffusion studies, had shown an opposite selectivity (reflecting its adsorption selectivity) in electrodialysis, and electrodialysis performance was also very much susceptible to the applied voltage. The MIP membrane behavior was summarized in a phenomenological relationship where the flux monotonically increased with the increase in

applied potential difference (ΔV) while the selectivity was ~1 at about 0.1 volts, showed a pronounced maximum selectivity (up to 6!) in the range of 1.5 – 2.5 V and leveled off again to ~1 at very high potential difference value of ~15 V [82]. The authors also argued that by applying a pressure difference such as in membrane filtration, a similar increase in selectivity could be expected. This, however, is hindered by the microporous structure of the thick MIP membranes [66].

By applying this alternative molecular imprinting method, any polymeric material, which can construct and keep its structure, might be converted into a molecularly imprinted membrane. The chiral recognition depends only on the absolute configuration of the adopted print molecule. Following these lines Yoshikawa and his coworkers successfully prepared the imprinted membranes from the synthetic, achiral carboxylated polysulfone [81] and the natural polymer, cellulose acetate [83] via imprinting with a chiral amino acid derivative by using the alternative molecular imprinting technique. The separation factor values obtained for MIM prepared from carboxylated polysulfone and cellulose acetate were very low: 1.2 and 2.3, respectively. A highly enantio-selective MIP membrane based on tetrapeptide derivatives and adopting racemic amino acid derivative as template were also synthesized by Yoshikawa et al. [85]. By using electrical potential as gradient, an optimum permselectivity of 5.9, which corresponds to adsorption selectivity, was achieved.

For strategy (3), preparation of MIPs on or in the support membranes with suited morphology is required and the molecularly imprinted membranes mentioned in figure 2.4 fall in this category.

Molecularly Imprinted Composite Membranes

The composite membranes are being used for the advanced molecular separations, e.g. via reverse osmosis, nanofiltration, pervaporation or membrane adsorption, where an optimized porous support membrane is functionalized with a suited thin selective layer. In the same way MIP composite membrane can also be prepared by adjusting the pore structure and MIP recognition sequentially and by two different materials. The functional polymer added to the base membrane is responsible for the separation performance of a composite membrane. In general there are three different types of composite MIM (cf. Figure 2.6): (i) thin film composite MIM, (ii) pore-filled composite MIM, and (iii) surface functionalized porous composite MIM.

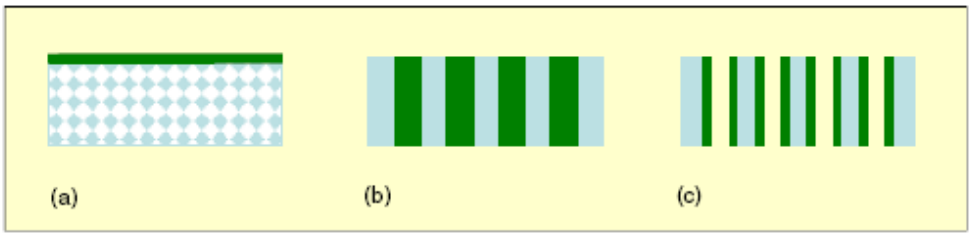

Figure 2.6. Schematic illustration of three main composite membrane types: (a) thin-film, (b) pore-filling, (c) pore surface-functionalized (relative dimensions not to scale) [66].

In membrane separation, not only permselectivity but also flux is an important factor for the evaluation of membrane performance, and the reduction in the thickness is required to enhance the flux through the membrane. In other words, molecularly imprinted, asymmetric or composite membrane with a very thin composite film acting as a selective barrier for higher fluxes (cf. Figure 2.6 a). With that intension, Martin et al. [13] had prepared ultra thin MIM via UV-initiated crosslinking polymerization of a monomer system MAA/EDMA for the preparation of bulk MIP skin (ca. 500 nm) across the surface of a 20 nm pore size alumina support

membrane. Theophylline or caffeine was adopted as a print molecule. The oxygen gas permeability measurements indicated the absence of any pinholes and that the thin film composite membranes were defect free. The observed transport selectivity for the MIP template in solution diffusion studies could be attributed to a facilitated transport through a "nanoporous" separation layer on the top of the porous support membrane [66].

The pore-filling of the porous base membrane with a porous polymer material via in situ polymerization is a very promising approach towards high performance, functional separation membranes (c.f. Figure 2.6 b). There are already the examples for filling the pores of membranes or filters via in situ crosslinking polymerization with polymer monoliths. MIP membranes were produced by using the established MIP synthesis protocols which are not well suited for the preparation of free standing films because of the brittleness. Piletsky et al. used mm-thick porous glass filters as base material to prepare "MIP membranes" by using established MIP synthesis mixture, e.g. MAA/EDMA. The sensors based on these membranes could detect the target molecules at concentrations of 1-50 μM in solution [86]. Imprinted polymer membranes were prepared by casting the polymer mixture MAA/TRIM containing a protected L-amino acid as a template in the pores of polypropylene microfiltration membranes. In diffusion experiments across the imprinted membranes, enantioselectivity was observed with the diffusion of the L-enantiomer (template) being faster than that of the D-enantiomer; however no real selectivities with mixtures had been observed [87]. Also, the very large fluxes indicated that those pore-filled composite membranes may have a considerable fraction of non-selective (i.e. large) pores.

Preparation methods for composite MIM with functionalized coating on the pore surfaces (cf. Figure 2.6 c) can be directly derived from surface modification by adopting a well established "grafting-from" approach [73]. Piletsky et al. [8] had first developed a macroporous

composite membrane, by evenly functionalizing the entire surface of polypropylene membrane via “grafting-from” with MIP layer to obtain high performance, substance-specific membrane adsorbers. By adopting this approach, the structure of the base membrane can be optimized by adjusting the pore size with the introduction of an additional functional layer to get a functional response in a desired application. By coating a photoinitiator (BP) on the surface, a photo-initiated cross-linking graft copolymerization yielded very thin MIP films which were covalently anchored and covered the entire surface of the base membrane [8]. Based on the results of surface and pore analyses, thicknesses of MIP layers with the highest affinity and selectivity were below 10 nm [88]. Moreover, it had been discovered that a previously prepared thin hydrophilic layer on the support membrane can have two functions [9], (i) matrix for the crosslinking polymerization and limiting monomer conversion to ‘filling’ the layer thus forming an interpenetrating polymer network, (ii) minimizing non-specific binding. A superior MIP composite membrane performance, especially high template specificity, could be achieved using this advanced composite structure [66].

In conclusion, the sequential approach will allow using the base membrane pore structure and layer topology as well as the location of the MIP, either on the top or inside the support membrane to prepare different types of MIM, with the MIP either as selective barrier or transport phase or as an affinity adsorber layer [4].

2.5. Strategy of the Work

In this work, molecularly imprinted composite membranes were prepared by adopting the well established molecularly imprinted scheme (cf. Figure 2.3) with the aim to enantioselectively separate the racemic mixture of Boc-D&L-PhA under diffusion (dialysis) and electrodialysis

conditions. The base membranes, polypropylene (PP) microfiltration and poly(ethylene terephthalate) (PET) track-etched membranes were in situ functionalized by filling the pores with porous polymer monoliths from methacrylic acid and ethyleneglycol dimethacrylate (poly(MAA-co-EDMA)). A molecular imprinting procedure based on hydrogen bonding interactions between the template Boc-D-phenylalanine (Boc-D-PhA) and the functional monomer methacrylic acid (MAA) (cf. Figure 2.7) was used to synthesize a porous molecularly imprinted polymer (MIP) with high binding selectivity in the pores of the membranes.

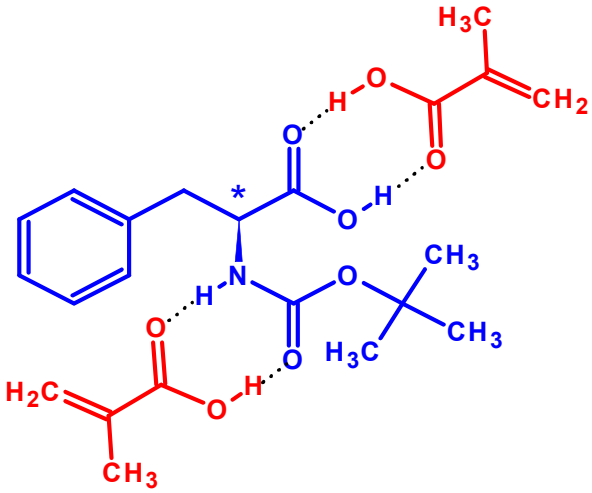

Figure 2.7. A postulated complex between template, butoxycarbonyl-D-phenylalanine (Boc-D-PhA) and methacrylic acid (MAA) based on hydrogen bonding.

The formation of voids at the monolith-mold interface, caused by shrinkage during polymerization, can be a big problem. This is especially true if an even and complete filling of the mold is necessary for the intended application, e.g. a chromatographic separation. The consequences become more severe with decreasing characteristic pore diameter of the monolith and, especially, decreasing dimension of the mold e.g. pores of a membrane. In a first attempt to

solve this problem, a porous polymer monolith had been covalently attached to the walls of channels in the plastic micro devices [89].

Surface modification of polymeric materials is a key technology in various fields of industrial applications, and "grafting-from" has proven to be the most effective and flexible method for tailored surface functionalization [90]. The surface functionalization of microfiltration membranes made from polypropylene (PP) and of track-etched membranes (TEM) made from poly(ethylene terephthalate) (PET) using photoinitiated graft copolymerization had already been explored in several previous studies [69,71,73]. With benzophenone (BP), a "type 2" photoinitiator, the initiation of a heterogeneous graft polymerization relies on a hydrogen abstraction reaction from the base (membrane) polymer (cf. Figure 2.8) [69,70,73,91].

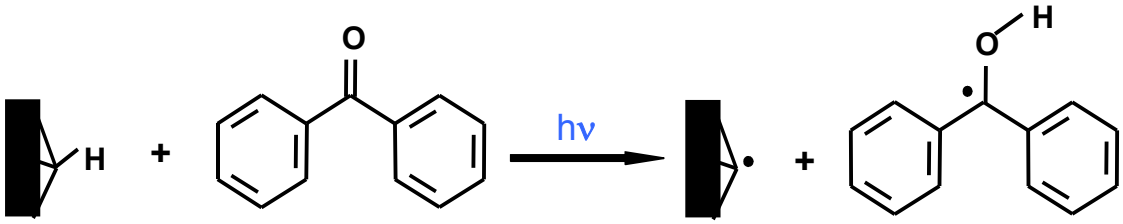

Figure 2.8. Mechanism of H-abstraction from the membrane surface using benzophenone (BP) photo-initiator.

For pre-modification of the membranes, a UV-initiated "grafting-from" functionalization of the entire membrane surface with poly(ethyleneglycol) dimethacrylate (*poly(PEGMA)*) was chosen (cf. Figure 2.9) which should enhance the non-covalent interactions between the polymer monoliths and the pore walls during the subsequent functionalization of the monolithic *poly(MAA-co-EDMA)* in the membrane pores. For the photo-grafting, porous PP membranes were coated using the "photoinitiator entrapping method", and track-etched PET membranes

were coated using the "photoinitiator adsorption method", in both cases with BP as the photoinitiator [73].

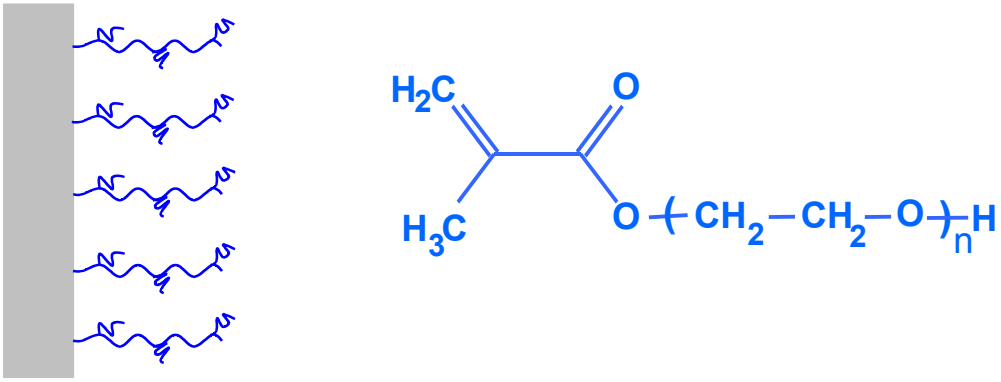

Figure 2.9. Pre-modification of polymer membrane surface with PEGMA (n~9).

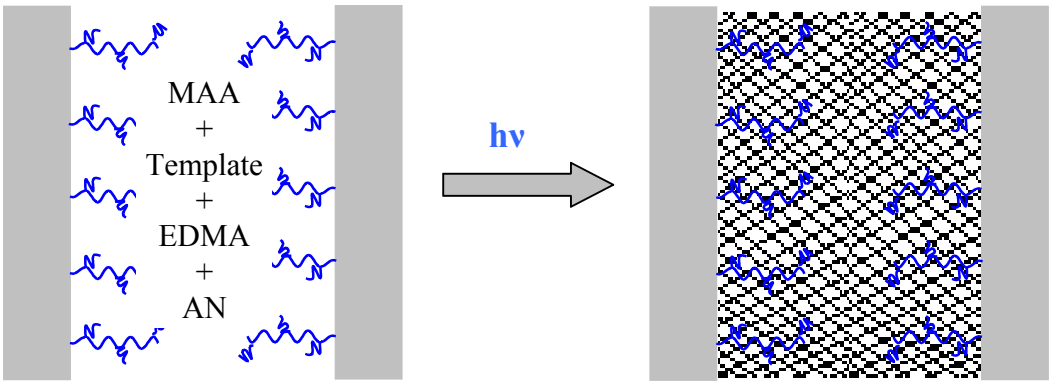

Figure 2.10. Pore-filling functionalization of polymer membrane with porous polymer monoliths from methacrylic acid and ethyleneglycol dimethacrylate (*poly(MAA-co-EDMA)*).

The subsequent in situ UV- initiated functionalization of these membranes (after pre-modification step) with *poly(MAA-co-EDMA)* by filling the pores with porous polymer monoliths was done using the conditions established for the bulk monoliths (cf. Table 3.2) (cf.

Figure 2.10). The resulting MIP and NIP composite membranes, including functionalized MIP and NIP membranes without pre-modification step for comparison, were characterized using gravimetry data, by SEM images, by data from nitrogen adsorption isotherms (BET) as well as by diffusion and electrodialysis etc.

Chapter 3

Experiments

3.1. Materials

Polypropylene (PP) microfiltration membranes (2E HF) with a nominal cut-off pore diameter of 0.4 μm and a thickness of 165 μm were obtained from Membrana GmbH (Wuppertal, Germany), poly (ethylene terephthalate) (PET) track-etched membranes with a nominal pore diameters of 0.4 and 3 μm and a thickness of 23 μm were purchased from Oxyphen GmbH (Dresden, Germany), and "Anodisc" alumina membranes with a nominal pore diameter of 0.2 μm and an average thickness of 60 μm were purchased from Whatman (UK). All the solvents and reagents purchased from commercial sources were of HPLC or analytical grade and were used without further purification. Methacrylic acid (MAA) was from Aldrich, ethylene glycol dimethacrylate (EDMA), 2,2-dimethoxy-2-phenylacetophenone (DMPAP), pure enantiomers Boc-D-PhA and Boc-L-PhA, ammonium acetate anhydrous and acetonitrile (AN) were from Arcos. Polyethylene glycol (400) monomethacrylate (PEGMA 400, the number indicates PEG molar mass in g/mol) was from Polysciences, methanol from VWR, 2,2'-azo-iso-butyronitrile (AIBN), benzophenone (BP), trifluoro acetic acid (TFA) and polyethylene glycols (PEG 1.5, PEG 3, PEG 6 and PEG 10, the numbers indicate molar masses in kg/mol) were from Fluka, sodium azide from Sigma and acetone and heptane were from J.T.Baker. Water purified with a Milli-Q system from Millipore GmbH (Eschborn, Germany) was used.

3.2. Analyses

The concentration of AIBN, Boc-D-PhA and Boc-L-PhA were calculated from their UV absorbance at 340, 255 nm, respectively, measured using the UV-Visible spectrophotometer CARY-50 Probe (Varian, Germany).

Gel permeation chromatography (GPC) was used to analyze the molar mass distribution of PEGs. All analyses using GPC were conducted in sodium azide solution (0.01 M). PEGs were analyzed using a MZ Hema Bio column (MZ Analytik, Mainz, Germany) coupled with a Waters refractive index detector. Calibration curves for the correlation of retention volume and molar mass were obtained using different PEG molar mass standards.

A microbalance (ME 215P Genius, Sartorius, Germany) was used for all gravimetric determination.

Decomposition of Initiators

The solutions of 0.0455 mol/L of azo-iso-butyronitrile (AIBN) and 0.0195 mol/L of dimethoxy phenyl acetophenone (DMPAP) corresponding to 1.5% and 1% of the weight of monomers in the pre-polymerization mixtures were prepared in acetonitrile, respectively. For thermal decomposition of AIBN, 2.5 mL of the AIBN solution was filled into cylindrical glass vessels (diameter 14 mm, height 44 mm) which were then tightly closed with caps, and thereafter placed in the oven at 70°C for different intervals of time. For UV-initiated decomposition of AIBN and DMPAP, 2.5 mL of the respective solutions were filled into each cylindrical glass vessel (diameter 14 mm, height 44 mm) which were then tightly closed with caps, and thereafter placed in the UV-box and irradiated at UV intensity of 4.3 ± 0.2 mW/cm^2 for different intervals

of time at room temperature. The AIBN concentrations were calculated from UV absorbencies at 340 nm measured using the UV-visible spectrophotometer CARY-50 Probe (Varian, Germany).

The DMPAP samples were analyzed using a HPLC system (Dionex, Germany) equipped with a column Kromasil 100 C18 (MZ Analysentechnik, Mainz, Germany). The chromatographic separations were performed using 20 vol % aqueous methanol as an eluent at 1 mL/min. Injection volume was 20 μL and elution was monitored using the UV detector set at 255 nm.

3.3. Syntheses

A small UV-box (CL-1000L, Upland, CA, U.S.A.) equipped with 5*8 Watt discharge type tubes with a wavelength of 365 nm were used for the decomposition study of initiators and for the synthesis of bulk polymer monoliths of different diameter sizes. The UV intensity was 4.3 ± 0.2 mW/cm^2 (measured with the UVA meter, Hönle AG).

A UV illumination system (UV A Print, Hönle AG, Graefelfing, Germany) equipped with a high pressure mercury lamp and a glass filter ($\lambda > 300$ nm) was used for the syntheses of bulk polymer monoliths (MIP and NIP), the pre-modification of the membranes and the preparation of the composite membranes. The UV intensity was 35 ± 5 mW/cm^2 (measured with the UVA meter, Hönle AG).

3.3.1. Polymer Monoliths in Bulk

At first step, the polymer monoliths in bulk were prepared via thermal and UV-initiated polymerization of the pre-polymerization mixture, composed of functional monomer and cross-linker in the ratio of 1:4 (w/w), initiator AIBN (1.5% wt. relative to mass of monomers) or

DMPAP (1% wt. relative to mass of monomers) and porogen solvent AN (in the ratio of 1:1 (v/w) relative to the monomer mixture) [35]. The pre-polymerization mixture compositions are summarized in the Table 3.1. About 2.5 mL of the polymerization mixture was filled into a cylindrical glass vessel (diameter 14 mm, height 44 mm) which was then closed tightly with a cap, and thereafter polymerization was done either thermally at 70°C for 24 hours or UV-initiated polymerization at UV intensity of 4.3 ± 0.3 mW/cm^2 for one hour depending upon the type of sample. In case of BM-MAA-UV, polymer monoliths with different diameters were also prepared. After polymerization, the bulk polymer monoliths matching the shape of the mold were taken out of the glass vessels, washed in methanol for one hour while shaking on a horizontal shaker, then extracted in a Soxhlet apparatus with methanol for about 18 hours and finally dried at 45°C, first for about six hours without vacuum and then for 18 hours under vacuum.

Table 3.1. Pre-polymerization mixture compositions for the synthesis of different polymeric monoliths.

Bulk Monolith Type	**Functional Monomer (g)**		**Crosslinker (g)**	**Solvent (mL)**	**Initiator (mg)**	
	MMA	**MAA**	**EDMA**	**Acetonitrile**	**AIBN**	**DMPAP**
BM-MMA-T	1		4	5	75	
BM-MMA-UV	1		4	5		50
BM-MAA-T		1	4	5	75	
BM-MAA-UV		1	4	5		50

3.3.2. MIP Monoliths in Bulk

After optimizing the synthesis conditions for the polymer monoliths with suited pore structure (i.e. no large macropores and with high specific surface area), large polymer monoliths were prepared by in situ polymerization of the pre-polymerization mixture, composed of functional monomer (MAA) and cross-linker (EDMA) in the ratio of 1:4 (w/w), photoinitiator DMPAP (1% wt. relative to mass of monomers) and porogen solvent AN (in the ratio of 1:1 (v/w) relative to the monomer mixture) (cf. Table 3.2).

Table 3.2. Syntheses compositions for MIP (Boc-D-PhA) and NIP (without template) monoliths and pore-filled membranes.

Polymer Type	**Functional monomer** MAA (g)	**Cross-linker** EDMA (g)	**Porogen** AN (mL)	**Initiator** DMPAP (mg)	**Template** Boc-D-PhA (mg)
MIP	1	4	5	50	250
NIP	1	4	5	50	--

Incase of MIP monoliths, the pre-polymerization mixture preparation involves, the mixing of the template Boc-D-PhA and MAA to have “pre arrangement complexes” based on electrostatic and hydrogen bonding interactions between template and functional monomer and then the subsequent addition of crosslinker and photoinitiator [44,92-94]. About 650 µL of the polymerization mixture was filled into a cylindrical glass vessel (diameter 7 mm, height 40 mm)

which was then closed with a rubber septum, and thereafter UV irradiated for 15 minutes. After polymerization, the bulk polymer monoliths matching the shape of the mold were taken out of the glass vessels, washed in methanol for one hour while shaking on a horizontal shaker, then extracted in a Soxhlet apparatus with methanol for about 40 hours and finally dried at 45°C, first for about six hours without vacuum and then for 18 hours under vacuum.

3.3.3. Membrane Pre-modification by Photografting

The UV-initiated grafting of the PP membranes using "photoinitiator entrapping method" and the PET membranes were pre-modified via UV-initiated grafting using the "photoinitiator adsorption method" were carried out according to Ulbricht and Yang [73]. The PP membranes were pre-modified with 25 g/L PEGMA solution in water, while PET membranes were pre-modified with 25 and 50 g/L PEGMA solution in water. The detailed procedures for pre-modification are given below:

Pre-modification of PP Microfiltration Membranes

Circular membrane samples with a diameter of 30 mm were pre-soaked for 15 minutes in 2.5 mL of a solution of 0.1 wt% BP in heptane. Thereafter samples were dried in air for 10 minutes and carefully immersed in 5 mL of methanol for 5 minutes. Then, the samples were quickly wiped with the filter paper in order to remove the adhering solvent and were immediately immersed into 4 mL of PEGMA solution in water in a petri dish (diameter of 55 mm) by placing them between two filter papers. Finally, this "sandwich" was tightly covered with a smaller glass Petri dish with a UV transmission > 300 nm (cf. Figure 3.1). After 30 minutes of equilibration, UV irradiation for 15 minutes followed. The membrane samples were

taken out and then washed while stirring sequentially with 80 mL of water in each step, first for 30 minutes at room temperature, second for 30 minutes at 60°C and third for 30 minutes at room temperature. Finally, the membranes were dried at 45°C overnight.

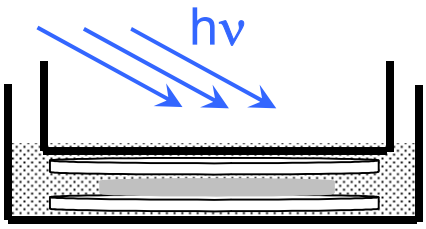

Figure 3.1. Pre-modification of membrane in a sandwich between two filter papers placed between two petri dishes.

Pre-modification of PET Track Etched Membranes

The circular membrane samples with a diameter of 46 or 48 mm were pre-soaked for 15 minutes in 4 mL of 0.1 M BP in acetone. The membranes were dried at 45°C for one hour and were placed between two filter papers in a petri dish (diameter of 55 mm) and immersed in 4 mL of PEGMA solution in water saturated with BP and tightly covered with a smaller glass petri dish and also used as a filter with UV transmission > 300 nm (cf. Figure 3.1). After 15 minutes of equilibration, UV irradiation for 15 minutes followed. Membrane samples were taken out and then washed in 60 mL of methanol for one hour. Finally, the membranes were dried at 45°C overnight.

3.3.4. Membrane Pore-filling Functionalization

Both PP and PET membranes were used for pore-filling functionalization. Synthesis of the MIP and NIP composite membranes was done by functionalization of the original and already pre-modified membranes with *poly(MAA-co-EDMA)*, using the same polymerization mixture

ratio which was used for the synthesis of bulk polymeric monoliths (cf. Table 3.2). The membranes were placed between two filter papers, put in a petri dish with 4 mL of polymerization mixture and covered with a smaller petri dish so that no gas bubbles were entrapped. After 15 minutes of equilibration, membrane samples were taken out, immediately placed between two glass plates (50×70 or 60×100 mm; UV transmission > 300 nm) and fixed tightly with clamps from the four corners followed by UV irradiation for 15 minutes (cf. Figure 3.2). Incase of PET membranes with pore diameter of 3 µm were UV irradiated under water in order to avoid heating of the sample during the polymerization. After polymerization, membranes samples were carefully removed from the glass plates and washed in 60 mL methanol for one hour while shaking on a horizontal shaker. Thereafter they were extracted in a Soxhlet apparatus with methanol for about 40 hours. The composite membranes were kept wet in AN. Whenever necessary the membranes were dried at 45°C, first for about two hours without vacuum and then for overnight under vacuum.

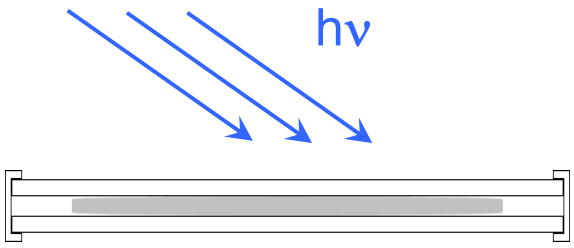

Figure 3.2. Fixing of the membrane between two glass plates for polymerization.

3.4. Characterizations

3.4.1. Degree of Grafting

The degree of grafting (DG) for both PP and PET membranes after each step (pre-modification and pore-filling functionalization) was determined gravimetrically from the weight of each sample before and after modification, using following equation:

$$\text{DG } (\mu g/cm^2) = \frac{W_1 - W_0}{A} \quad (3.1)$$

Where W_0 and W_1 represent the sample's weight in μg before and after modification and A (cm^2) is the outer (geometric) membrane area or the specific surface area of the membrane, respectively.

3.4.2. Surface and Cross-sectional Morphology

Principle

Scanning electron microscopy (SEM) is a very simple and useful technique for characterizing the polymeric materials and membranes for surface and cross-sectional morphology. A clear and concise picture of the membrane can be obtained in terms of the top layer, cross-section and bottom layer. In addition, the porosity and the pore size distribution can also be estimated from the photographs [95].

The SEM is an instrument that produces a largely magnified image by using electrons instead of light to form an image. A beam of electrons is produced at the top of the microscope by an electron gun. The electron beam follows a vertical path through the microscope, which is held within a vacuum. The beam travels through electromagnetic fields and lenses, which focus

the beam down toward the sample (cf. Figure 3.3). Once the beam hits the sample, electrons and X-rays are ejected from the sample.

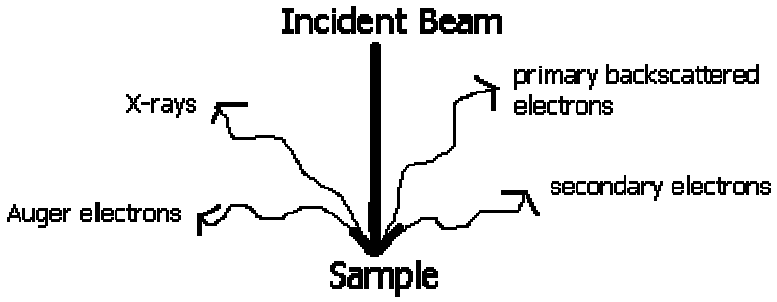

Figure 3.3. Working principal of a scanning electron microscope.

Detectors collect these X-rays, backscattered electrons, and secondary electrons and convert them into a signal that is sent to a screen similar to a television screen. This produces the final image.

Because the SEM utilizes vacuum conditions and uses electrons to form an image, special preparations must be done to the sample. All water must be removed from the samples because the water would vaporize in the vacuum. All metals are conductive and require no preparation before being used. All non-metals need to be made conductive by covering the sample with a thin layer of conductive material. This is done by using a device called a "sputter coater."

The sputter coater uses an electric field and argon gas. The sample is placed in a small chamber that is at a vacuum. Argon gas and an electric field cause an electron to be removed from the argon, making the atoms positively charged. The argon ions then become attracted to a negatively charged gold foil. The argon ions knock gold atoms from the surface of the gold foil. These gold atoms fall and settle onto the surface of the sample producing a thin gold coating.

Procedure

For present work an environmental scanning electron microscope (ESEM), Quanta 400 FEG (FEI, USA) was used to characterize the bulk monoliths, as well as the PP and PET membranes before and after functionalization. A sputter coater K550 (Emitech, UK) was used for coating of the outer surface and cross-section of the samples with gold / palladium.

3.4.3. Pore Morphology

Principle

The gas adsorption is a well known technique for determining the specific surface area and pore size distribution in porous materials. The relationship of volume of gas adsorbed vs. relative pressure at constant temperature is known as an adsorption isotherm. The adsorption isotherm of an inert gas (e.g. N_2) is determined as a function of the relative pressure ($P_{rel} = P_S/P_o$, i.e. the ratio between the sample or applied pressure and the saturation pressure). The experiments are carried out at boiling liquid nitrogen temperature (at 1 bar). The adsorption isotherm starts at a low relative pressure. At a certain minimum pressure the smallest pores will be filled with liquid nitrogen (with minimum radius size of about 2 nm). By increasing pressure further, larger pores will be filled and near the saturation pressure all the pores are filled. The total pore volume is determined by the quantity of the gas adsorbed near the saturation pressure [96]. The specific surface area is derived from Brunauer-Emmett-Teller (BET) gas adsorption method. The BET surface area (which includes all internal structures) is calculated from a multilayer adsorption theory which assumes that the first layer of molecules adsorbed on the sample surface involves adsorbate-adsorbent energies and subsequent layers of molecules adsorbed involve the energies

of condensation of the adsorbate-adsorbate interaction. The BET equation should produce a straight line plot and the linear form of which is presented as:

$$\frac{P_S}{V_A(P_0 - P_S)} = \frac{1}{V_M C} + \left[\frac{C-1}{V_M C}\right] \times \frac{P_S}{P_0} \tag{3.2}$$

Where V_A is the volume adsorbed at the relative pressure P_S/P_o, V_M is the volume of monolayer and C is a constant related to enthalpy of adsorption but generally used to characterize the shape of the isotherm in BET range.

The BET equation requires a linear relationship between $P_S/V_A(P_o\text{-}P_S)$ and P_S/P_o and the range of linearity is restricted to a limited part of the isotherm usually not outside the P_S/P_o range of 0.05 to 0.3. After getting the volume of monolayer (V_M), the BET surface area can be calculated from following expression.

$$S_{BET} = \frac{V_M \times N_A \times A_M}{M_V} \tag{3.3}$$

Where S_{BET} is the BET surface area, N_A is the Avogadro's number, M_V is the molar volume (22414 mL) and A_M is the cross-sectional area occupied by each adsorbate molecule and for BET determinations it is assumed to be 0.162 nm^2.

The pore size distribution is the distribution of pore volume with respect to pore sizes. For the calculation of pore size distribution, a cylindrical pore model is assumed and the method used is based on BJH (Barrett, Joyner and Halenda) method which involves the area of the pore walls and uses the Kelvin equation to correlate the relative pressure of the nitrogen in equilibrium with porous solid, to the size of the pores where capillary condensation takes place. The mesopores are filled progressively with adsorbate by the process of capillary condensation. At relative pressure of near unity, all meso and macropores are full of liquid adsorbate.

The volume adsorbed by the sample at different increasing relative pressure values are converted to equivalent liquid volumes, because it is assumed that capillary condensation has taken place and the pores are filled with liquid rather than gas. The Kelvin equation in the following form is used to calculate the core radius of the liquid in the capillary:

$$RT \ln\left(\frac{P_S}{P_0}\right) = -2\gamma \frac{V_{mol}}{R_K} \qquad (3.4)$$

Where R_K is the Kelvin radius, γ is the adsorbate surface tension at T, in mN/m, R is the gas constant, T is the boiling point of nitrogen and V_{mol} is the molar volume of nitrogen.

If the actual radius of the cylindrical pore is R_P and a correction is made for the thickness of a layer already adsorbed on the pore walls i.e. for the multilayer thickness, t, then

$$R_P = R_K + t \qquad (3.5)$$

Values of t are obtained from the data for the adsorption of the same adsorptive on a nonporous sample having a similar surface to that of the sample under investigation.

Procedure

A surface area analyzer SA 3100 (Beckmann-Coulter, U.S.A.) and nitrogen with a purity > 99.99% were used to measure adsorption isotherms and to determine the BET specific surface area and BJH cumulative pore volume for all the different materials.

The swelling, the solvent uptake (wet porosity) of the bulk polymeric monoliths were determined by measuring the volume and the mass increase relative to the dry state. The initial weight and volume were measured for the polymeric monoliths which were then immersed in 5 mL of AN in a tightly sealed glass vessel for 24 hours while shaking. The final weight and volume were measured, and wet porosity was calculated using following formula:

$$\text{Wet Porosity (\%)} = \frac{\Delta m}{\rho \times V_W} \times 100 \qquad (3.6)$$

Where, Δm is the weight difference between wet and dry state (g), V_w is the volume of the wet monolith (mL) and ρ is the density of the wetting liquid (g/mL).

Swelling of the bulk monolith was calculated from the volume difference between dry monolith volume (V_d) and wet monolith volume (V_w) after wetting with the solvent. A digimatic micrometer (IP 65; Mitutoyo, Japan) was used to measure the diameter and length of the monoliths.

3.4.4. Chiral Chromatography

Principle

Chiral chromatography is a technique for separating enantiomers. Such a separation is based on the differently strong interaction of the enantiomers with the chiral stationary phase. As a result, one enantiomer is more retarded than the other, so that they pass through the chromatographic column at different times. The enantiomers cannot be distinguished in achiral environments, such as a solvent system or by normal silica gel chromatography; they can be distinguished in chiral environments, such as in the active site of an enzyme, or in a chiral stationary phase of a column. In a chiral column, achiral silica gel (SiO_2) is converted into a chiral stationary phase by a reaction with a chiral molecule. Once the enantiomers that need to be separated are run down the column, one enantiomer will "stick" to the stationary phase better than the other, and there will be a separation.

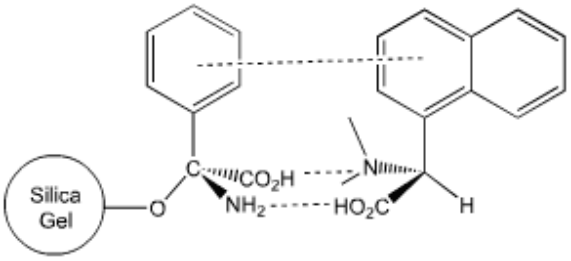

Figure 3.4. A three point interaction between chiral stationary phase and an enantiomer of a biphenyl derivative.

In Figure 3.4, the hypothetical example of an interaction between a chiral stationary phase (left) with an enantiomer of a biphenyl derivative (right), there is a three-point interaction, with the carboxy groups aligning with the amino groups and the aromatics lining up with each other to form π- π interactions. The counter enantiomer of this biphenyl would not be able to have all three of these interactions because its groups would not be aligned correctly, and, consequently, it would stick less to the chiral stationary phase and filter off the column first.

Procedure

A HPLC system (Dionex, Germany) equipped with a chiral column Sumichiral OA-3300 (Sumika Chemical Analysis Service, Japan) or a chiral column Nucleocel Alpha-RP-S (Macherey-Nagel GmbH & Co., Germany) was used to characterize MIP and NIP monoliths and the respective PP and PET composite membranes for their equilibrium binding and enantioselectivity for the template (Boc-D-PhA) and its counterpart in the racemic mixtures of different concentrations and for the amounts of D- and L- isomers that permeated through the PET composite membranes during diffusion and electrodialysis experiments. The chromatographic separations were performed using 6 mM ammonium acetate solution in

methanol as an eluent at 1 mL/min with a chiral column Sumichiral OA-3300 or a 0.08% trifluoro acetic acid (TFA) in 60 vol % aqueous AN as an eluent at 0.5 mL/min with a chiral column Nucleocel Alpha-RP-S. Injection volume was 20 µL and elution was monitored using the UV detector set at 217 nm.

In chromatography, the smallest detectable signal cannot be less than the double height of the biggest noise signal. For qualitative analysis, the signal to noise ratio can be from 3 to 5 but should not be less than 3 [97]. The qualitative detection limits of Boc-D-PhA and or Boc-L-PhA in MeOH, AN, and 50 vol % aqueous AN are given in table 3.3. The values equal to or below these limits fall in the qualitative analysis range.

Table 3.3. The HPLC detection limits for Boc-D/L-PhA in different solvents for qualitative analysis.

Solvent	**Detection Limit for Boc-D/L-PhA [µmol/L]**
Methanol	2.0
Acetonitrile	8.0
50 vol % aqueous AN	15.0

3.4.5. Static Adsorption Experiments

About 150 mg of MIP and NIP bulk monoliths were placed in glass sample tubes. These samples were equilibrated with 5 mL of AN or 50 vol % aqueous AN, for overnight while shaking on horizontal shaker. Likewise about 100 mg of MIP and NIP composite PP and PET membranes prepared with and without pre-modification were equilibrated with 3 mL of AN for

overnight while shaking on horizontal shaker, respectively, After removing the AN or 50 vol % aqueous AN, a racemic mixture (Boc-DL-PhA) of different concentrations in AN or 50 vol % aqueous AN, was added to each sample bottle (1 mL/50 mg of sample) and tightly sealed. The samples were then left on the horizontal shaker for 24 hours. In case of bulk monoliths, the samples were also equilibrated for longer time to study the effect of time on equilibrium conditions. The supernatant was analyzed by chiral HPLC. The free amount of Boc-D-PhA and Boc-L-PhA was determined by measuring the peak heights using the calibration curve obtained from the different racemate concentrations.

3.4.6. Diffusion and Electrodialysis

Diffusion

"Diffusion" is the movement of molecules from a region in which they are highly concentrated to a region in which they are less concentrated. It depends on the motion of the molecules and continues until the system in which the molecules are found reaches a state of equilibrium, which means that the molecules are randomly distributed throughout the system.

$$\frac{\partial c}{\partial t} = -D\frac{\partial^2 c}{\partial x^2} \tag{3.7}$$

The above expression, also known as Fick's second law, gives the change in concentration as a function of distance and time. 'D' is the diffusion coefficient. The rate of diffusion of a molecule can be characterized as diffusion coefficient.

$$D_{eff} = \frac{n.d}{t \cdot A \cdot \varepsilon \cdot \Delta c} \tag{3.8}$$

Where, 'D_{eff}' is effective diffusion coefficient, 'n' is permeated amount of solute in moles, 'd' is the membrane thickness, 't' is the time, 'A' is the membrane area, 'ε' is the membrane porosity, and 'Δc' is the concentration gradient.

The order of magnitude of the diffusion coefficients of molecules permeating through membranes depends on the size of the diffusing particles and on the nature of the material through which the diffusion occurs. In general, diffusion coefficients decrease as the particle size increases. The diffusion coefficient values for the low molecular weight liquids ranges from 10^{-8} – 10^{-9} m^2/sec [98]. The diffusion coefficient increases with the increase in swelling of the membrane and under such circumstances the effect of the particle size will become less important.

Dialysis is a process where salutes diffuse from feed side to the permeate side according to their concentration gradients. Separation between the salutes is obtained as a result of differences in diffusion rates across the membrane arising from differences in molecular size and difference in solubility. In order to obtain a high flux, the membranes should be as thin as possible. Transport in dialysis proceeds via diffusion through nonporous membranes. As a result of swelling, diffusion coefficients are high in comparison to those in the unswollen membrane which in turn implies that the membrane selectivity will decrease. Dialysis is referred as the diffusion of neutral molecules. If electrolytes are separated with neutral membranes or with charged membranes, then 'Donnan effects' arising from the unequal distribution of ions, interfere with the normal dialysis process. This type of dialysis is called Donnan dialysis or diffusion dialysis [99].

Diffusion dialysis is a diffusion process in which ions are transported across an ionic membrane due to a concentration difference and can be described in a similar way as the dialysis

process. If an ion exchange membrane in contact with an ionic solution is considered, then ions with the same charge as the fixed ions in the membrane are excluded and can not pass through the membrane. This effect is known as Donnan exclusion [100].

Procedure

The diffusion method where concentration difference was adopted as a driving force for membrane permeation was used to quantify the amount of solute on the permeate side as well as the effective diffusion coefficient. As shown in Figure 3.5, the diffusion cell consisted of two half-cells, i.e. the feed cell (high concentration) and the permeate cell (low concentration). Each cell was equipped with a stirring system. The membrane with an effective area of ~12.56 or 10.75 cm^2 was placed between the two cells and sealed with O-rings.

Both feed and permeate cells were filled at the same time. The feed cell was filled with a solution of either PEG (1 g/L in 0.01 M sodium azide solution) or racemic mixture (Boc-DL-PhA, 0.3 or 1 mmol/L in AN or MeOH or 50 vol % aqueous AN solution) and the permeate cell was filled with a respective solvent either 0.01 M sodium azide solution or AN or MeOH or 50 vol % aqueous AN solution, depending upon the nature of experiment. In order to minimize the resistance of boundary layers, the two half-cells were stirred at the same stirring rate. The diffusion of PEG and Boc-DL-PhA through the membrane was monitored by measuring their concentrations in permeate cell at certain time intervals and the effective diffusion coefficient values were calculated subsequently.

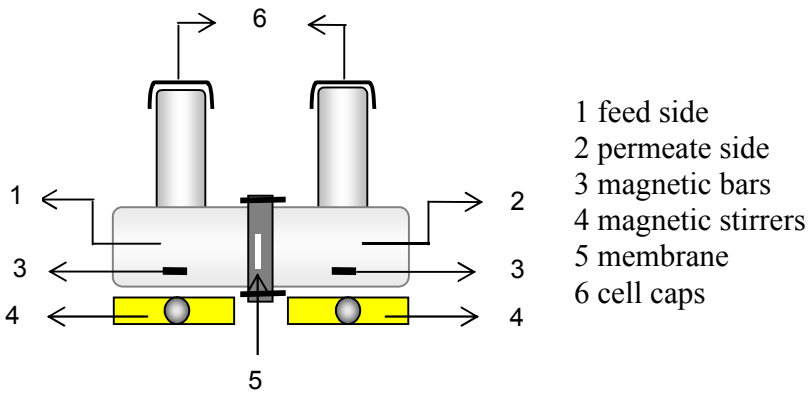

Figure 3.5. Experimental setup for diffusion measurements.

Electrodialysis

Membrane processes in which an electrical potential difference acts as the driving force used the mobility of charged ions or molecules to conduct an electrical current. If an electrical potential difference is applied to a salt solution, then the positive ions (the cations) migrate to the negative electrode (the cathode) where as the negative ions (the anions) migrate to the positive electrode (the anode) (cf. Figure 3.6). Uncharged molecules are not affected by applied electrical potential difference and hence electrically charged components can be separated from their uncharged counterparts [101].

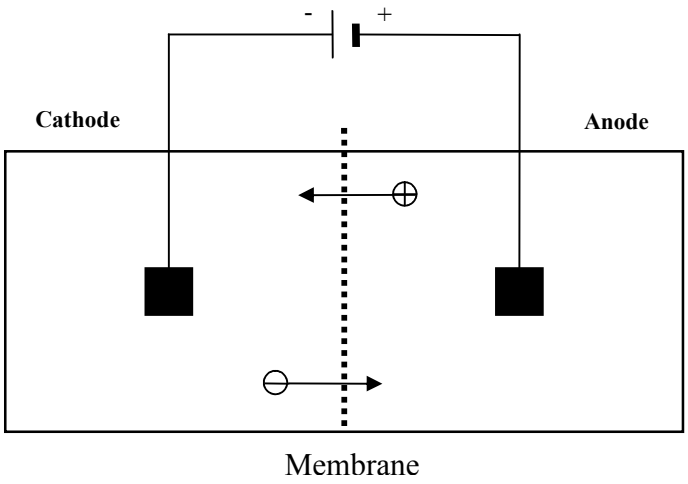

Figure 3.6. Transport of ions or charged molecules in an electrically driven membrane process.

"Electrodialysis" is a process in which ions are transported through membranes because of an applied electrical potential difference and as a consequence of a direct electrical current flow. In this process electrically charged membranes are used to remove ions from an aqueous solution. In order to make the membranes selective for ions, ion-exchange membranes that either allows the transfer of cations or anions are used. Thus, the ion-exchange membranes can be sub-divided into anion-exchange and cation-exchange membranes. Anion-exchange membranes contain positively charged groups attached to a polymer, for example those derived from ammonium salts. Positively charged cations are repelled from the membrane because of this fixed charge. On the other hand, cation-exchange membranes contain negatively charged groups, primarily sulfonic or carboxylic acid groups. Negatively charged anions are now repelled by the membrane. The transport of ions across an ionic membrane is based on the Donnan exclusion mechanism.

Procedure

The electrodialysis where applied potential difference was adopted as a driving force for membrane permeation was used to quantify the amount of solute on the permeate side. As shown in Figure 3.7, the diffusion cell consisted of two half-cells, i.e. the feed cell (high concentration) and the permeate cell (low concentration). Each cell was equipped with a stirring system. The membrane with an effective area of ~ 10.75 cm^2 was placed between the two cells and sealed with O-rings.

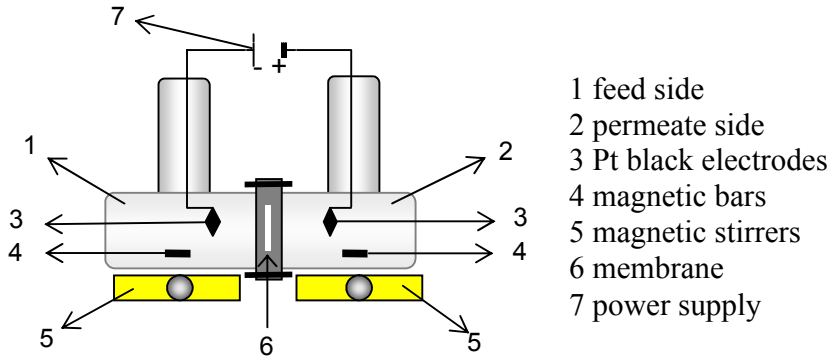

Figure 3.7. Experimental setup for electrodialysis measurements.

The feed and permeate cells were filled at the same time with a solution of either Boc-D-PhA/Boc-L-PhA (1 and 0.5 mmol/L in 50 vol % aqueous AN solution) or racemic mixture (Boc-DL-PhA, 0.3 or 1 mmol/L in 50 vol % aqueous AN solution) and a 50 vol % aqueous AN solution, respectively. The diffusion of Boc-DL-PhA through the membrane as function of applied potential difference was monitored by measuring their concentrations on permeate-side at different time intervals.

Chapter 4

RESULTS AND DISCUSSION

The experimental results obtained are classified into following four main sections: (i) Preparations and pore characterizations, (ii) Equilibrium binding and enantioselectivity, (iii) Transport experiments (diffusion and electrodialysis), (iv) Correlations between synthesis, pore-structure, binding and transport properties.

4.1. Preparations and pore characterizations

This section is further divided into four subsections which include (i) Development of synthesis conditions for polymer monoliths, (ii) Pre-modification and pore-filling of PP and PET Membranes, (iii) Pore characterization of PP and PET based composite membranes, and (iv) Pore-filling functionalization of "Anodisc" alumina membranes.

4.1.1. Development of Synthesis Conditions for Polymer Monoliths

General Consideration

The pore size distribution within a monolith has a direct effect on the performance of the material. Large macropores are required for the mobile phase to flow through the monolith at low pressures, while mesopores (2-50 nm) and micropores (< 2 nm) afford a high surface area for increased capacity [31]. Optimization of pore size distribution is necessary to get the suited pore structure (no large macropores and high specific surface area) within the polymer monolith. Initially by adopting the procedure from Santora et al., the polymer monoliths in bulk were prepared via thermal polymerization of MMA as a functional monomer and EDMA as across-

linker in the ratio of 1:4 (w/w), AIBN as an initiator and AN as a porogen solvent [35]. Later MMA was replaced with MAA as functional monomer to get imprinting effect for its intended use in the synthesis of molecularly imprinted composite membranes. The thermal polymerization was done at ~70°C for 24 hours while the UV-initiated polymerization was done at room temperature and at an UV-intensity of 4.3 ± 0.2 mW/cm^2 for one hour. The detailed pre-polymerization mixture compositions are summarized in the Table 3.1. After establishing the synthesis conditions, the MIP monoliths were prepared from the pre-polymerization mixture (cf. Table 3.2) where Boc-D-PhA was used as template in the ratio of 1:4 to the functional monomer (MAA) and the NIP monoliths were prepared without template molecule for control experiments. Both MIP and NIP monoliths were polymerized at an UV-intensity of 35 ± 5 mW/cm^2 for 15 minutes.

Decomposition Behavior of Photo-Initiators (AIBN & DMPAP)

The choice of an initiator and the mode of polymerization are very important to obtain the polymer monoliths with suited pore morphology. The AIBN and DMPAP solutions in AN were used to study their decomposition behavior thermally and photochemically. All the thermal decompositions were done at ~70°C and the UV-initiated decompositions were done at room temperature and at a UV-intensity of 4.3 ± 0.2 mW/cm^2. The thermal decomposition of AIBN follows the first order kinetics while UV-initiated decomposition of AIBN & DMPAP follows initially the zero order and then the first order kinetics. The thermal-decomposition of AIBN and UV-decomposition of both AIBN and DMPAP were studied as a function of time. The experimental conditions and the rate constants for zero order (k_0) and for first order (k_1) reactions with experimental half life values are detailed in Table 1. Under present conditions for thermal

decomposition, AIBN has a half life of 5.5 hrs which is quite in agreement with half life from the literature. AIBN has a half-life of 74 hours at 50°C, 4.8 hours at 70°C, and 7.2 minutes at 100°C [102,103].

Table 4.1. Experimental conditions and reaction rate constants for the decomposition of initiators, AIBN and DMPAP.

Initiator	**Concentration**	**Mode of Polymerization**	**Results**
AIBN	0.0455 mol/L (1.5% of Wt. of monomers)	Thermal, Temp.: ~ 70°C,	$k_1 = 3.5*10^{-5}$ sec^{-1} $t_{1/2} = 5.5$ hrs.
AIBN	0.0455 mol/L (1.5% of Wt. of monomers)	UV, 4.3 ± 0.2 mW/cm^2 Room temperature	$k_0 = 5*10^{-6}$ mol/L.sec $k_1 = 3.65*10^{-}5$ sec^{-1} $t_{1/2} = 1.27$ hrs.
DMPAP	0.0195 mol/L (1.0% of Wt. of monomers)	UV, 4.3 ± 0.2 mW/cm^2 Room temperature	$k_0 = 2.16*10^{-5}$ mol/L.sec $k_1 = 1.43*10^{-3}$ sec^{-1} $t_{1/2} = 7.5$ min.

A UV-initiated decomposition is much faster than thermal decomposition because the reaction kinetics initially depends upon the light intensity. From the figure 4.1, DMPAP decomposes initially with time and irrespective of the concentration and then a plateau showed decomposition depend upon the concentration. Almost 90% of DMPAP was decomposed in first 20 minutes of irradiation. Consequently most of the preparation had been performed at higher UV-intensities (35 ± 5 mW/cm^2) in order to make sure the complete monomer conversions. While the AIBN decomposed only about 60% and 20% of its original concentration during UV- and thermal-decomposition for 100 minutes respectively (cf. Figure 4.1).

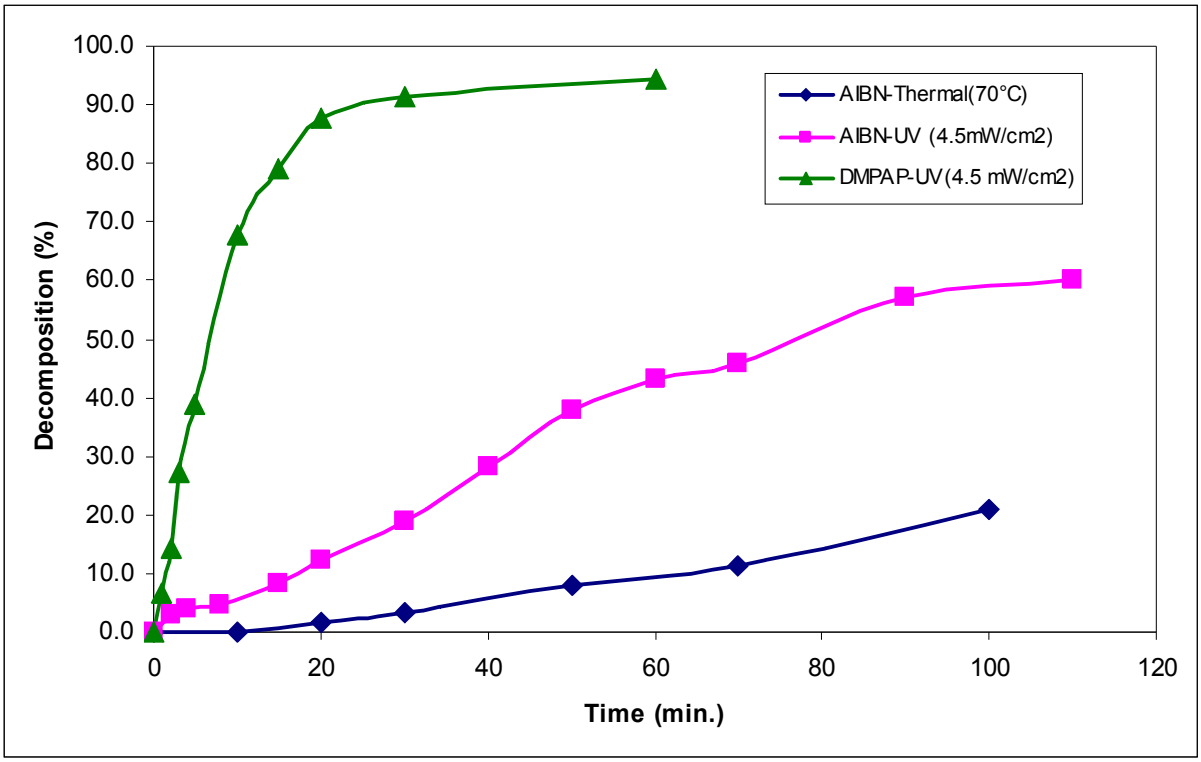

Figure 4.1. Decomposition of initiators, AIBN and DMPAP, as a function of time.

Polymerization with complete monomer conversion depends upon the mode of polymerization and the decomposition of initiator. The UV-initiated polymerization provides the fast decomposition of DMPAP to generate an increased number of free radicals which would be responsible for the fast initiation and increased number of growing chains. Hence by using DMPAP as photoinitiator a polymerization with complete monomer conversion can be achieved even at low radiation power which is in agreement with the results obtained in a similar study [104].

General Properties

It was observed gravimetrically that the weights inside the sample vessels remained constant during the course of polymerization. The selected reaction conditions lead to the formation of opaque monoliths of about the same volume compared to the initial reaction mixture; semi-quantitative analysis of the washing and extraction steps indicated almost complete monomer conversion. The polymeric monoliths were analyzed for wet porosity (57.5 ± 1.4%), pore volume (1.11 ± 0.02 mL/g) and volumetric swelling (23 ± 1.4%) in AN. The data are typical for materials obtained from the same monomers under similar conditions [44]. Irrespective the high content of crosslinker monomer (EDMA), the swelling upon solvent uptake from dry state (and vice versa) was considerably high.

Cross-sectional Morphology of Polymer Monoliths

The cross-sectional morphologies from SEM for the bulk polymeric monoliths which were prepared from different monomers and under different polymerization conditions (cf. Table 3.1 and 3.2) are shown in Figure 4.2. The both *poly(MMA-co-EDMA)* based monoliths BM-MMA-T and BM-MMA-UV which were prepared from thermally- and UV-initiated polymerization, respectively, have the homogeneous pore structure (see figure 4.2a and b). The material in figure 4.2a is composed of comparatively larger polymeric globules and hence larger voids between them than the material in figure 4.2b. In case of *poly(MAA-co-EDMA)* based material, both monoliths, BM-MAA-T and BM-MAA-UV have the homogeneous pore structure (see figure 4.2c and d). The material in figure 4.2c which was prepared by thermal polymerization contains much larger polymeric globules and hence larger voids between them than the materials which were prepared from UV-initiated polymerization (cf. Figure 4.2d).

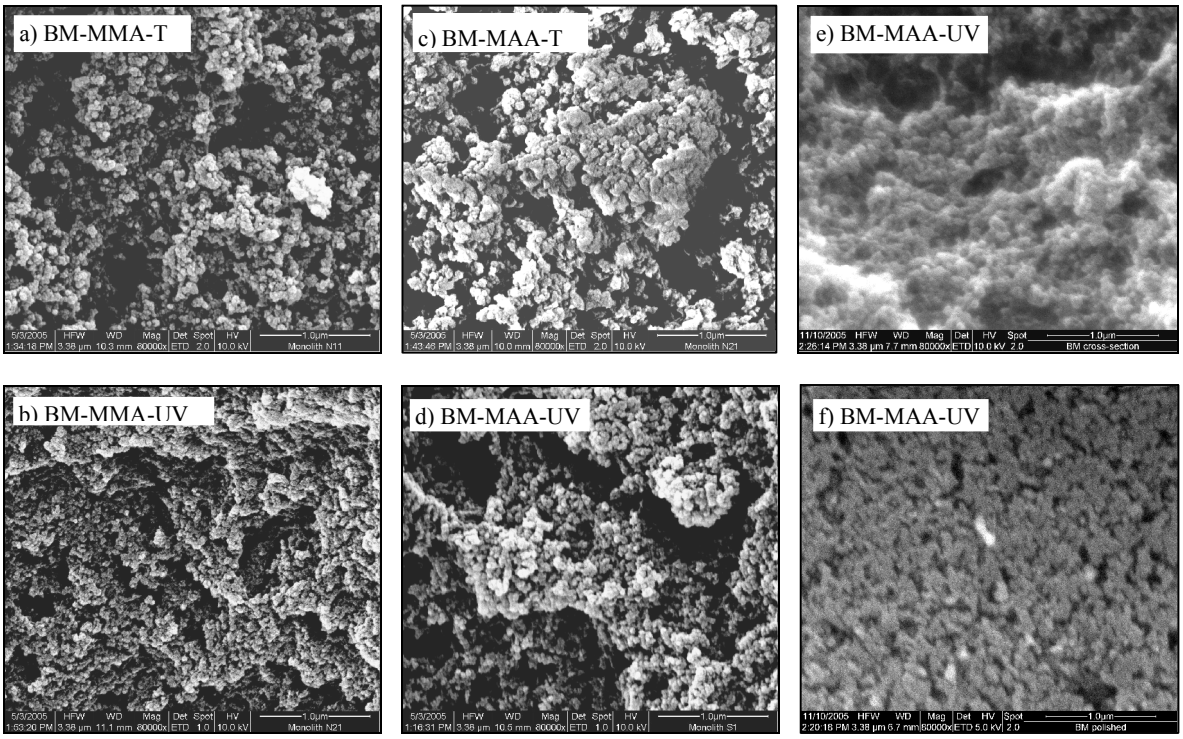

Figure 4.2. SEM images of the cross-section of *poly(MMA-co-EDMA)* based monoliths prepared via (a) thermal polymerization at ~70°C and (b) UV-polymerization at 4.3 ± 0.2 mW/cm^2 and *poly(MAA-co-EDMA)* based monoliths prepared via (c) thermal polymerization at 70°C, (d) UV-polymerization at 4.3 ± 0.2, (e) UV-polymerization at 35 ± 5 mW/cm^2 respectively; the samples were prepared by breaking the large monoliths and (f) view of outer surface at interface with the mold of the same *poly(MAA-co-EDMA)* based monolith given in figure (e).

Both cross-sectional and outer surface views reflect the homogeneous with few macropores and porous polymer monoliths which were prepared from UV-initiated polymerization at 35 ± 5 mW/cm^2 (Figure 4.2e and f). The findings from SEM images were also fully supported by the data obtained from pore structure studies by nitrogen adsorption (cf. Table 4.2 below). All the polymeric materials which were prepared by in situ UV-polymerization had a more homogeneous pore structure composed of small polymeric globules and revealing only a few

macropores. Such morphology is typical for materials obtained under similar synthesis conditions [44,105]. The porosity is also confirmed by the high specific surface area (cf. Tables 4.2 below).

Pore Structure of Polymer Monoliths

The polymeric monoliths were analyzed by nitrogen adsorption for specific surface area and pore volume determinations. The shape of isotherms resembled "type II" according to IUPAC classification (cf. Figure 4.3) [106].

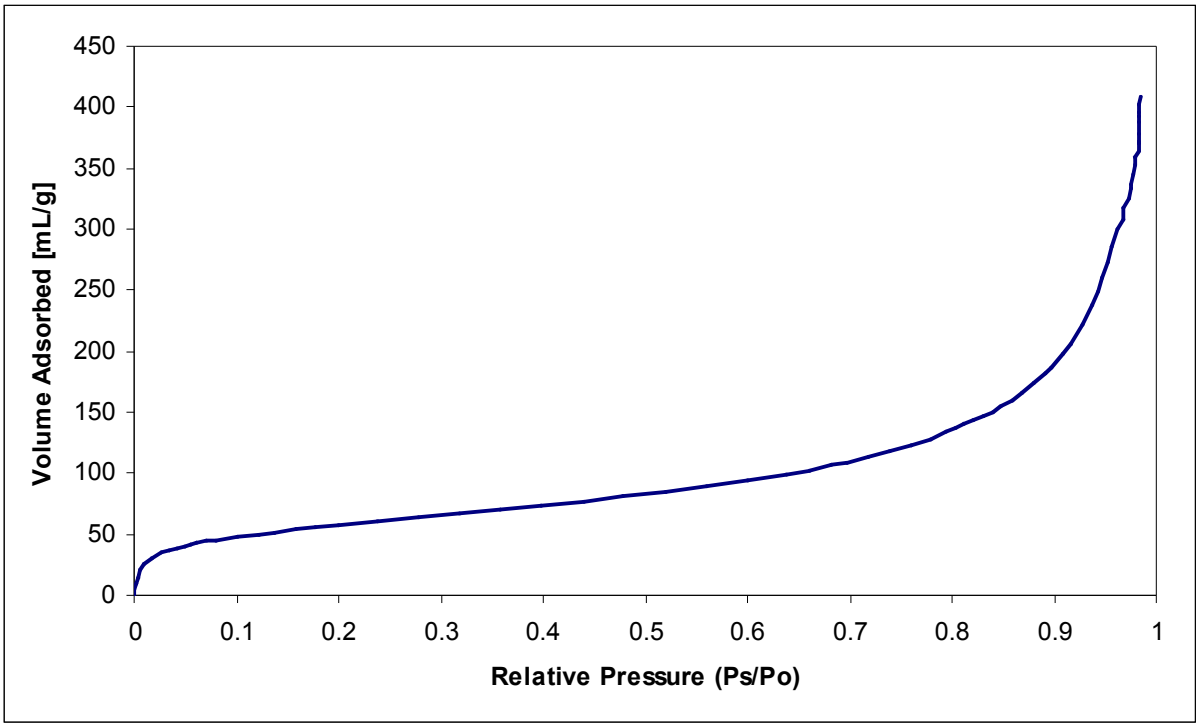

Figure 4.3. A typical BET isotherm for a *poly(MAA-co-EDMA)* based monolith.

The specific surface area data were derived using the BET method and the pore size distribution was obtained by BJH method [106,107]. The properties of the monoliths synthesized by UV- or thermal initiation are shown in Table 4.2).

Table. 4.2. Specific surface area and cumulative pore volume of *poly(MMA-co-EDMA)* and *poly(MAA-co-EDMA)* based bulk monoliths with different diameters. Using this method only the pore volume of the pores having a pore diameter less than ~191 nm can be measured. Here the polymer monoliths were prepared via thermal- or UV-initiated polymerization at 70°C for 24 hours or @ 4.3 ± 0.2 mW/cm^2 for 1 hour, otherwise stated.

Bulk Monolith Type	**Monolith Diameter (mm)**	**Sp. Surface Area (m^2/g)**	**Cumulative pore Volume (mL/g)**
BM-MMA-T	9.0	209 ± 5.9	0.59 ± 0.035
BM-MMA-UV	9.0	375 ± 6.1	0.6 ± 0.01
BM-MAA-T	9.0	111 ± 7.2	0.33 ± 0.026
BM-MAA-UV	9.0	211	0.64
BM-MAA-UV	5.0	217	0.60
	12.0	240	1.58
BM-MAA-UV 35 ± 5 mW/cm^2, 15 min.	5.0	214.5 ± 4.9	0.60 ± 0.01
Powder BM-MAA-UV 35 ± 5 mW/cm^2, 15 min.	(50-100 μm)	210 ± 0.7	0.62 ± 0.01

The *poly(MMA-co-EDMA)* based bulk monolith BM-MMA-UV has much larger specific surface area value (375 ± 6.1 m^2/g) than the polymer monolith BM-MMA-T (209 ± 5.9 m^2/g). Identical results were obtained for the similar materials when prepared under similar conditions (via thermal polymerization) [35]. *The poly(MAA-co-EDMA)* based bulk monolith (BM-MAA-UV) has larger values for both specific surface area and pore volume than the bulk monolith BM-MAA-T (cf. Table 4.2). A complete polymerization of monomers depends upon the

decomposition of initiator and the mode of polymerization. The UV-initiated decomposition of DMPAP causes an increased number of free radicals and therefore a larger number of growing nuclei and globules. The increase in number of nuclei is at the cost of their size. Since the globules obtained are smaller and more numerous, smaller voids are obtained resulting in a shift in the pore size distribution.

The bulk monolith BM-MAA-UV, polymerized in the molds with different diameter sizes were also characterized for specific surface area and pore volume (cf. Table 4.2). The bulk monolith with a diameter of 12 mm had the highest values for the specific surface area and pore volume (cf. Table 4.2). The value is (still) surprising, and it can not be well explained (especially because the cumulative pore volume of registered pore size is up to ~200 nm only).

By looking into the pore volume fractions for various pore size ranges (in nm); it was observed that the monolith with 12 mm diameter has much larger pore volume value for the pores above 80 nm. The monolith with a diameter of 9 mm has larger pore volume value than that of 5 mm diameter monolith (cf. Figure. 4.4). The increase in pore volume with the increase in diameter is due to temperature gradient because of ineffective heat dissipation in the mold during the process of polymerization, which in turn leads to heterogeneous pore structures throughout the monolith. This temperature gradient results in significant difference in the pore size distribution between the center core and the outer shell of the monolith [108]. By decreasing the dimensions of the mold, the monolith with more homogeneous pore structure can be obtained. From figure 4.4, it is clear that the monolith with smallest diameter size (5 mm) has most of the pores in the range of $\leq$ 80 nm which is the prime requirement to get the more suited pore structure for higher specificity and enantioselective separations.

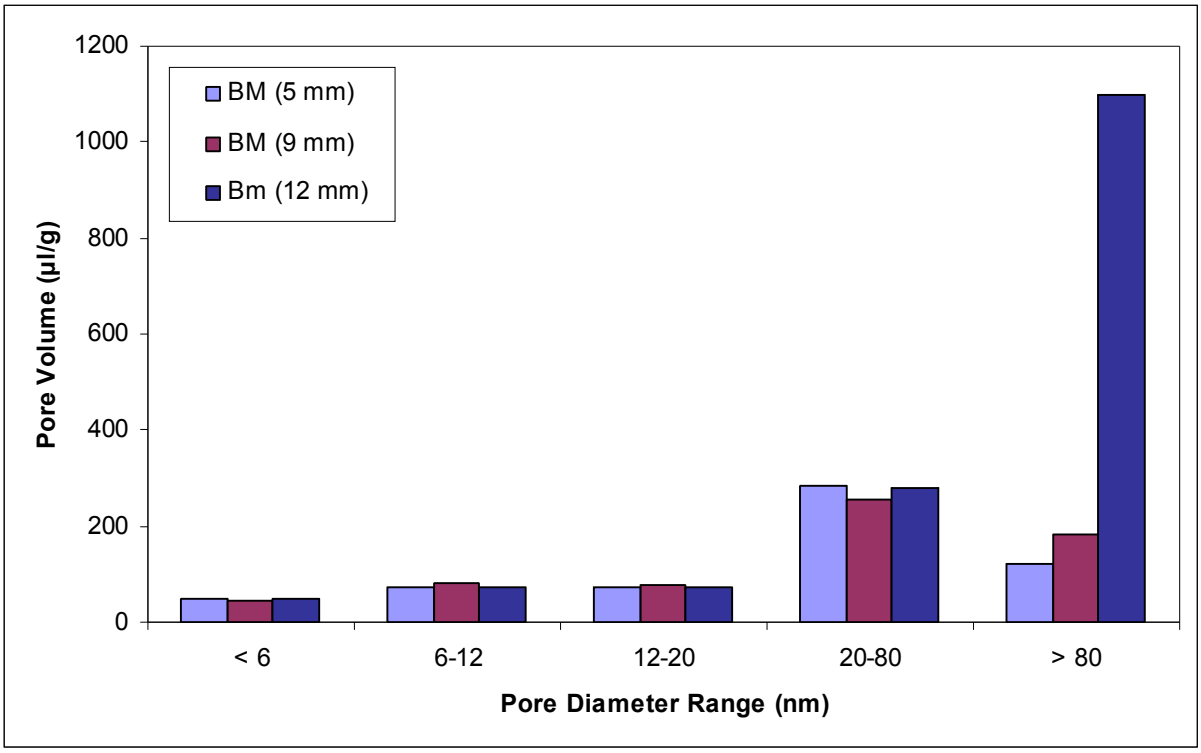

Figure 4.4. Pore volume from the nitrogen adsorption isotherm for *poly(MAA-co-EDMA)* based bulk monoliths "BM-MAA-UV" prepared with different diameter sizes at a UV-intensity of 4.3 ± 0.2 mW/cm^2: fractions of pore volume for various pore size ranges (in nm).

Increase in the polymerization temperature/irradiation power, results in an increase in the volume fraction of the smaller pores [33,30]. The bulk monoliths BM-MAA-UV polymerized at UV-intensity of 35 ± 5 mW/cm^2 for 15 minutes were analyzed for specific surface area and pore volume and results were compared with the monolith having same dimensions but polymerized at 4.3 ± 0.2 mW/cm^2 for one hour (cf. Table 4.2). Although both the monoliths which were prepared from same pre-polymerization mixture but under different polymerization conditions had almost same specific surface area and pore volume values (cf. Table 4.2). By looking into the fractions of pore volume for various pore sizes in nm ranges, there was a significant shift in the pore size distribution in the 20-80 nm and above pore diameter ranges (cf. Figure 4.5). This

can easily be explained by the difference in irradiation power during the process of polymerization. Hence the increase in irradiation power increases the volume fraction of smaller pores present in the polymeric monolith [30]. The values for the powdered (50-100 µm) polymer monolith were identical to that data for the large monolith prepared @ 35 ± 5 mW/cm^2, 15 min.; hence, a reduction in size by more than two orders of magnitude had no significant effect on the (internal) pore structure of the monolith (cf. Table 4.2).

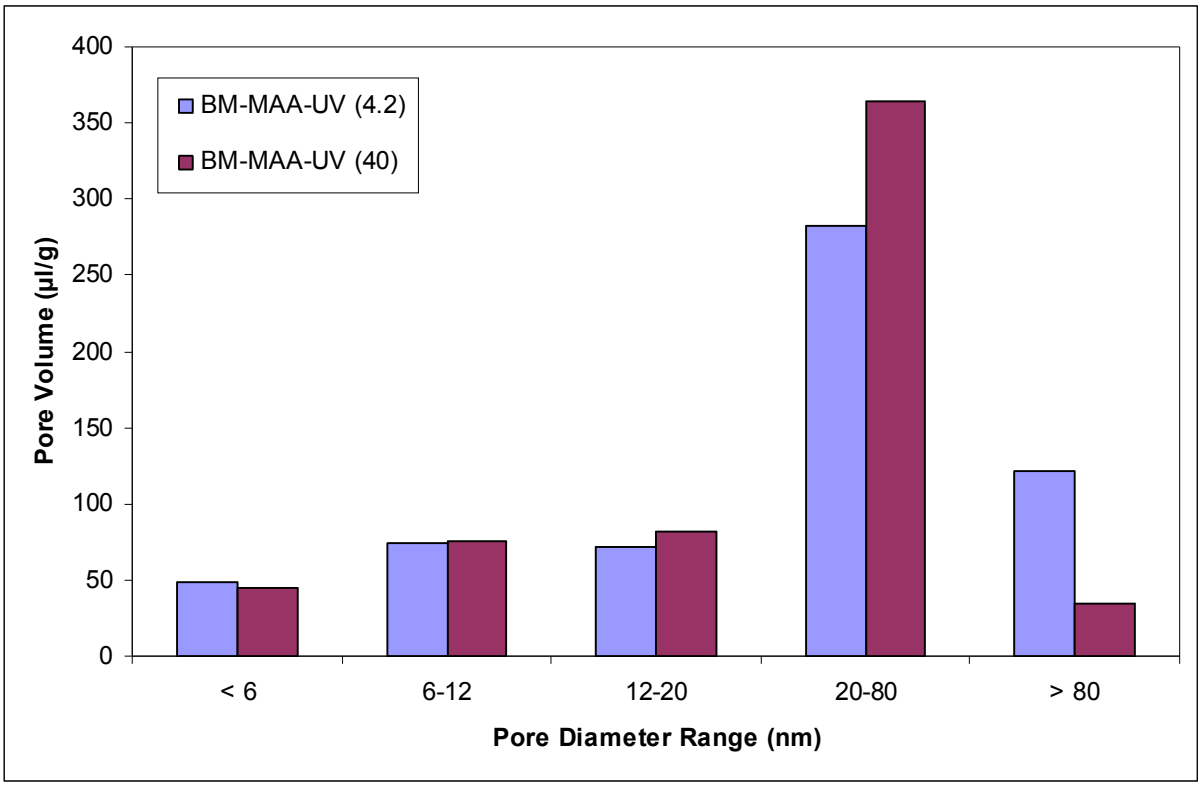

Figure 4.5. Pore volume from the nitrogen adsorption isotherm for bulk monoliths prepared under different polymerization conditions (@ 4.2 & 40 mW/cm^2): fractions of pore volume for various pore size ranges (in nm).

MIP and NIP Polymer Monoliths

After establishing the synthesis conditions for polymer monoliths with suited pore structure i.e. no large macropores and high specific surface area, the MIP and NIP monoliths were prepared from pre-polymerization mixture (cf. Table 3.2) in situ polymerization at UV-intensity of 35 ± 5 mW/cm^2 for 15 minutes.

Both *poly(MAA-co-EDMA)*MIP and NIP monoliths were characterized for specific surface area and cumulative pore volume before and after their excessive washing in AN and drying in vacuum. The specific surface area values before and after exposure of the monoliths to an organic solvent (AN) were identical, indicating the rigidity and stability of the porous crosslinked polymeric structure (cf. Table. 4.3). In this particular study it was also observed that the MIP monoliths had slightly higher specific surface area and cumulative pore volume values than NIP monoliths (cf. Table 4.3).

Table 4.3. BET specific surface area and BJH cumulative pore volume for MIP and NIP poly(MAA-co-EDMA) based monoliths before and after exposure to acetonitrile.

Bulk Monolith Type	**Sp. Surface Area (m^2/g)**	**Cumulative pore Volume (mL/g)**
Before exposure to acetonitrile		
BM-MIP	215	0.62
BM-NIP	198	0.58
After exposure to acetonitrile		
BM-MIP	219	0.62
BM-NIP	193	0.56

4.1.2. Pre-modification and Pore-filling of PP and PET Membranes

The PP microfiltration membranes with a nominal cut-off pore diameter of 0.4 μm and PET track etched membranes with nominal pore diameters of 0.4 and 3.0 μm were used for pre-modification with 25 and 50 g/L of PEGMA in water and the their subsequent functionalization with *poly(MAA-co-EDMA)*. The degree of grafting (relative to the geometric and to the specific surface area) of PP and PET membranes after the pre-modification and the subsequent functionalization steps were determined gravimetrically and results are summarized in Table 4.4 and 4.5 respectively.

Assuming an even coverage of the specific surface area of the membranes with grafted *poly(PEGMA)* and a density of *poly(PEGMA)* of 1.1 g/cm^3, the DG values correspond to an average layer thickness in the dry state of 3.5 nm for PP and 9.1 nm for PET. Previous work with the same base materials and similar grafting methods had revealed that these assumptions are justified [71,91]. After the same photo-grafting conditions i.e. 25 g/L of PEGMA, the DG values for PET were about three times larger (cf. Table 4.4). This can be explained by a lower grafting density achieved by the "photoinitiator entrapping method" as compared with the – less controlled – "photoinitiator adsorption method" [73], and the larger pore volume relative to the pore wall area for the track-etched membrane may also contribute to this difference. The DG values for PET were almost doubled when it was photo-grafted with 50 g/L of PEGMA under the similar polymerization conditions (cf. Table 4.4). For all membranes, the grafted layer thickness was much smaller than the (average) membrane pore radius.

Table 4.4. Degree of grafting after the pre-modification with grafted *poly(PEGMA)* of PP microfiltration and PET track etched membranes (specific surface area (Sp. S.A): for unmodified PP from nitrogen adsorption = 27.6 m^2/g, for unmodified PET with nominal pore diameters of 0.4 and 3.0 µm, calculated from permeability and permporometry data) = 1.81 and 0.245 m^2/g, respectively [91]); average results of minimum three different samples with their standard deviations.

Type	**DG after Pre-modification**	
	Relative to Facial Area ($\mu g/cm^2$)	**Relative to Sp. S.A. ($\mu g/cm^2$)**
PP-25P&F	299 ± 32	0.38 ± 0.04
PET-0.4-25P&F	40 ± 4.7	1.01 ± 0.12
PET-3-25P&F	6.7 ± 1.3	1.09 ± 0.21
PET-3-50P&F	12.43 ± 2.09	2.03 ± 0.34

The porosity of the unmodified PP microfiltration membrane (79 ± 5.3 %) was calculated from the water and ethanol uptake. The thickness decreased from 195 ± 9.6 µm for the unmodified PP membrane to 172 ± 6.7 µm for the composite membrane. One possible reason is that during the functionalization step the membrane was pressed tightly between the two glass plates. However, the slightly reduced sample diameter indicated that the reaction conditions of monolith synthesis may also contribute to the contraction, and this may well be related to the reversible swelling of the monolith (cf. above).

Considering the initial membrane porosity (cf. above) and a pore volume contraction during the polymerization process estimated from the change of membrane thickness (13 ± 1.6 %), the theoretical value for a complete pore filling is 7.71 mg/cm^2 (relative to geometric area). The experimental values for both PP composite membranes were somewhat larger than this theoretical value (cf. Table 4.5). Possible reasons could be an overestimation of the porosity reduction during polymerization and the weight of the very thin (<1 μm) continuous film of porous polymer monolith on both outer surfaces of the composite membranes (cf. "Surface and cross-sectional morphology", below). Overall, the DG data indicate that a complete pore-filling of the porous PP membranes with polymeric monoliths had been achieved. Further, the identical data for the composite membranes, PP membrane functionalized without pre-modification (PP-F) and PP membrane functionalized after pre-modification (PP-25P&F) indicate that the pre-modification has no macroscopic effect on the functionalization with polymeric monoliths.

In case of PET membranes there was no contraction observed after the functionalization step. With the ideal porosity of the isotropic track etched membranes, the theoretical value for the PET membrane with nominal pore diameter of 0.4 μm calculated for complete pore-filling is 428 μg/cm^2 (relative to facial area). This is much less than the experimental value (cf. Table 4.5). Also, in case of PET membranes with nominal pore diameter of 3 μm, the theoretical value for complete pore-filling is 232 μg/cm^2 (relative to facial area), which is much less than the experimental values (cf. Table 4.5). Again, one possible reason could be weight of the continuous film of porous polymer monolith on both sides of the membranes (cf. "Pore characterization of composite membranes", below). However, large "caverns" in the interior of the membrane structure which have no effect onto the pore diameter of the membrane had already been observed in earlier studies using this type of membrane (and can be seen

occasionally also in the cross-section of the membranes used in this work; cf. Fig. 4.8a and b) [69]. Such artifacts will lead to a higher porosity and surface area than expected for the ideal capillary pore structure. This could be another reason for larger degrees of pore-filling.

Table 4.5. Degree of grafting after functionalization with *poly(MAA-co-EDMA)* of PP microfiltration and PET track etched membranes (specific surface area (Sp. S.A): for unmodified PP from nitrogen adsorption = 27.6 m^2/g, for unmodified PET with nominal pore diameters of 0.4 and 3.0 µm, calculated from permeability and permporometry data) = 1.81 and 0.245 m^2/g, respectively [91]); average results of minimum three different samples with their standard deviations.

Type	**DG after Functionalization**	
	Relative to Facial Area (mg/cm^2)	**Relative to Sp. S.A. ($\mu g/cm^2$)**
PP-F	8.43 ± 0.45	10.84 ± 0.58
PP-25P&F	8.51 ± 0.57	10.94 ± 0.73
PET-0.4-25P&F	1.12 ± 0.14	28.3 ± 3.5
PET-3-F	1.02 ± 0.15	166 ± 25
PET-3-25P&F	1.06 ± 0.25	174 ± 41
PET-3-50P&F	1.11 ± 0.20	181 ± 33

Overall, the gravimetric data confirmed that a complete pore filling had also been achieved for all types of PET membranes. Analogous to PP membranes, the almost identical data for the composite membranes, PET membrane functionalized without pre-modification (PET-F) and

PET membrane functionalized after pre-modification (PET-25P&F and PET-50P&F) indicate that the pre-modification has no macroscopic effect on the functionalization with polymeric monoliths.

Both PP and PET composite membranes functionalized with and without pre-modification step were characterized for solvent uptake (pore volume) using acetonitrile. The PP membranes had larger values for solvent uptake than the PET membranes (cf. Figure 4.6).

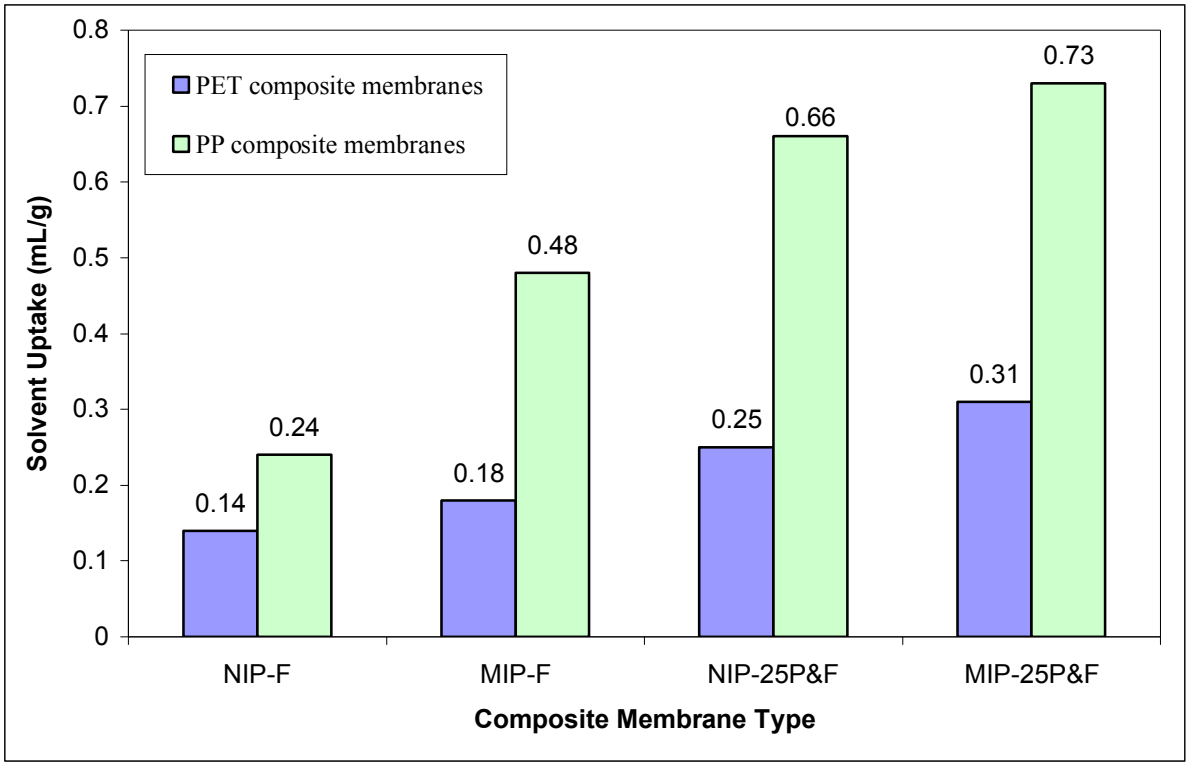

Figure 4.6. Solvent uptake (pore volume) of MIP and NIP *poly(MAA-co-EDMA)* monolith based PP and PET composite membranes, prepared with and without pre-modification.

The solvent uptake increases with the increase in the monolith thickness from PET to PP composite membranes. However these values were significantly lower than the value obtained for bulk monolith (1.11 ± 0.02 mL/g). The composite membranes pre-modified with PEGMA

had larger solvent uptake values than the composite membranes which were prepared without pre-modification. The possible reason could be the swelling of thin grafted *poly(PEGMA)* layer which is well compatible with most of the organic solvents. In addition, in all cases, MIP composite membranes imprinted with Boc-D-PhA had shown larger pore volume values than the respective NIP composite membranes. The imprinting effect seems to improve the porosity due to formation of inter-connected pores within the polymer materials.

4.1.3. Pore Characterization of PP and PET based Composite Membranes

The composite membranes prepared from PP microfiltration and PET track etched membranes with their nominal pore diameter of 0.4 μm after pore-filled functionalization (*poly(MAA-co-EDMA)*) with and without pre-modification were used for their pore characterization. The characterization of the composites membranes was mainly done by SEM and by gas adsorption method.

Surface and Cross-sectional Morphology

Typical cross-sectional morphologies for unmodified PP membranes and the PP monolith composites obtained without and with pre-modification are shown in Fig. 4.7, more details for pore-filled PP membranes are presented in Fig. 4.8. The SEM images of PP-F and PP-25P&F membranes confirm the homogeneous porous polymeric monolith in the membrane pores (cf. Fig. 4.7b and c, Fig. 4.8b) and also as a thin (<1 μm) continuous film with homogeneous pore structure on the outer membrane surface (cf. Fig. 4.8). Also, the entire membrane thickness seemed to be evenly functionalized (cf. Fig. 4.8b), and this supports the conclusion based on the

DG values that a complete pore filling had been achieved (cf. "Pre-modification and pore-filling of PP and PET membranes", above). However, in case of PP-F, the polymeric monolith was not

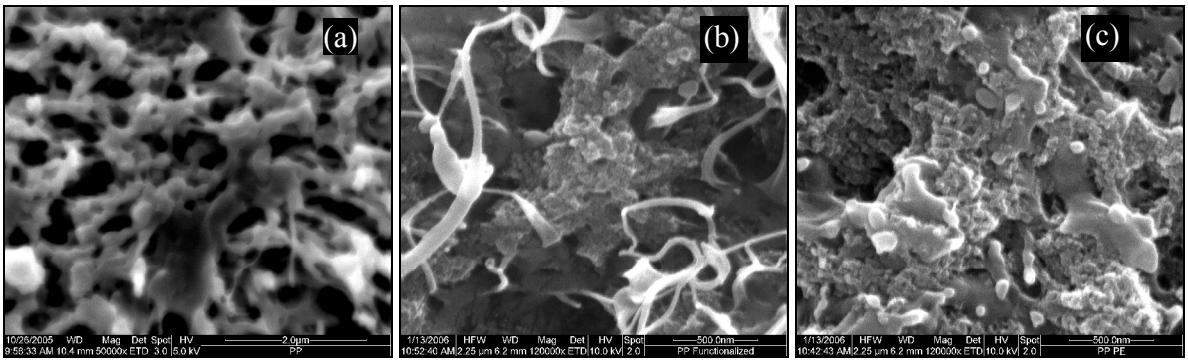

Figure 4.7. SEM images of the cross-section of PP membranes. (a) original PP membrane, (b) *poly(MAA-co-EDMA)* monolith PP composite membrane, prepared with out pre-modification, and (c) *poly(MAA-co-EDMA)* monolith PP composite membrane, prepared with pre-modification, respectively.

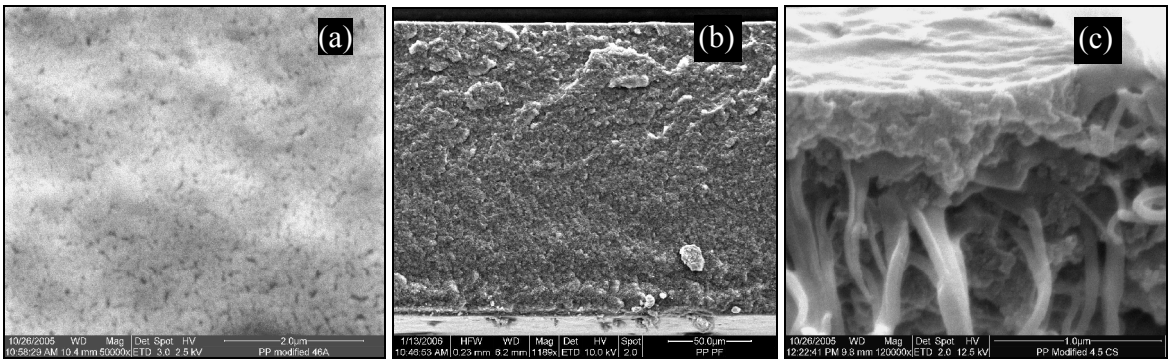

Figure 4.8. SEM images of a *poly(MAA-co-EDMA)* monolith PP composite membrane. (a) porous outer surface, (b) full cross-sectional view of the PP composite membrane with a thin top layer of polymer monolith and (c) magnified view of the thin top layer (thickness <1 μm).

well adhering to the PP matrix, voids were clearly seen between the fibers forming the pore walls and the monolith (cf. Fig. 4.7b). This resembles observations made for syntheses of polymeric monoliths in polymeric microfluidic channels [89]. In case of PP-P&F, the monolith was tightly

connected to PP membrane structure without voids between the two polymers. The polymer monolith has a better compatibility with the pore walls after the pre-modification step, yielding a much more even pore-filling (cf. Fig. 4.7c).

Cross-sections of PET track etched membranes with nominal pore diameter of 0.4 µm, functionalized with *poly(MAA-co-EDMA)* without pre-modification step revealed that the cylindrical pores had been filled with rod-shaped polymeric monoliths, and additional layers on both outer surfaces could be identified as well (Fig. 4.9a). However, a closer inspection (see Fig. 4.9b) revealed that there was no adhesion of the polymeric "nano-monolith rods" to the pore walls of the PET membrane, because the monoliths were either missing (see left part of the figure) or there was a gap between monolith and pore wall (see right part of the figure).

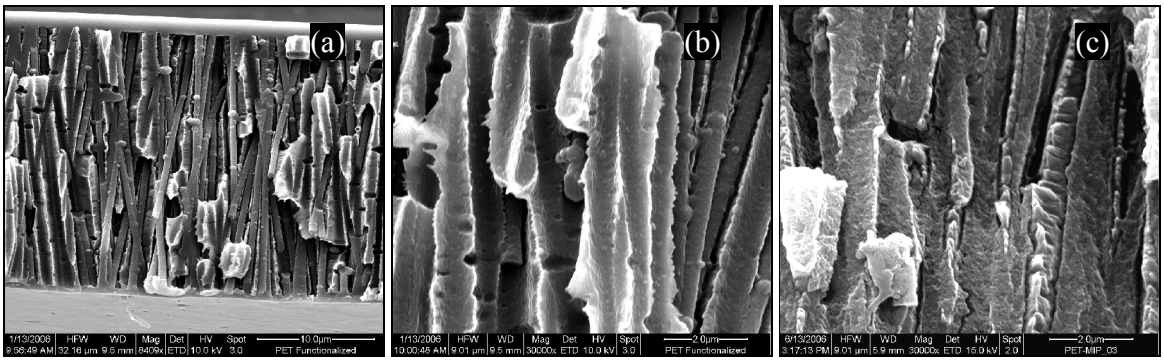

Figure 4.9. SEM images of the cross-section of track etched PET membranes. (a) *poly(MAA-co-EDMA)* monolith PET composite membrane, prepared with out pre-modification, (b) same sample as (a), but other location at larger magnification, (c) *poly(MAA-co-EDMA)* monolith PP composite membrane, prepared with pre-modification, same magnification as (b).

The loss of the "nano-monolith rods" from the pores can be easily explained because the samples had been prepared by breaking the membranes. In contrast, in case of PET membrane functionalized after pre-modification (PET-25P&F), the polymer monoliths were evenly and

tightly attached to the PET pore walls (Fig. 4.9c). Obviously, during breaking the membrane, the monoliths were also broken, and no detachment or voids between the two polymers could be seen. Hence a very clear and pronounced effect of the pre-modification step, a largely improved adhesion, could be identified for the two composite materials with otherwise identical preparation and DG value.

Overall, a better compatibility of the polymeric monoliths with the pore walls after the pre-modification step was confirmed in case of both PP and PET membranes. Due to the much more regular pore structure, the effect was more clearly identified for the track-etched PET membranes. The improved adhesion of the polymeric monoliths to the two different membrane polymers can be well explained with an even functionalization of the entire pore surface with a thin grafted *poly(PEGMA)* layer which is well compatible with the polyacrylate based monolith.

Pore Structure from Gas-Adsorption Isotherms

The PP-based composite membranes were analyzed by nitrogen adsorption and the respective data for porous polymeric monoliths was used for comparison. Only PP-based composite membranes had been studied because – due to larger porosity and membrane thickness – the effects were much easier to analyze than for the PET membranes. The shape of the isotherms resembled “type II” according to IUPAC classification (cf. Figure 4.3) [106]. Hence, the pore volume was mainly determined by meso- and smaller macro-pores. The specific surface area data were derived using the BET method and the pore size distribution was obtained by using the BJH method (cf. Table 4.6) [106,107]. The pore size distribution data in the range which could be analyzed under the experimental conditions are summarized in Fig. 4.10.

Table 4.6. BET specific surface area and BJH cumulative pore volume for bulk (diameter 5 mm) and powder (size 50-100 μm) polymer monolith, un-modified and functionalized PP membranes, average results of minimum two different samples with their standard deviations, for PP-unmodified results of one measurement. All these preparations were carried out at UV-intensity of 35 ± 5 mW/cm^2 with the exception of PP membrane unmodified.

Bulk Monolith Type	**Sp. Surface Area (m^2/g)**	**Cumulative pore Volume (mL/g)**
Bulk Monolith	214.5 ± 4.9	0.60 ± 0.01
PP membrane unmodified	27.6	0.08
PP-F	87 ± 1.4	0.16 ± 0.01
PP-25P&F	97.2 ± 3.2	0.21 ± 0.02

The highest values for surface area and pore volume were observed for the bulk polymeric monolith. The accumulated pore volume from nitrogen adsorption was smaller than the total pore volume (cf. "Development of synthesis conditions for polymer monoliths", above). This can easily be explained by the fraction of larger pores in the porous polymeric monolith (cf. Fig. 4.2e and 4.2f) and the incapability of the method to measure the pore volume of the pores having a pore diameter larger than ~191 nm. The surface area and pore volume values for the composite membranes were much lower than for the bulk monoliths but also much larger than the data for the unmodified PP membrane (cf. Table 4.6).

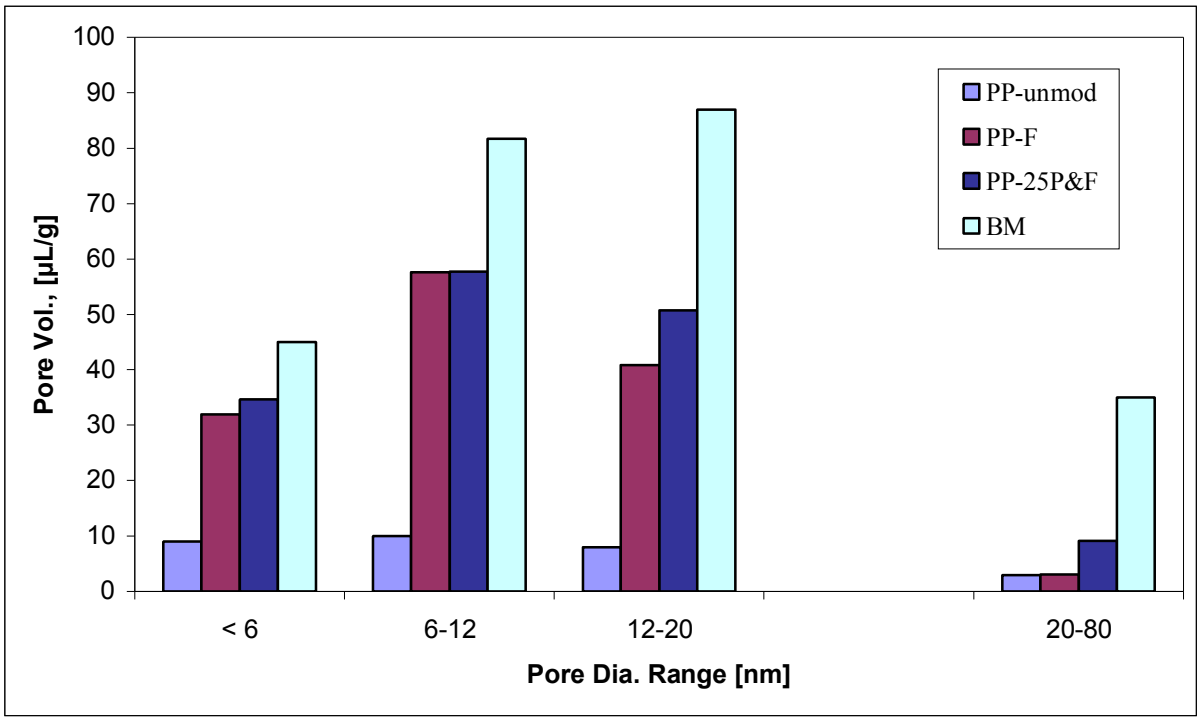

Figure 4.10. Pore volume from nitrogen adsorption isotherm for PP membranes (data for bulk monolith "BM" for comparison): fractions of pore volume for various pore-size ranges (in nm). Note that the values for the pore size fraction 20-80 nm have been reduced on the y-scale by a factor of 10.

However, the membranes PP-25P&F had significantly larger specific surface area and pore volume values than the membranes PP-F. Analogous trends were seen for the pore volume distributions (cf. Fig. 4.10). In particular, membranes PP-25P&F had for all pore fractions a larger pore volume than membranes PP-F, and a pronounced maximum shift to larger pore sizes was observed for PP-25P&F relative to PP-F. This indicates that the pre-modification contributed to a larger content of pores in the meso- to macro-pore range (20-80 nm). The pore volumes were significantly lower than for the bulk monolith, but the shape of the pore size

distribution for the composite materials prepared with pre-modification was more similar to the one for the bulk monolith than without pre-modification.

Considering the membrane porosity as well as the observed slight shrinkage and related decrease in porosity during functionalization (cf. above), the theoretical value for the specific surface area of a PP membrane where the entire pore volume is filled with polymer having the pore structure of a large bulk monolith should be ~145 m^2/g. This estimate is significantly larger than the experimental values (cf. Table 4.6). These differences in pore structure between large (mm scale) and small (nm scale) monoliths could be due to different structural heterogeneity. On the one hand, it could be speculated that UV initiation of the polymerization could be more even for the very thin (~195 μm) membranes when compared with the large bulk polymer materials (diameter 7 mm, height 40 mm). On the other hand, the membranes have a wide pore size distribution, and incomplete filling of smaller membrane pores during polymerization as well as shrinkage of monolith could cause disturbed monolith morphology as compared to the large samples. Nevertheless, the pre-modification of the pore walls seems to reduce the undesired consequences of those problems.

For pre-modification, a UV-initiated ”grafting-from” functionalization of the entire membrane surface with *poly(PEGMA)* was chosen to enhance the non-covalent interactions and to avoid the formation of voids between the polymer monoliths and the pore walls during the subsequent functionalization of the monolithic *poly(MAA-co-EDMA)* in the membrane pores (cf. Figure 4.11). From SEM and pore characterization studies, a better compatibility of the polymeric monoliths with the pore walls after the pre-modification step was confirmed in case of both PP and PET membranes.

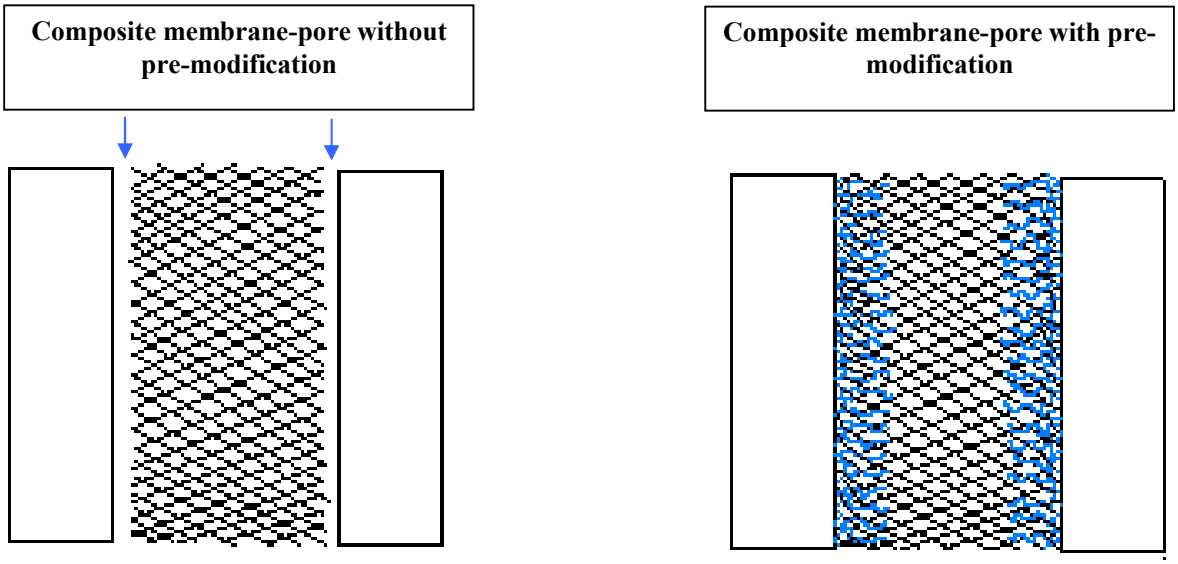

Figure 4.11. Schematic illustration of the effect of pre-modification in membrane pores.

4.1.4. Pore-filling Functionalization of Anodisc Alumina Membranes

In order to attain permselective transport, the more rigid and inert inorganic (alumina) membranes with higher porosities (~50 %) would be a more suitable alternate for PET base membranes (cf. Figure 4.12a and b). Although alumina membranes are thicker (~65 µm) than PET membranes (~23 µm) but the higher porosity of the former material would be advantageous to use these membranes as base material to synthesize *poly(MAA-co-EDMA)* monolith based composite membranes (cf. Figure 4.13a) for enantio-selective separation under diffusion (dialysis) and electrodialysis conditions. A magnified SEM image confirms the complete filling of the alumina membrane pore with porous polymer materials having pore diameters <100 nm (cf. Figure 4.13b). A porous alumina membrane with additional porosities of porous pore-filled polymer would be a very promising composite material for enantioselective transport with high throughput properties.

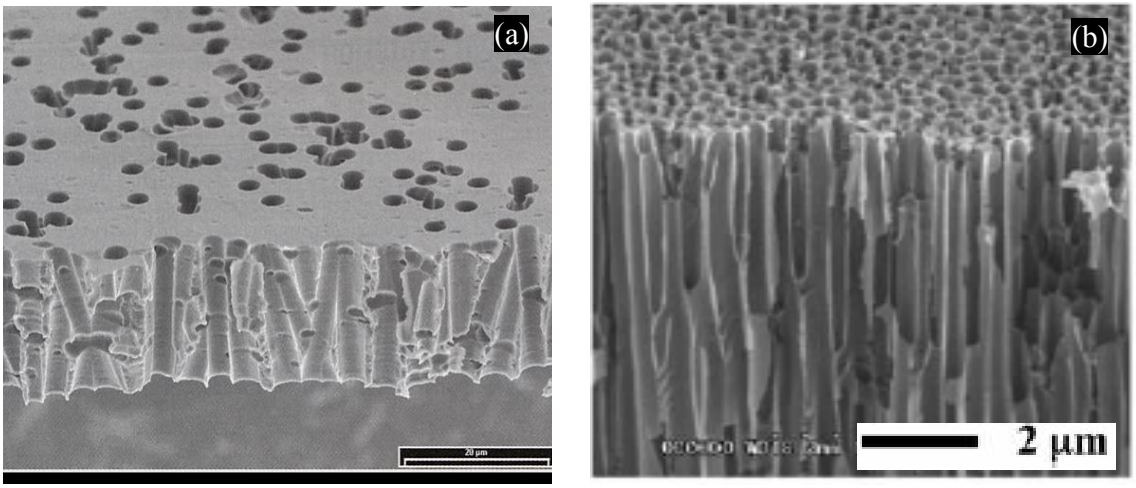

Figure 4.12. SEM images of cross-section cum top views of (a) PET track etched membrane and (b) inorganic alumina membrane "Anodisc".

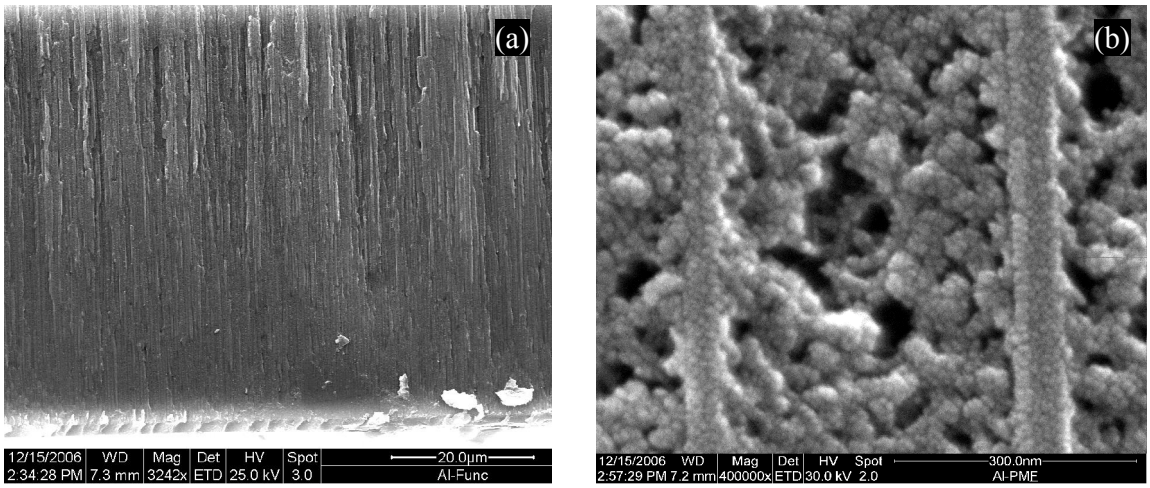

Figure 4.13. SEM images of cross-section of Anodisc alumina membranes with a nominal pore diameter of 0.2 µm. (a) full cross-sectional view of *poly(MAA-co-EDMA)* monolith composite membrane and (b) magnified view of a pore of *poly(MAA-co-EDMA)* monolith composite membrane.

4.2. Equilibrium Binding and Enantioselectivity

For equilibrium binding studies, all the MIP and NIP monoliths (diameter 5 mm) and monolith-filled PP and PET composite membranes with and without pre-modification were prepared by in situ polymerization at UV-intensity of 35 ± 5 mW/cm^2 for 15 minutes. For composite membranes, the PP microfiltration membrane with nominal cut-off pore diameter of 0.4 μm and PET track etched membranes with nominal pore diameter of 3 μm were used as base materials.

4.2.1. Equilibrium Binding and Enantioselectivity of MIP Monoliths

The MIP *poly(MAA-co-EDMA)* based polymer monolith imprinted with Boc-D-PhA were analyzed for their binding isotherms and the enantioselectivity for the imprint molecule (Boc-D-PhA) in the racemic mixture of Boc-D-PhA and Boc-L-PhA and NIP monoliths (without imprint) were used for control experiments. The NIP monoliths adsorbed both Boc-D-PhA and Boc-L-PhA in almost equal amounts at different equilibrium concentrations of the racemic mixture and, hence, did not show specificity for the template molecule in the racemic mixture (Figure 4.14a). The amount adsorbed by the NIP monolith increased with the increase in the equilibrium concentrations. The maximum amounts of Boc-D-PhA and Boc-L-PhA adsorbed by the NIP monolith at ~0.35 mmol/L solution concentration were ~0.49 μmol/g. However, when considering the shape of the isotherms, a complete saturation of the adsorber materials had not been achieved in the studied concentration range.

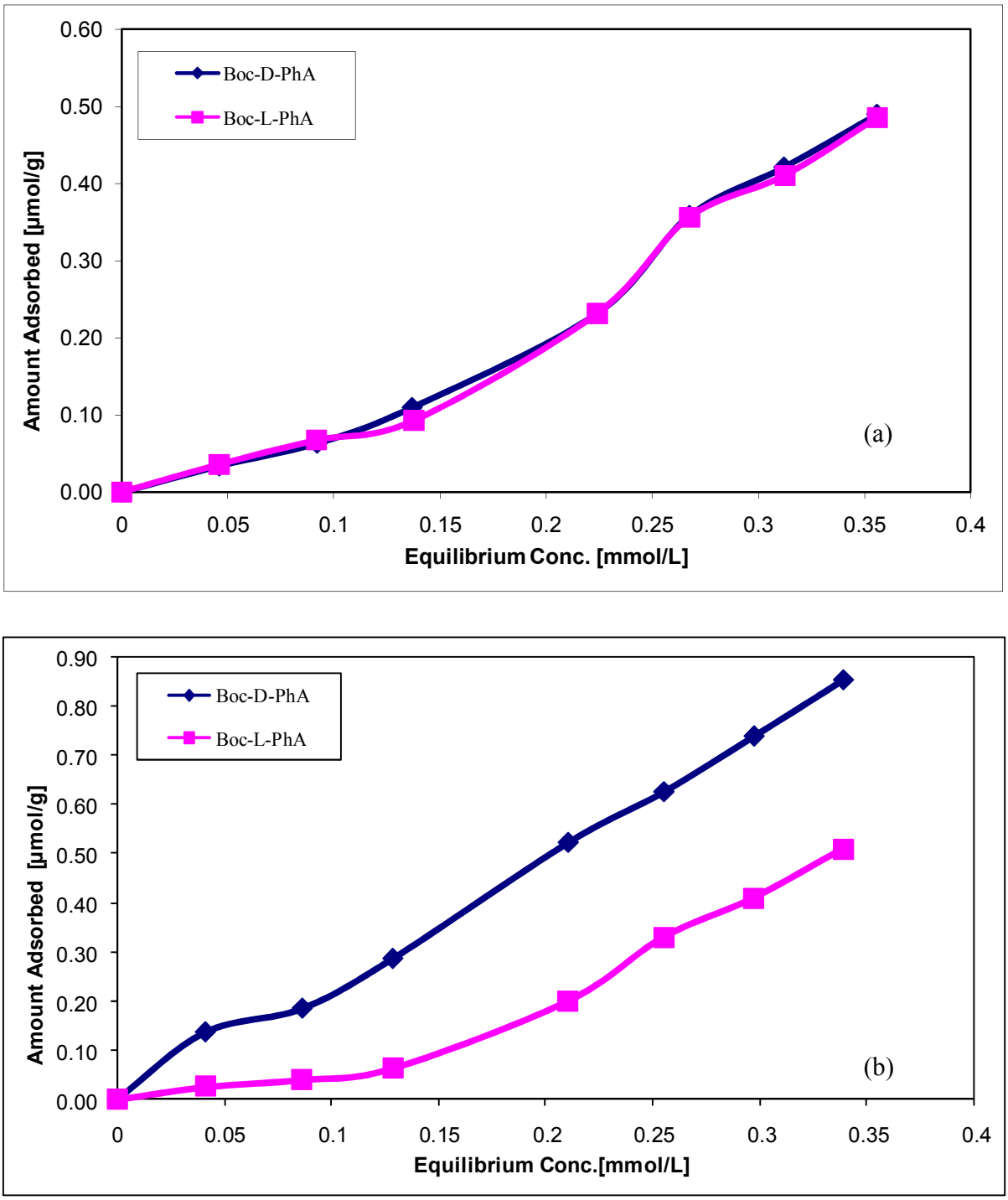

Figure 4.14. Adsorption isotherms for *poly(MAA-co-EDMA)* based monoliths measured with enantiomeric mixtures (Boc-DL-PhA) of different concentrations after 24 hours of adsorption, a) NIP monolith and b) MIP monolith.

The MIP (Boc-D-PhA) monolith adsorbed the template Boc-D-PhA in significantly higher amounts as compared to its counterpart Boc-L-PhA in the racemic mixture at all equilibrium concentrations (Figure 4.14b). The maximum amounts of Boc-D-PhA and Boc-L-PhA, adsorbed by the MIP monolith at ~0.35 mmol/L solution concentration were ~0.85 and ~0.50 μmol/g, respectively. Related to this imprinting effect the MIP monolith has shown higher overall binding capacity as compared to NIP monolith. However, significant non-specific binding was also observed. A possible reason could be the structure of the monoliths with non-specific binding sites, for example carboxylic groups of MAA which are not part of the ("concave") imprinted site [44].

Consequently, MIP monoliths have shown a significant enantioselectivity as was clear from the high values of separation factor α (adsorbed amount of Boc-D-PhA divided by the adsorbed amount of Boc-L-PhA at the same equilibrium concentration) at all equilibrium concentrations while the NIP monolith has shown no enantioselectivity as indicated by the separation factor value of almost one for all equilibrium concentrations (Figure 4.15).

The separation factor value tends to decrease systematically with increasing equilibrium concentration. At low equilibrium concentration, the imprinted sites with high affinity (for the template) are available to a relatively low number of template molecules and their counterparts. Consequently, the template molecules will fill these imprinted cavities first. Non-specific binding sites with lower affinity will only be occupied (by both enantiomers) at higher concentrations, i.e. driving force for adsorption. Therefore, selectivity tends to decrease upon increasing racemate concentration, because an increasing number of molecules are competing for the limited number of imprinted sites.

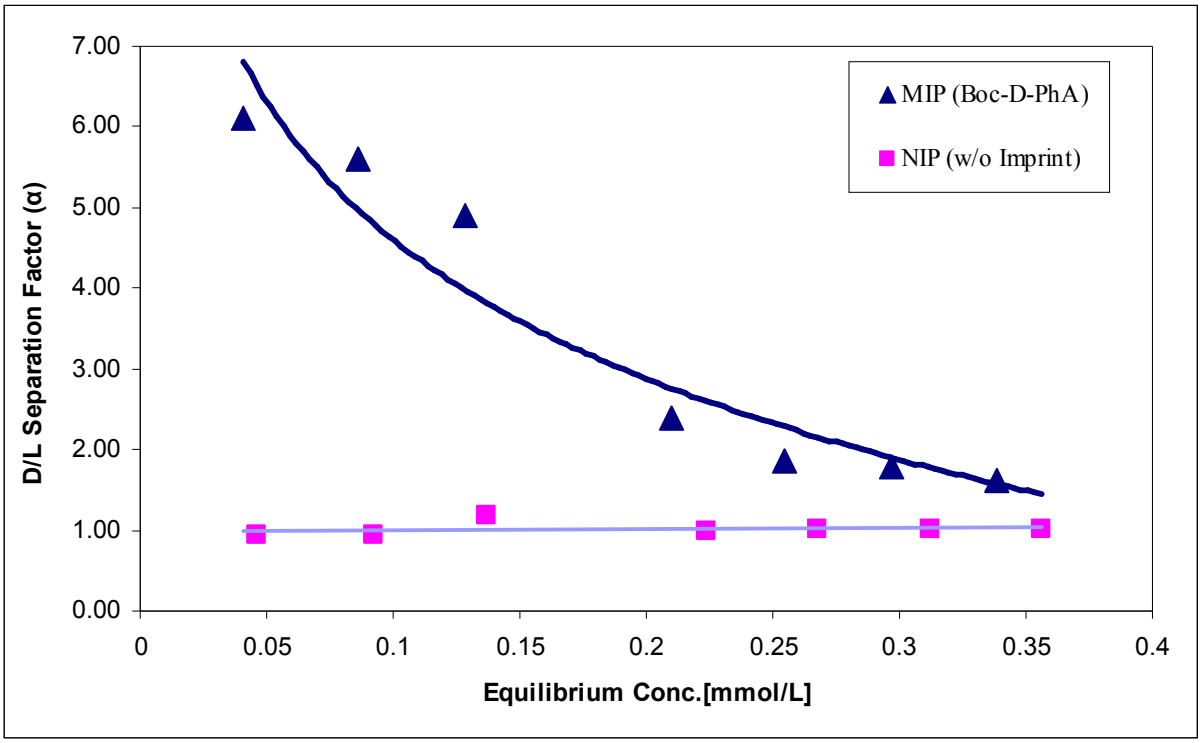

Figure 4.15. Enantioselectivity of MIP and NIP *poly(MAA-co-EDMA)* monoliths at different equilibrium concentrations after 24 hours.

Effect of Time on Equilibrium Binding and Enantioselectivity of Polymeric Monoliths

Both MIP and NIP *poly(MAA-co-EDMA)* monoliths were also analyzed for their binding isotherms and the enantioselectivity for the imprint molecule (Boc-D-PhA) in the racemic mixture of Boc-D-PhA and Boc-L-PhA with respect to time to attain the maximum adsorption capacity (Figure 4.16). The NIP monoliths adsorbed both Boc-D-PhA and Boc-L-PhA in almost equal amounts at different equilibrium concentrations of the racemic mixture and, hence, did not show specificity for the template molecule in the racemic mixture (Figure 4.17). However, overall binding capacity of NIP monolith was increased with the increase in the time for

adsorption (cf. figure 4.16). The maximum amounts of enantiomers adsorbed by the NIP monolith after 24 and 96 hours were ~1.01 and 1.35 µmol/g, respectively.

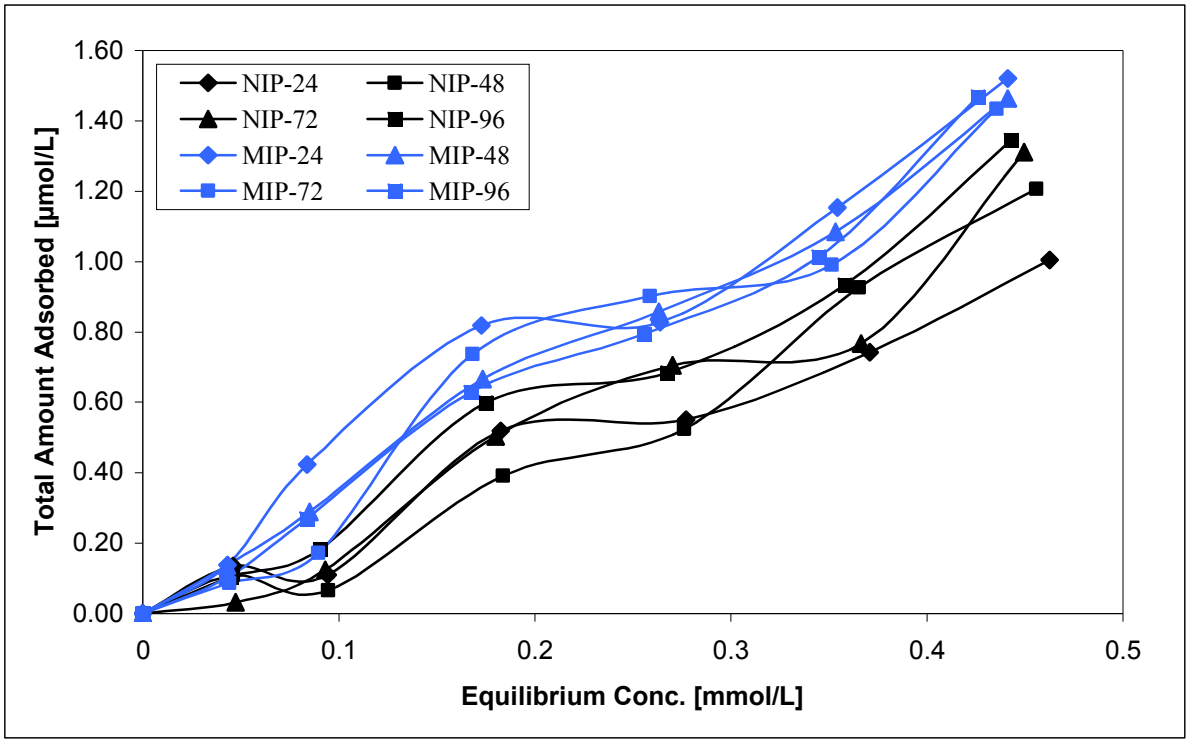

Figure 4.16. Total amount of racemic mixtures adsorbed by the *poly(MAA-co-EDMA)* based MIP and NIP monoliths at different equilibrium concentrations w.r.t. time.

Again the MIP (Boc-D-PhA) monolith adsorbed the template Boc-D-PhA in significantly higher amounts as compared to its counterpart Boc-L-PhA in the racemic mixture at all equilibrium concentrations and hence has shown a significant specificity for the template molecules in the racemic mixtures, as clear from the high values of separation factor (Figure 4.17). Related to this imprinting effect the MIP monolith has shown higher overall binding capacity as compared to NIP monolith. However, there was not a clear difference in the total

binding capacity of MIP monoliths with the increase in the adsorption time, especially at the highest equilibrium concentration (cf. figure 4.16).

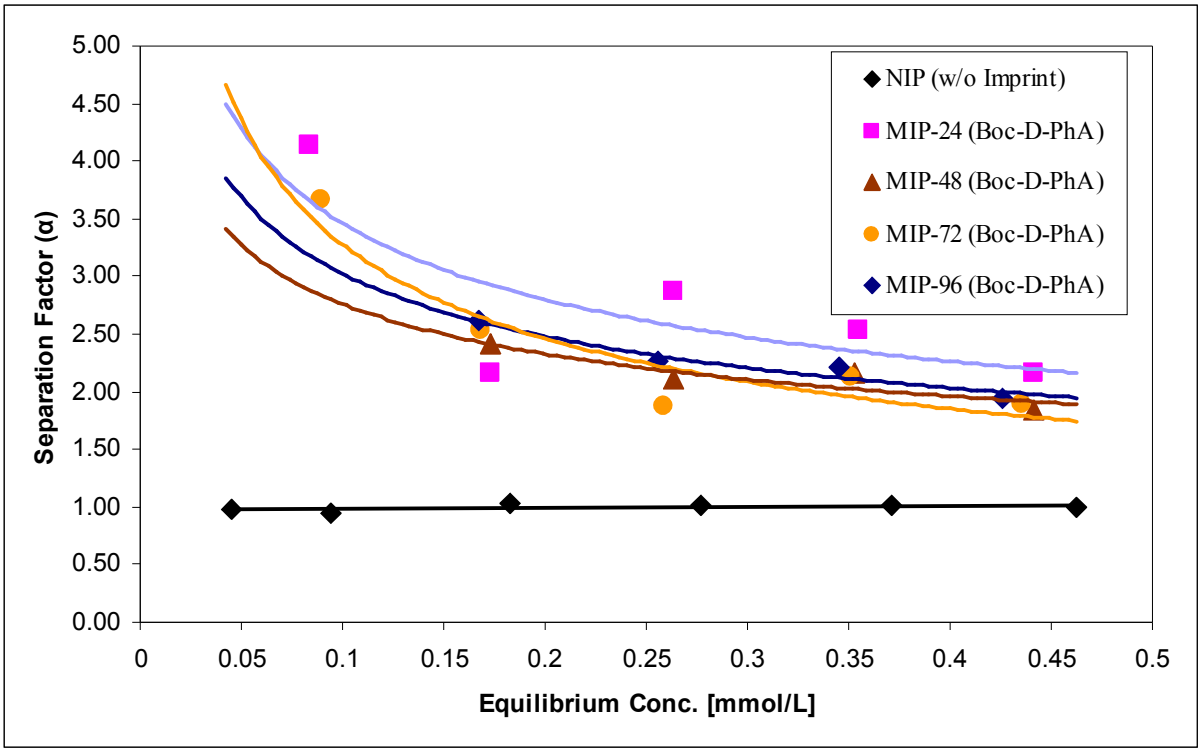

Figure 4.17. Enantioselectivity of MIP and NIP *poly(MAA-co-EDMA)* monoliths at different equilibrium concentrations w.r.t. time.

The maximum amounts of enantiomers adsorbed by the MIP monolith after 24 and 96 hours were ~1.52 and 1.47 µmol/g, respectively. Although the MIP monolith had shown higher adsorption capacity than NIP monolith and significant enantioselectivity for the template molecules but this trend was tend to decrease with the increase in the adsorption time. The MIP monolith after 24 hours of adsorption (MIP-24) had shown overall larger separation factor value for all concentrations (Figure 4.17).

4.2.2. Equilibrium Binding and Enantioselectivity of MIP Composite Membranes

Poly(MAA-co-EDMA) monolith based PP and PET composite membranes, prepared with and without pre-modification were used for adsorption binding studies. For both PP and PET composite membranes, all the results were normalized to the mass of monolith.

The PP NIP composite membranes adsorbed both Boc-D-PhA and Boc-L-PhA in almost equal amounts at different equilibrium concentrations of the racemic mixture and had, consequently, not shown specificity for the template molecule (Boc-D-PhA) in the racemic mixture (Figure 4.18a & 4.19a). The maximum amounts of Boc-D-PhA and Boc-L-PhA adsorbed by the NIP composite membranes prepared with pre-modification was 0.93 μmol/g at ~0.35 mmol/L solution concentration, while the respective data for the NIP composite membranes prepared without pre-modification was 0.95 μmol/g.

Both PP MIP composite membranes adsorbed the template Boc-D-PhA in larger amounts as compared to its counterpart Boc-L-PhA in the racemic mixture at all equilibrium concentrations (Figure 4.18b & 4.19b). In case of MIP membranes, the composite PP membranes prepared with pre-modification have shown slightly higher binding capacity and specificity towards template molecule as compared with PP composite membrane prepared without pre-modification (cf. Figure 4.18b & 4.19b). The maximum amount of the template molecule (Boc-D-PhA) and Boc-L-PhA adsorbed by MIP composite membranes prepared with pre-modification at ~0.35 mmol/L solution concentration were ~1.10 and ~0.80 μmol/g, respectively, while the respective data for composites prepared without pre-modification were ~1.06 and ~0.90 μmol/g, respectively. The non-specific binding was observed in both types of MIP composite membranes.

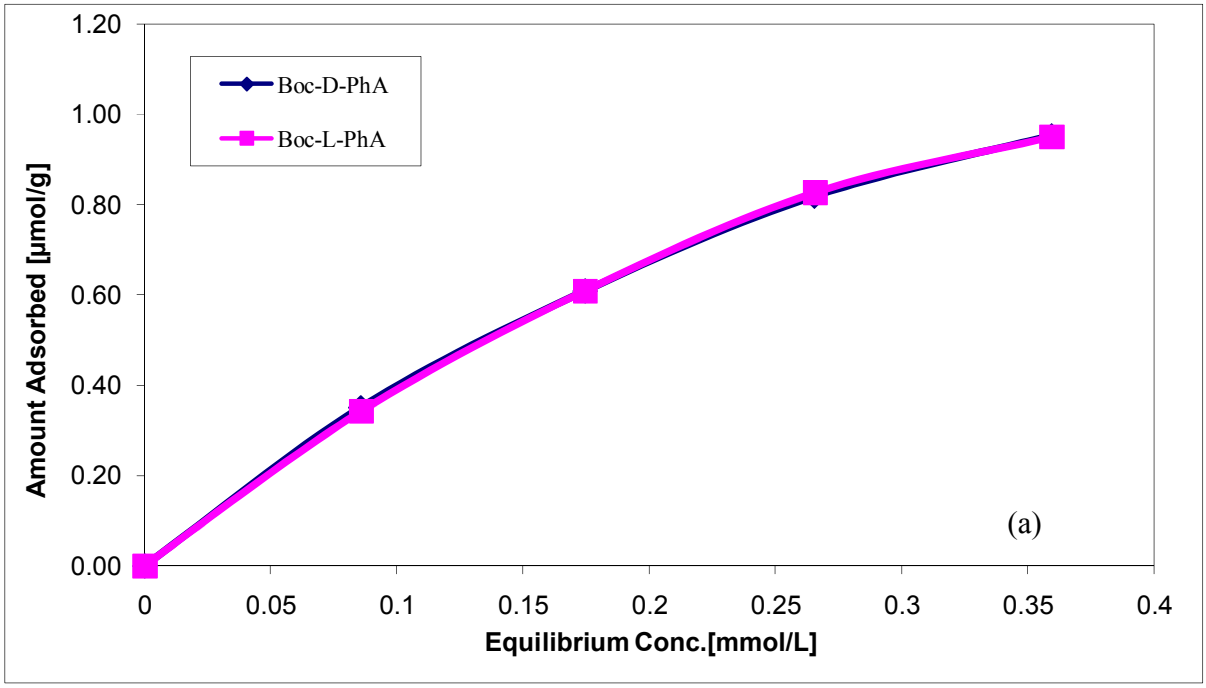

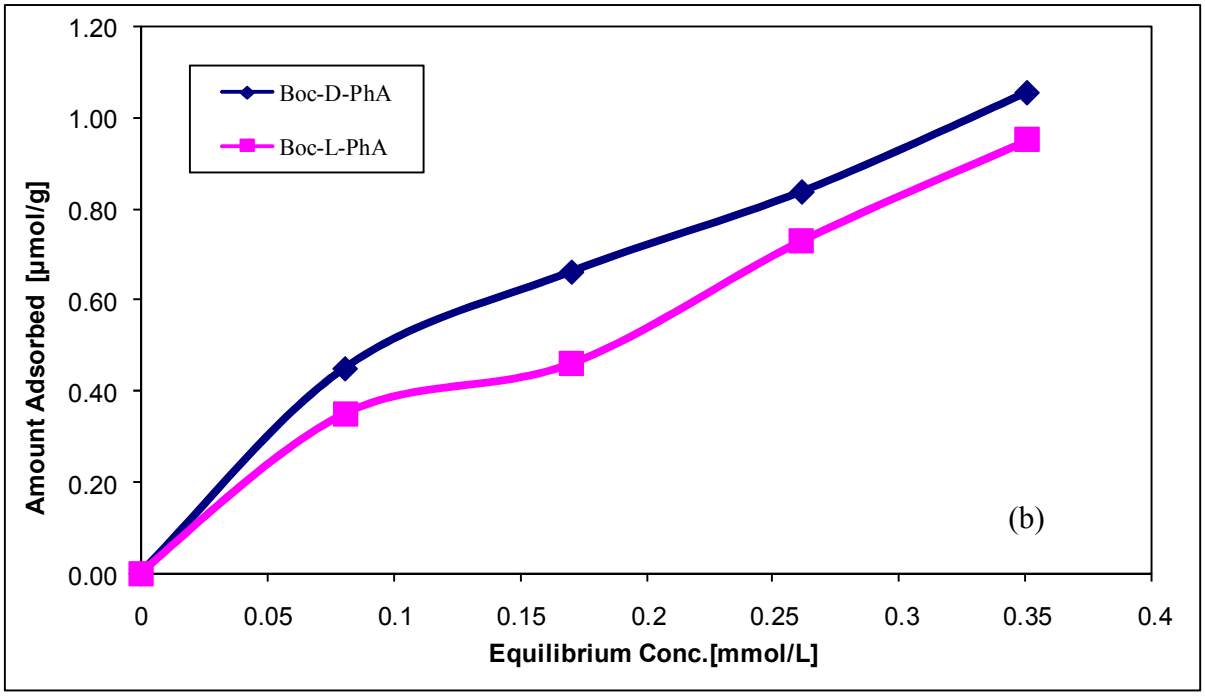

Figure 4.18. Adsorption isotherm for *poly(MAA-co-EDMA)* monolith based PP composite membranes, prepared without pre-modification a) NIP membrane, b) MIP membrane. PP membranes with nominal cut-off pore diameter of 0.4 µm were used as base material.

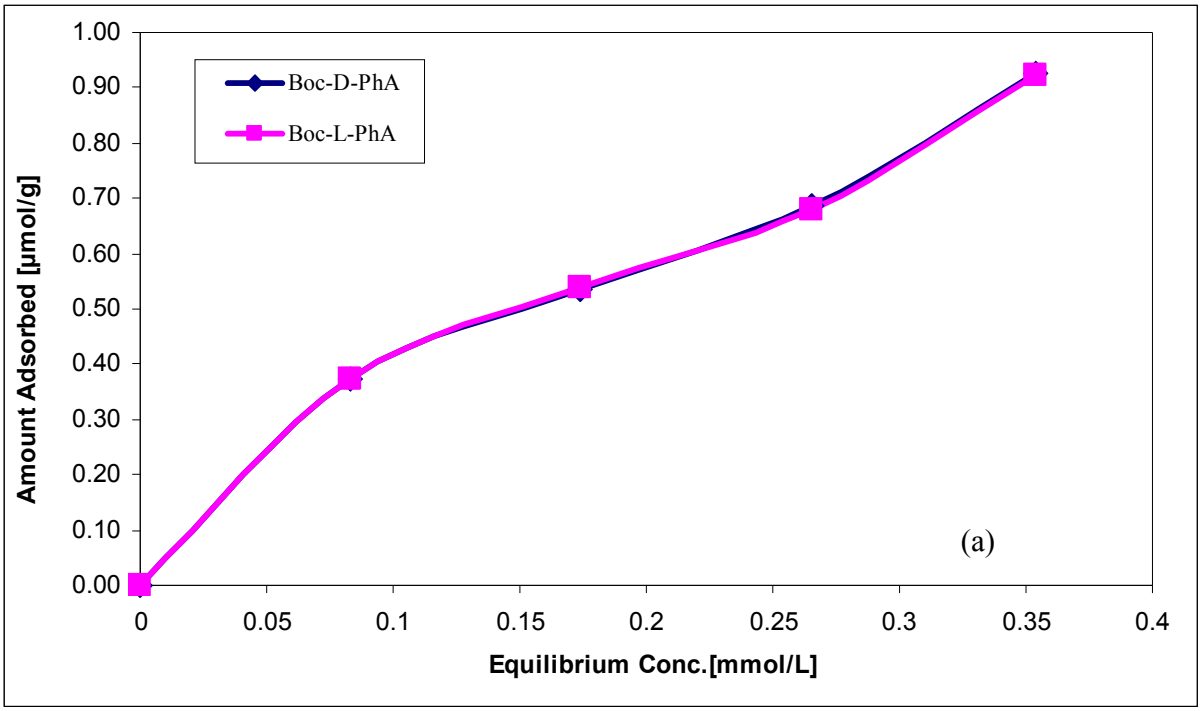

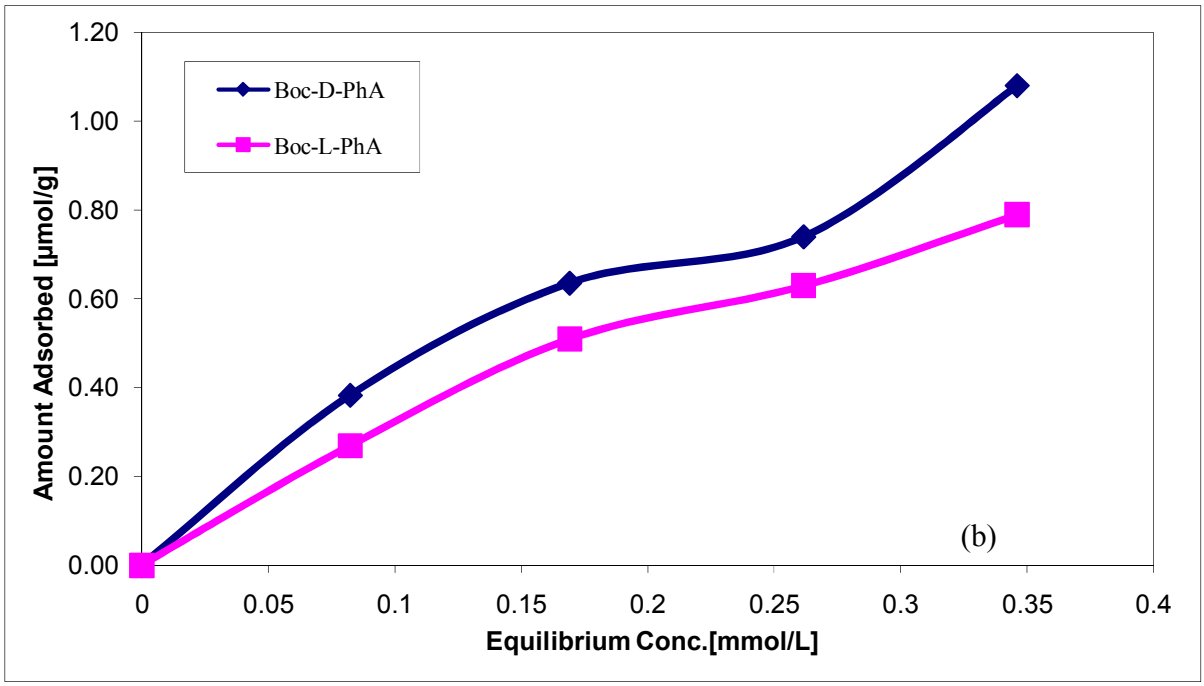

Figure 4.19. Adsorption isotherm for *poly(MAA-co-EDMA)* monolith based PP composite membranes, prepared with pre-modification a) NIP membrane, b) MIP membrane. PP membranes with nominal cut-off pore diameter of 0.4 µm were used as base material.

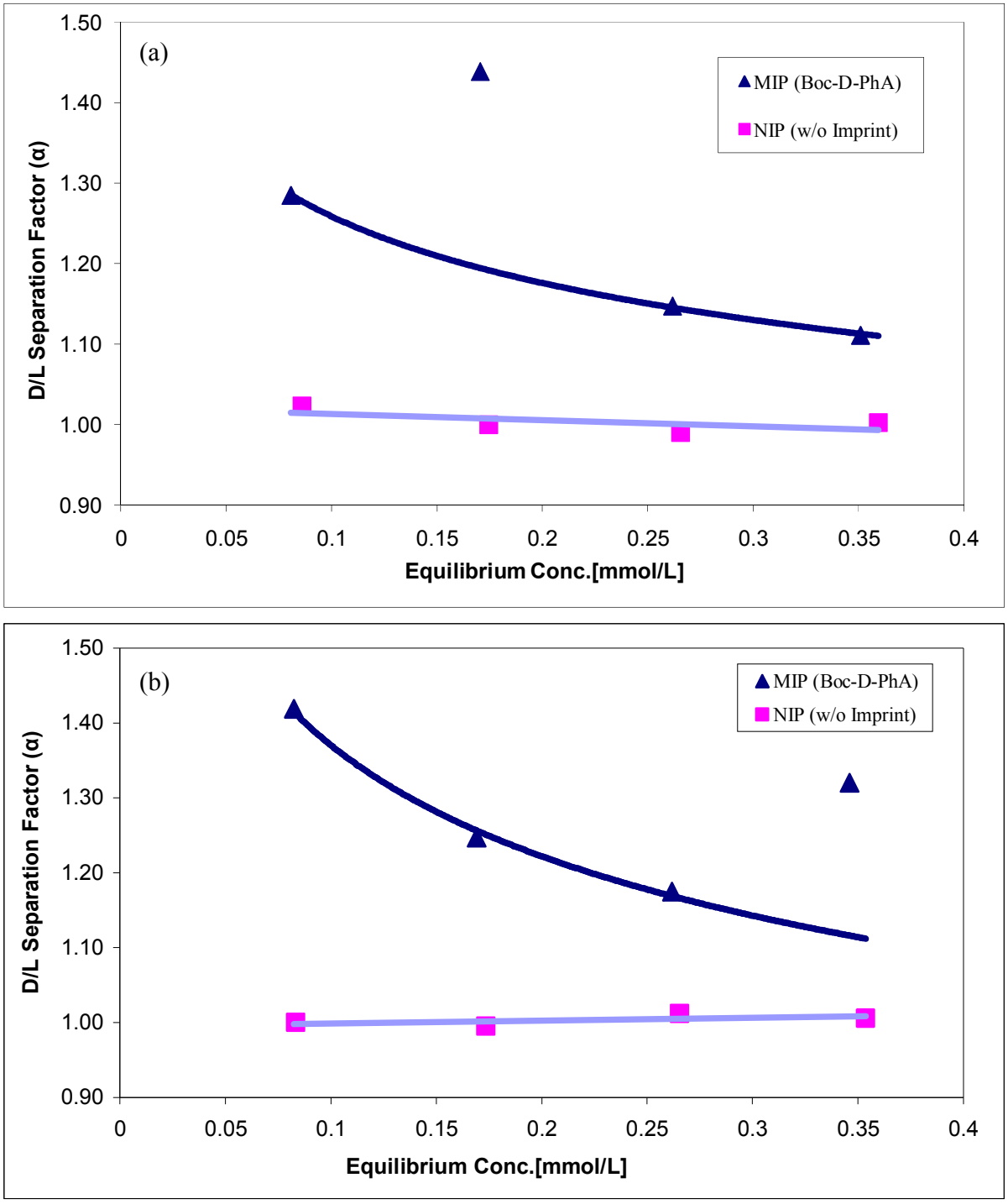

Figure 4.20. Enantioselectivity of MIP and NIP *poly(MAA-co-EDMA)* monolith PP composite membrane functionalized a) without pre-modification and b) with pre-modification. PP membranes with nominal cut-off pore diameter of 0.4 µm were used as base material.

Consequently, both MIP composite membranes prepared have shown a significant enantioselectivity as clear from the higher values of separation factor at all equilibrium concentrations while the NIP composite membranes have shown no enantioselectivity as indicated by the separation factor value of almost one for all equilibrium concentrations (Figure 4.20). Although the MIP composite membrane prepared without pre-modification has shown one higher separation factor value, the overall trend of the separation factor curves indicates that the MIP composite membrane prepared with pre-modification have a better enantioselectivity, even at higher equilibrium concentrations (cf. Figures 4.20a & 4.20b).

The PET NIP composite membranes adsorbed the counterpart Boc-L-PhA in slightly larger amounts than the template Boc-D-PhA at different equilibrium concentrations of the racemic mixture. The maximum amounts of Boc-D-PhA and Boc-L-PhA adsorbed by the NIP composite membranes prepared with pre-modification at ~0.36 mmol/L solution concentration were ~1.74 and ~1.94 μmol/g, respectively, while the respective data for composites prepared without pre-modification were ~2.77 and ~2.91 μmol/g, respectively.

Both PET MIP composite membranes adsorbed the template Boc-D-PhA in larger amounts as compared to its counterpart Boc-L-PhA in the racemic mixture at almost all equilibrium concentrations. The maximum amount of the template molecule (Boc-D-PhA) and Boc-L-PhA adsorbed by MIP composite membranes prepared with pre-modification at ~0.36 mmol/L solution concentration were ~3.03 and ~3.07 μmol/g, respectively, while the respective data for composites prepared without pre-modification were ~3.05 and ~3.02 μmol/g, respectively. The non-specific binding was observed in both types of MIP composite membranes. In case of MIP membranes, the composite PET membranes have shown overall higher binding capacity and slightly less specificity towards template molecule as compared with PP composite membrane.

Possible reasons for these differences could be the error in analysis and also due to more complex structure in case of PET composite membranes. Both the PET MIP composite membranes have shown higher total binding capacity than the PET NIP composite membranes (Figure 4.21). Incase of MIP membranes, the composite PET membranes prepared with and without pre-modification have shown almost same binding capacity at higher equilibrium concentrations. However, PET composite membranes prepared with pre-modification have shown higher specificity towards template molecule as compared with PET composite membrane prepared without pre-modification (cf. Figure 4.21).

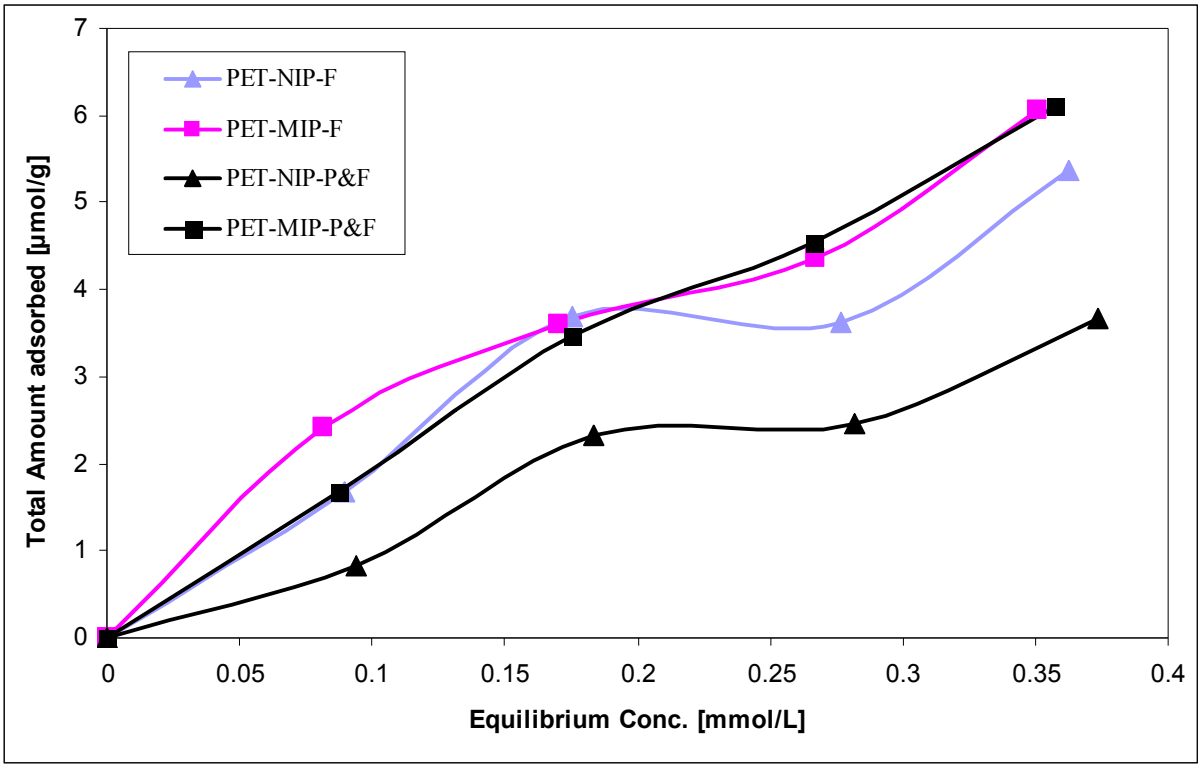

Figure 4.21. Total amount of racemic mixtures adsorbed at different equilibrium concentration by *poly(MAA-co-EDMA)* monolith based MIP and NIP PET composite membranes, prepared with and without pre-modification. PET membranes with nominal pore diameter of 3.0 µm were used as base material.

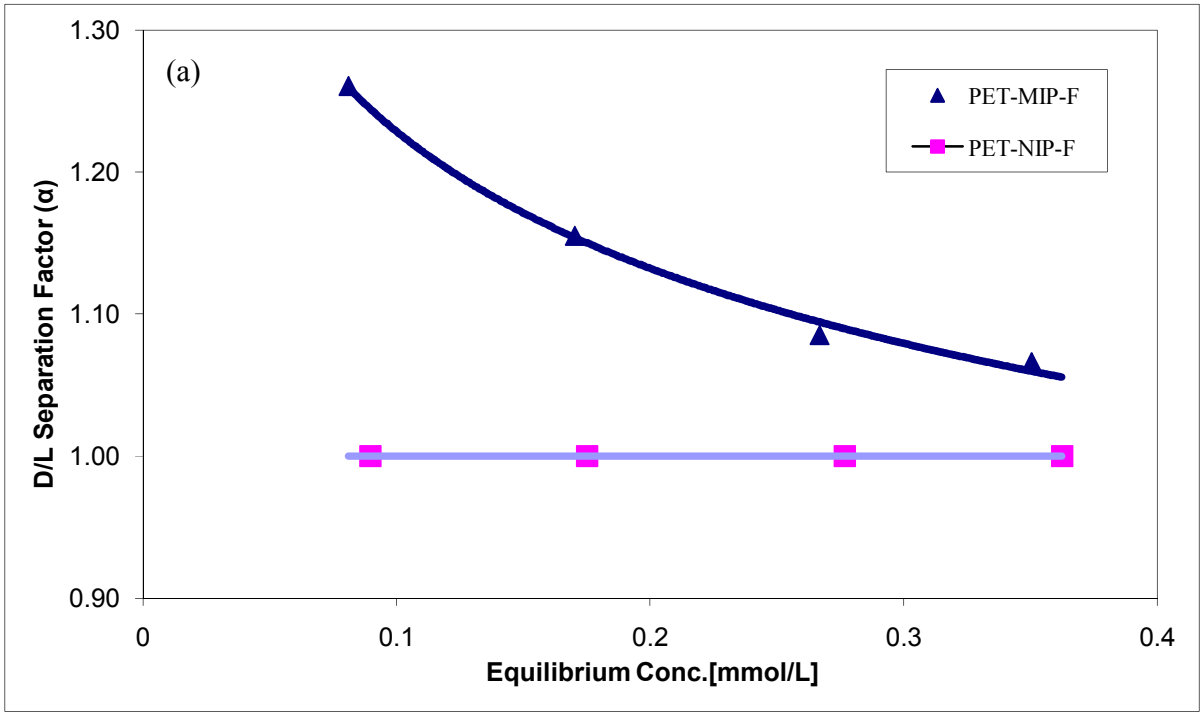

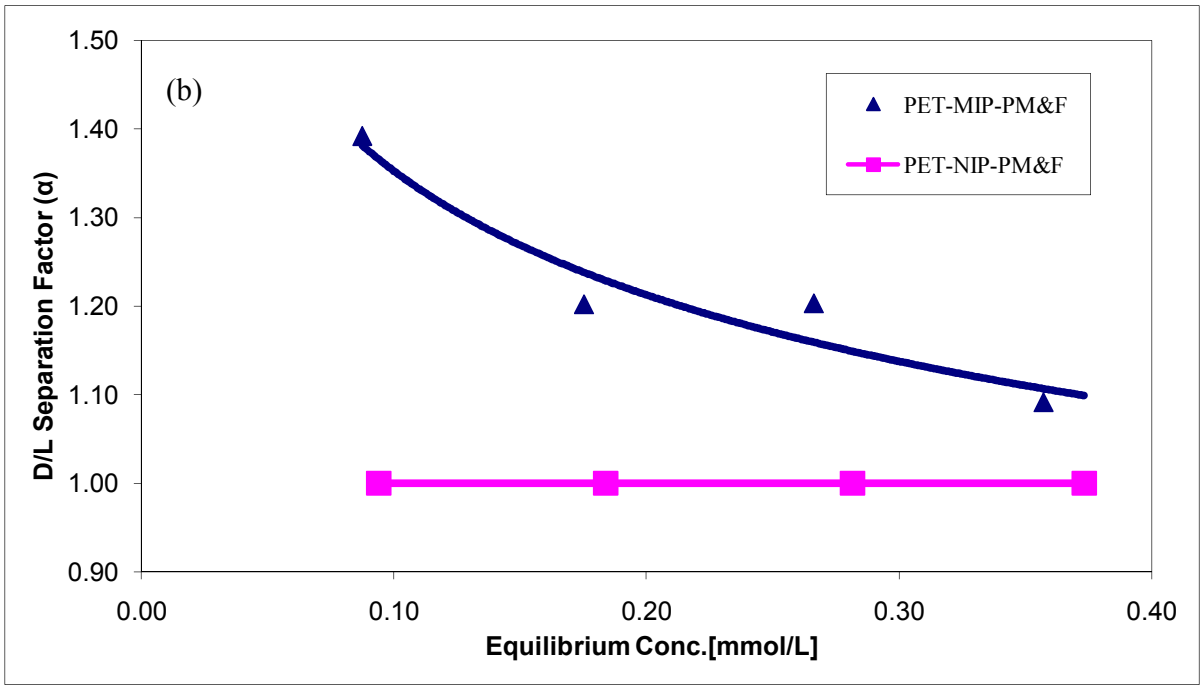

Figure 4.22. Enantioselectivity of MIP and NIP *poly(MAA-co-EDMA)* monolith PET composite membrane functionalized a) without pre-modification and b) with pre-modification. PET membranes with nominal pore diameter of 3.0 μm were used as base material.

In case of PET membranes, both MIP composite membranes prepared have shown net enantioselectivity as clear from the higher values of separation factor at all equilibrium concentrations. All the separation factor values for PET MIP membranes were normalized by taking the separation factor value of one for NIP composite membranes. The overall trend of the separation factor curves indicates that the MIP composite membrane prepared with pre-modification have a better enantioselectivity, even at higher equilibrium concentrations (cf. Figures 4.22a & 4.22b).

The MIP monoliths and monolith-filled PP and PET composite membranes as compared to the respective NIP materials have shown specificity, higher binding capacity and significant enantioselectivity for the template molecule (Boc-D-PhA) in the racemic mixture. For the PP and PET monolith composite membranes, the pre-modification of the pore walls with grafted *polyPEGMA* has improved the imprinting efficiency by providing a compatible interface between membrane material and *poly(MAA-co-EDMA)* as well as a larger number of specific imprinted binding sites within the monolith.

4.3. Transport Experiments (Diffusion and Electrodialysis)

This section can be further divided into three parts, i) Effective diffusion coefficient for polyethylene glycols, ii) Electrodialysis through MIP composite membranes and iii) Diffusion (dialysis) through MIP composite membranes.

4.3.1. Effective Diffusion Coefficient for Polyethylene Glycols

PET track etched membranes with nominal pore diameter of 3 μm, after pre-modification with PEGMA and pore filled functionalization with *poly(MAA-co-EDMA)*(cf. Section 4.1.2.

"Pre-modification and pore-filling of PP and PET membranes") were characterized for effective diffusion coefficient (D_{eff}) using 1 g/L PEG mixture (1500, 3000, 6000 and 10,000 g/mol) in water. The molecular weight distribution of PEG mixture obtained from GPC is given in Figure 4.23.

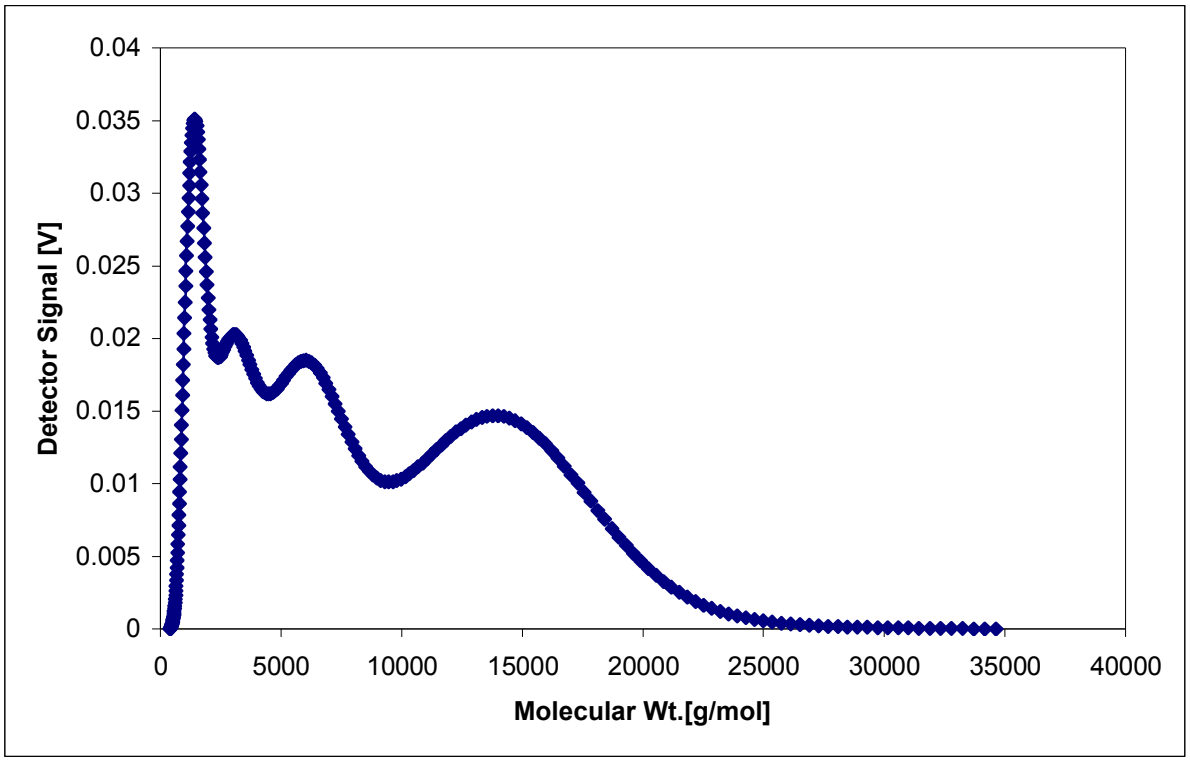

Figure 4.23. Molecular weight distribution of different PEG's in PEG mixture from GPC.

The effective diffusion coefficient for MIP (imprinted with Boc-D-PhA) and NIP (without imprint) PET *poly(MAA-co-EDMA)* based composite membranes pre-modified with 25 and 50 g/L of PEGMA are given in Table 4.7. The PET composite membrane MIP-25PM&F had shown larger D_{eff} values for both PEG's than non-imprinted composite membrane NIP-25PM&F. Likewise MIP-50PM&F had shown larger D_{eff} values for PEG's than non-imprinted composite membrane NIP-50PM&F. Overall the imprinted membranes had shown much larger D_{eff} values

than the non-imprinted membranes and the composite membranes pre-modified with 25 g/L PEGMA had larger D_{eff} value than the composite membranes pre-modified with 50 g/L PEGMA.

Table 4.7. Effective Diffusion coefficient – determined with PEG mixture in water (1 g/L) through MIP and NIP composite membranes pre-modified with 25 and 50 g/L of PEGMA. PET membranes with nominal pore diameter of 3.0 µm were used as base material.

PET-3 µm Membranes	**Effective Diffusion Coefficient, D_{eff} (m^2/s)**	
	MW, PEG = 1500 g/mol	**MW, PEG = 13500 g/mol**
MIP-25PM&F	7.64×10^{-11}	5.64×10^{-11}
NIP-25PM&F	1.61×10^{-11}	3.80×10^{-12}
MIP-50PM&F	1.39×10^{-11}	2.92×10^{-12}
NIP-50PM&F	6.91×10^{-12}	4.25×10^{-13}

The presence of imprints within the composite structure may be responsible for this increased pore connectivity in case of imprinted composite membranes. Also, the low D_{eff} values in case of composite membranes pre-modified with 50 g/L of PEGMA showed that the increase in the DG value of pre-modification may have significant effects on the composite pore structure i.e. decrease in the porosity. The detail study of this possible change in porosity was not possible. This however, had not been studied due to the limitation of the method (cf. Section 4.1.3. "Pore characterization of PP and PET based composite membranes").

4.3.2. Electrodialysis through MIP Composite Membranes

PET track etched membrane were used to study the phenomenon of electrodialysis and to optimize the suitable conditions for the electrodialysis using MIP *poly(MAA-co-EDMA)* monolith PET composite membranes. Initially original PET membranes with nominal pore diameter of 30 nm were used to study the effect of potential difference on transport electrodialysis of Boc-D-PhA. In parallel diffusion experiments where concentration difference was adopted as a driving force for membrane permeation were run as control experiments. The change of solvent to aqueous system had been necessary because the process of electrodialysis proceed only in conductive environment. Incase of electrodialysis pH of the feed and permeate were kept same. Boc-D/L-PhA is acidic in nature and 1 mmol/L solution of Boc-D/L-PhA in 50 vol % aqueous AN solution had a pH of ~ 4.0. Boc-D/L-PhA was negatively charged in the present conditions and was transported to the anode.

The effect of potential difference on the transport of Boc-D-PhA through original PET membrane with nominal pore diameter of 30 nm is given in Figure 4.24. The maximum transport of Boc-D-PhA was observed at applied potential difference of 3 volts as compared with diffusion permeation. It was also observed that by reversing the applied potential i.e. -3 volts, electrodialysis permeation was less than the diffusion permeation for all intervals of time. At an applied potential of 2 and 4 volts, the transport of Boc-D-PhA was less than that in diffusion experiment for almost all time intervals (cf. Figure 4.24). However, the effects were small, and not in all cases larger than the experimental error.

The effect of applied potential difference on the permeation of Boc-D-PhA after the same period of time can be explained in Figure 4.24, which showed slightly higher permeation concentration at 3 volts after 4 hours of electrodialysis. The applied potential difference of 3

volts was found to be a favorable condition for the high permeation of Boc-D/L-PhA using electrodialysis.

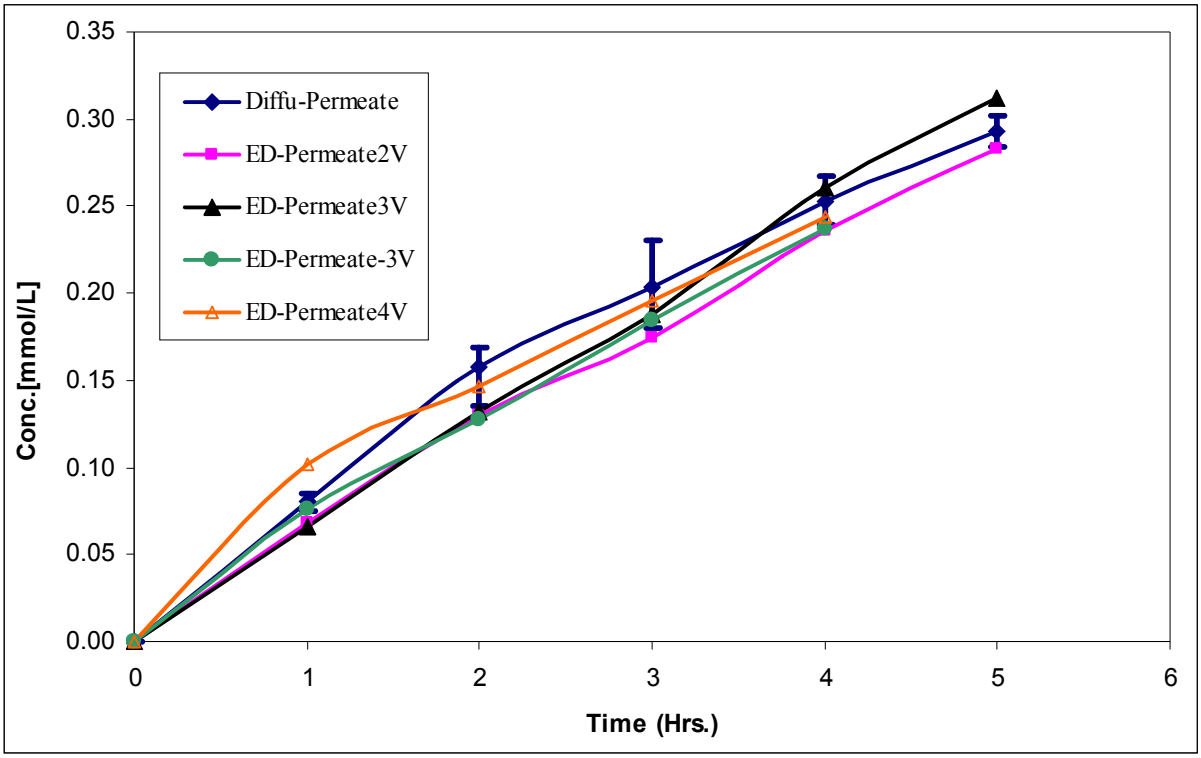

Figure 4.24. Comparison of permeate concentration during diffusion and electrodialysis at different applied voltages. Original PET membranes with nominal pore diameter of 30 nm and initial concentration difference of 1 mmol/L of Boc-D-PhA in 50 vol % aqueous AN solution were used in this experiment. The permeate concentrations for diffusion are average values with their error bars.

From above study, it was observed that the electrodialysis at an applied potential of 3 volts gives the comparatively fast transport of the Boc-D-PhA than in diffusion experiment. In all next experiments, PET composite membranes were used for electrodialysis at an applied potential difference of 3 volts.

Electrodialysis using MIP Composite Membranes

The MIP (imprinted with Boc-D-PhA) and NIP (without imprint) PET composite membranes, pre-modified with 25 g/L PEGMA prior to pore-filling functionalization were used for electrodialysis and for diffusion (control experiment) studies. All the composite membranes were prepared under similar conditions with almost same thickness. In all steps of sequential diffusion studies with one membrane under varied condition, 0.5 mmol/L Boc-D-PhA or Boc-L-PhA in 50 vol % aqueous AN solution was used as feed and a 50 vol % aqueous AN solution was used on permeate side for both electrodialysis and diffusion experiments. During the electrodialysis, pH of the feed and permeate were kept same at ~4.2. Incase of diffusion, the pH on feed and permeate sides were ~4.2 and ~7.1, respectively. In between every step, the membranes were extracted in methanol for 24 hours and wetted in 50 vol % aqueous AN solution before using for next step. The details about experimental steps and composite membranes used during these steps are summarized in Table 4.8.

Table 4.8. The composite membranes and the feed solutions used for different steps during electrodialysis and diffusion experiments.

Step No.	**Composite Membrane for Electrodialysis**	**Composite Membrane for Diffusion**	**Feed Solution [0.5 mmol/L]**
Step 1	MIP-3-25P&F-01	MIP-3-25P&F-02	Boc-D-PhA
Step 2	MIP-3-25P&F-01	MIP-3-25P&F-02	Boc-L-PhA
Step 3	MIP-3-25P&F-01	MIP-3-25P&F-02	Boc-D-PhA
Step 4	MIP-3-25P&F-02	MIP-3-25P&F-01	Boc-D-PhA

In step 1, 0.5 mmol/L Boc-D-PhA in 50 vol % aqueous AN solution was used as feed and the maximum concentration of Boc-D-PhA on the permeate-side through the MIP composite membrane during electrodialysis was ~0.04 mmol/L. While nothing was permeated through the membrane during diffusion (cf. Figure 4.25) for same period of time. In the second step, 0.5 mmol/L Boc-L-PhA in 50 vol % aqueous AN solution was used as feed and the maximum concentrations of Boc-L-PhA permeated through the MIP composite membrane during electrodialysis and diffusion were ~0.043 and ~0.018 mmol/L respectively (Figure 4.26). In this step, the MIP composite membrane used for diffusion had shown some permeation of Boc-L-PhA while the same membrane did not show any transport of Boc-D-PhA in step 1.

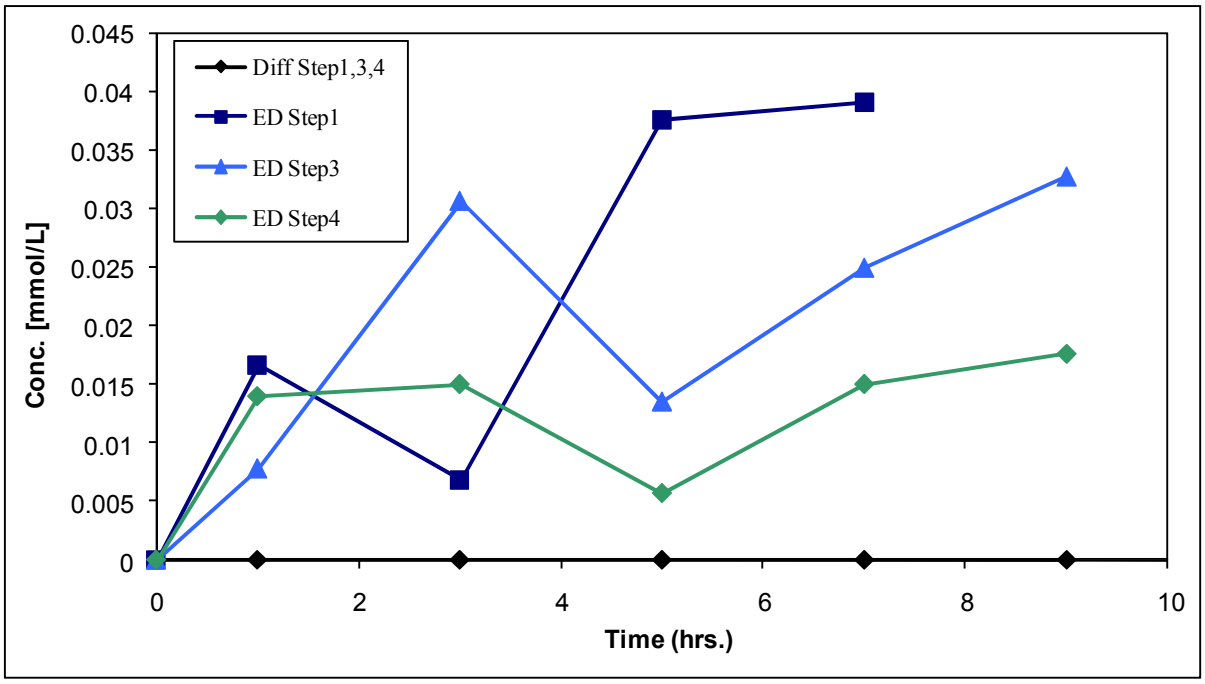

Figure 4.25. Concentration of Boc-D-PhA in AN/H_2O permeated through MIP *poly(MAA-co-EDMA)* monolith PET composite membrane during electrodialysis and diffusion after steps 1, 3 and 4. In step 4, the MIP composite membranes used for electrodialysis and diffusion in previous steps were interchanged with each other.

In step 3, 0.5 mmol/L Boc-D-PhA in 50 vol % aqueous AN solution was used as feed for electrodialysis and diffusion. Again electrodialysis results into permeation of Boc-D-PhA and the maximum concentration obtained was ~0.033 mmol/L while no permeation was observed during diffusion process (cf. Figure 4.25). Again in this step, the composite membrane used for diffusion did not show any transport of Boc-D-PhA on the permeate side as in step 1 (cf. Figure 4.25) while the same membrane had already shown permeation of Boc-L-PhA in step 2 (cf. Figure 4.26). As the MIP composite membranes were imprinted with Boc-D-PhA and may have shown more affinity towards the template Boc-D-PhA than its counter part Boc-L-PhA. So it may be thought that these MIP membranes are behaving as an adsorber for the template molecule (Boc-D-PhA) and do not offer any affinity for Boc-L-PhA.

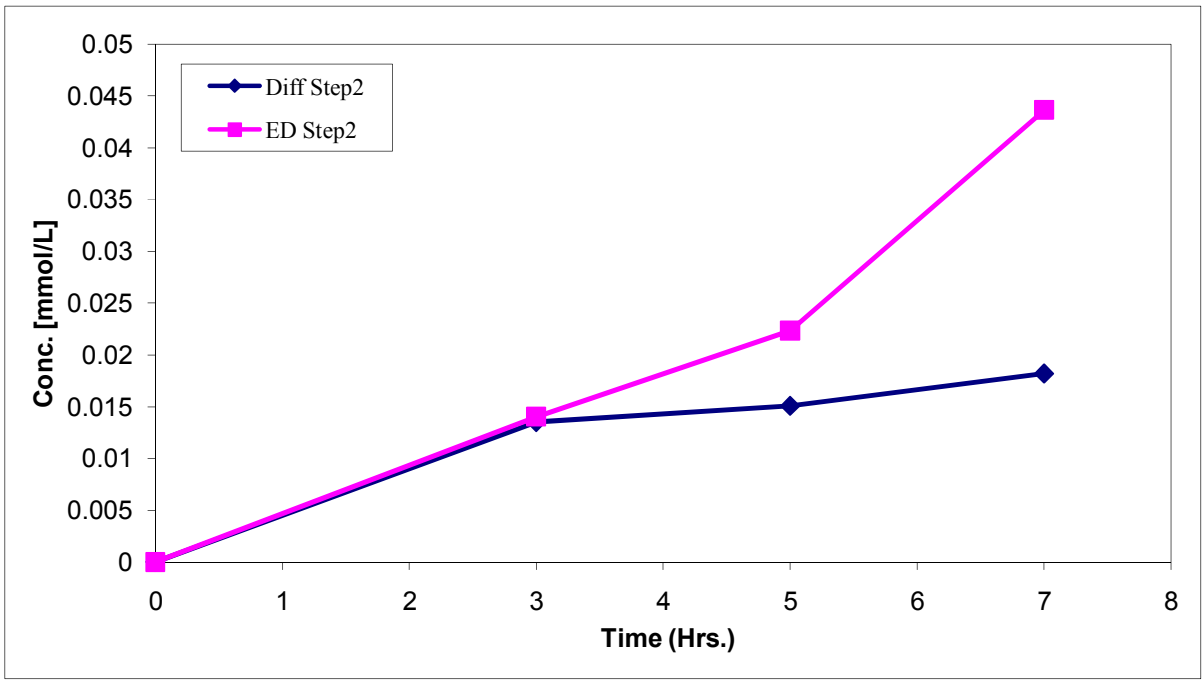

Figure 4.26. Effect of time on permeate concentration of Boc-L-PhA in AN/H_2O through MIP *poly(MAA-co-EDMA)* monolith PET composite membranes during diffusion and electrodialysis.

In order to further investigate this adsorber effect, in step 4, both MIP composite membranes were interchanged with each other i.e. membrane which had been used for diffusion in previous steps will be used for electrodialysis and vice versa (cf. Table 4.8). A 0.5 mmol/L Boc-D-PhA in 50 vol % aqueous AN solution was used as feed for both electrodialysis and diffusion. Once again electrodialysis results into permeation of Boc-D-PhA and the maximum concentration obtained was ~0.018 mmol/L while almost zero permeation was observed during diffusion process at the same time (cf. Figure 4.25). The MIP composite membrane which had earlier been used for electrodialysis did not show any transport of Boc-D-PhA when employed in diffusion cell. Again, during the diffusion process, the MIP composite membrane may behave as an adsorber for the template Boc-D-PhA. The estimated binding capacity of these membranes was found to be ~4 nmol/membrane (~15 mg of monolith). During the diffusion process, there was no permeation through the MIP composite membranes when Boc-D-PhA was used as feed (cf. Figure 4.25) and the same MIP membrane had shown permeation when Boc-L-PhA was used as feed solution (cf. Figure 4.26). As the binding capacity is not significant enough to claim these membranes as adsorber, these membranes may behave like “gate” due to an increase of membrane swelling as a consequence of binding of the template to imprinted sites. The “gate effect” will further be discussed in Section 4.4.

On the other hand if we look into the electrodialysis processes, the amount transported through the MIP composite membranes on the permeate side was always higher than in diffusion processes irrespective of the type of the feed solution (cf. Figure 4.25 and 4.26). The applied potential difference seems to facilitate the transport of charged species through the composite

membrane during electrodialysis. During electrodialysis a significant decrease in the transport rate through the MIP composite membranes was observed after each step (cf. Figure 4.25).

Effect of Time on Electrodialysis using MIP Composite Membranes

Analogous results were obtained when the above experiment was repeated with fresh MIP *poly(MAA-co-EDMA)* monolith PET composite membranes and for longer period of time. A 0.5 mmol/L Boc-D-PhA in 50 vol % aqueous AN solution was used as feed. In the first step, the maximum concentration of Boc-D-PhA transported through MIP composite membranes during electrodialysis and diffusion were ~0.058 and ~0.019 mmol/L respectively (cf. Figure 4.27).

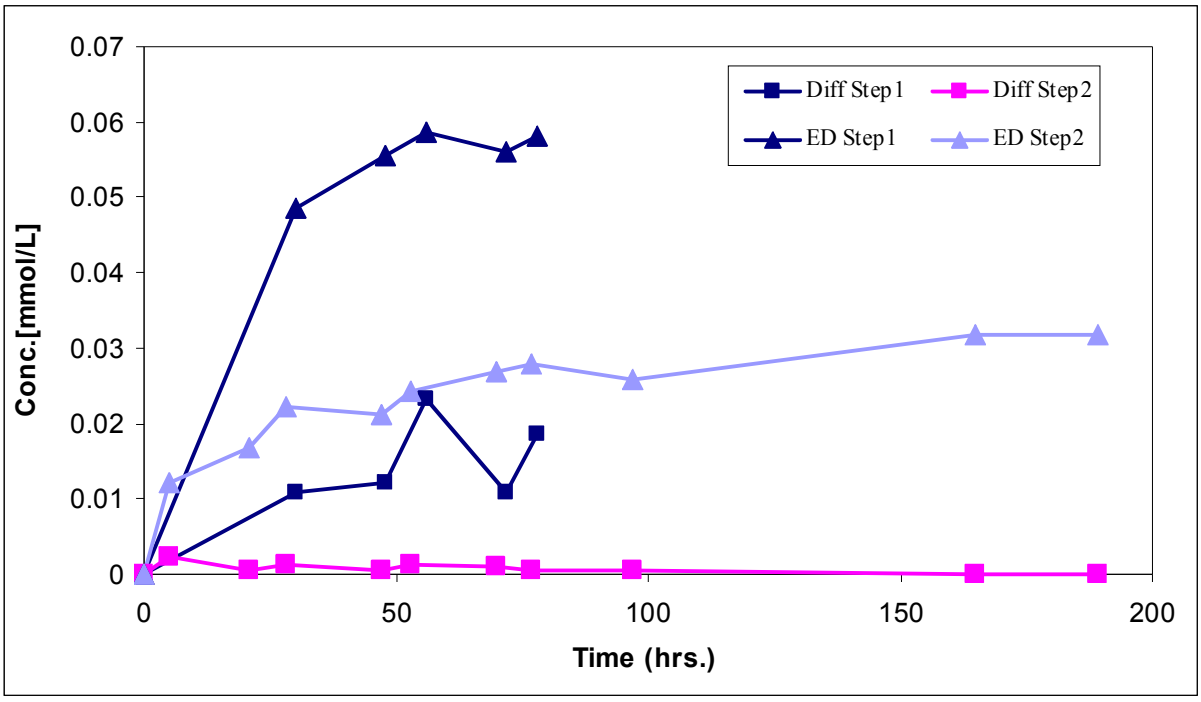

Figure 4.27 Effect of time on permeate concentration of Boc-D-PhA in AN/H_2O through MIP *poly(MAA-co-EDMA)* monolith PET composite membranes during diffusion and electrodialysis over the longer period of time.

In the second step, feed was kept same. In this case, the pH on the feed and permeate sides were kept same for both electrodialysis and diffusion to get the homogeneous ionic charge effect on permeate side for both processes. For second step, the maximum amounts of Boc-D-PhA transported through MIP composite membranes during electrodialysis and diffusion were ~0.032 and ~0.0 mmol/L respectively (cf. Figure 4.27). Again, a significant flux reduction was observed for the second set of experiments which reflects some structural changes towards pore morphology within the composite membranes.

NIP composite membranes were also employed to study the transport behavior through the membranes. The electrodialysis resulted in the facilitated transport of Boc-D-PhA through the NIP composite membrane and the maximum concentration on the permeate side was ~0.028 mmol/L while no transport was observed through NIP composite membrane during diffusion dialysis.

From above study, it is very much evident that applied potential across the MIP *poly(MAA-co-EDMA)* monolith PET composite membranes imprinted with Boc-D-PhA, facilitates the transport of Boc-D-PhA through these membranes while there was no significant transport of the Boc-D-PhA through these membranes during the diffusion process.

Electrodialysis was found to be one way to permeate the isomer, which is preferentially incorporated into the membrane by using the same concentration on both feed and permeate sides and adopting the applied potential difference as an only driving force for transport through the membrane [82,85,109]. Hence, the MIP composite membrane imprinted with Boc-D-PhA was used for enantioselective permeation of racemic mixture through the membrane. In order to use the potential difference as a only driving force for the membrane transport a 50 vol % aqueous AN solution of 1 mmol/L racemic Boc-PhA was placed in both chambers of the

diffusion cell. The pH value for the racemic mixture (Boc-DL-PhA) in present study was around 4.0. Boc-DL-PhA was negatively charged under the present conditions and was transported to the anode.

Figure 4.28 shows a concentration spectrum of Boc-D-PhA and Boc-L-PhA on feed and permeate side across the composite membrane imprinted with Boc-D-PhA as function of time and no measureable change was observed.

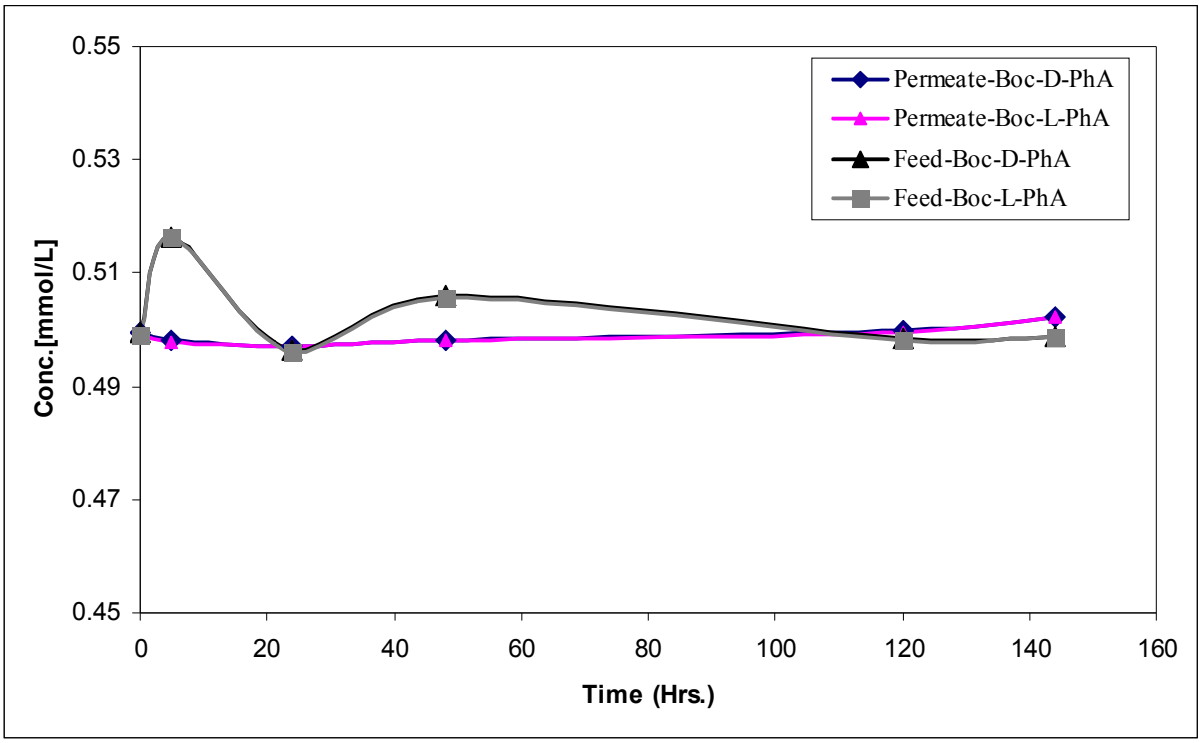

Figure 4.28. Effect of time on permeate-concentration of racemic mixture (Boc-DL-PhA) solution in AN/H_2O through *poly(MAA-co-EDMA)* monolith PET composite membrane imprinted with Boc-D-PhA during electrodialysis.

In order to investigate this non-enantioselective permeation through MIP *poly(MAA-co-EDMA)* monolith PET composite membranes in 50 vol % aqueous AN solution, the imprinted

(Boc-D-PhA) monoliths were investigated for their equilibrium binding and enantioselectivity in a racemic mixture of Boc-D-PhA and Boc-L-PhA in 50 vol % aqueous AN solution.

Equilibrium Binding and Enantioselectivity of Monolith in Aqueous-AN Medium

After wetting in 50 vol % aqueous AN solution (pH = ~ 7.1), both MIP (imprinted with Boc-D-PhA) and NIP *poly(MAA-co-EDMA)* based monoliths were analyzed for their binding isotherms and the enantioselectivity for the imprint molecule (Boc-D-PhA) in the racemic mixture of Boc-D-PhA and Boc-L-PhA of different concentrations in 50 vol % aqueous AN solution. Both NIP and MIP monoliths adsorbed significantly less amounts of enantiomers at different equilibrium concentrations of the racemic mixture and did not show specificity for the template molecule in the racemic mixture. The maximum amounts of Boc-D-PhA and Boc-L-PhA adsorbed by the NIP monolith at ~0.47 mmol/L solution concentration were ~0.09 μmol/g each. The maximum amounts of Boc-D-PhA and Boc-L-PhA adsorbed by the MIP monolith at ~0.46 mmol/L solution concentration were 0.24 and 0.22 μmol/g, respectively. These values were significantly less than the amount adsorbed at the same racemate concentrations in AN (see Figure 4.29) where enantioselective binding was observed at the same time (cf. Figure 4.14).

In its aqueous AN solution, Boc-D/L-PhA is acidic (pH = ~4.2) and exhibit the affinity binding within monolith structure. As these monoliths were already wetted with 50 vol % aqueous AN solution (pH = ~7.1). It may speculate that the ionic repulsion at the boundary of monolith could be responsible for less adsorption of Boc-D-PhA and Boc-L-PhA in both MIP and NIP monoliths. In addition, for MIP monoliths, the possible reason for the absence of enantioselective behavior could be due the presence of water molecules which are responsible

for the excessive H-bonding with the Boc-D/L-PhA molecules in the solution as well as with the imprinted sites present within the cross-linked structure of the polymer monoliths.

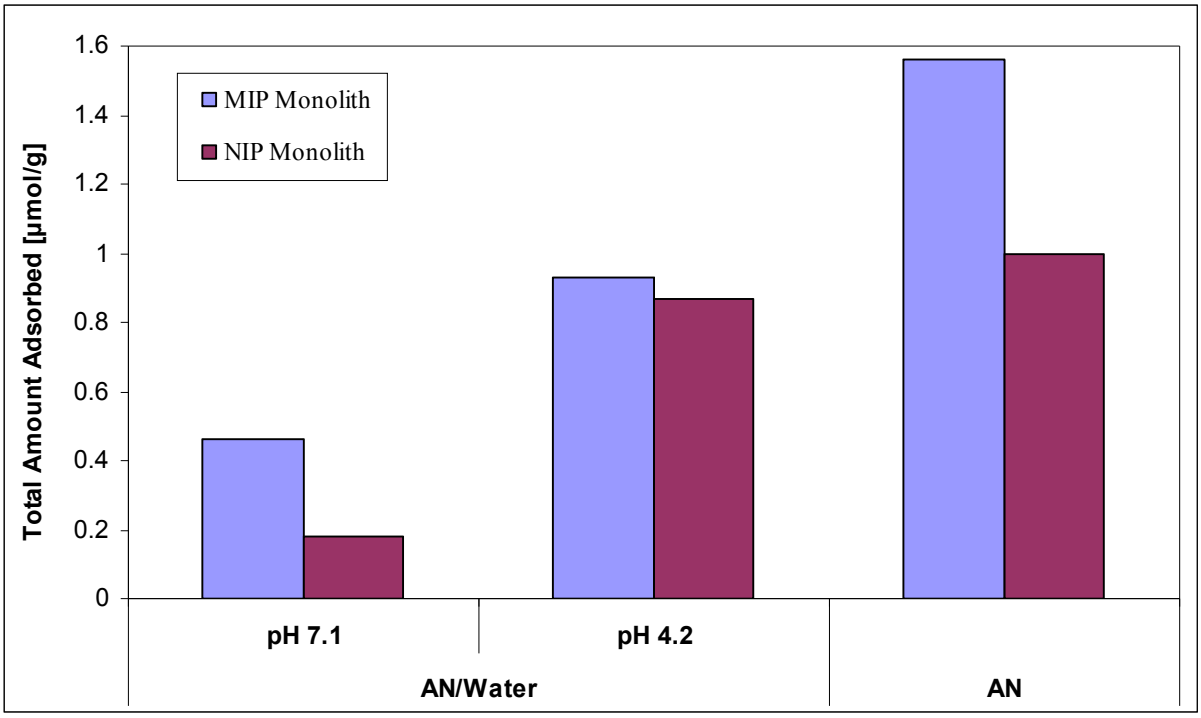

Figure 4.29. Comparison of amount of Boc-DL-PhA adsorbed at the same racemate concentration by the MIP and NIP *poly(MAA-co-EDMA)* based monoliths under different solvent conditions. Enantioselectivity was only observed for MIP in AN.

In order to further investigate the ionic repulsive effect (Donnan Exclusion) in the polymer monoliths and non-enantioselective behavior of MIP monoliths, both MIP and NIP *poly(MAA-co-EDMA)* monoliths were first wetted in 50 vol % aqueous AN solution which had a pH value equal to that of racemic mixture (pH = ~4.2). Both MIP and NIP monoliths were analyzed for their binding isotherms and the enantioselectivity for the imprint molecule (Boc-D-PhA) in the racemic mixture of Boc-D-PhA and Boc-L-PhA in 50 vol % aqueous AN solution for 24 hours.

Both MIP and NIP monoliths did not show any specificity for the template molecule in the racemic mixture. The maximum amounts of Boc-D-PhA and Boc-L-PhA adsorbed by the NIP monolith at ~0.455 mmol/L solution concentration were ~0.43 μmol/g each. The maximum amounts of Boc-D-PhA and Boc-L-PhA adsorbed by the MIP monolith at ~0.445 mmol/L solution concentration were 0.46 and 0.47 μmol/g (cf. Figure 4.29). However, NIP and MIP monoliths had adsorbed larger amount of enantiomers at different equilibrium concentrations of the racemic mixture than the same monoliths when wetted in 50 vol % aqueous AN solution at pH=7.1. But these values are comparatively less than the amounts adsorbed by the similar monoliths when wetted in AN. In case of NIP monoliths, the amounts adsorbed were comparable with that obtained from racemic mixture in AN (cf. Figure 4.29). While in case of MIP monoliths the values for amount adsorbed were significantly less than the amount adsorbed at the same racemate concentration in AN (cf. Figure 4.29) and also the MIP monolith had shown no enantioselectivity for the imprint molecule.

The solvent and its pH are very much important for the transport of molecules within the polymer monolith. At equilibrium the accessibility of pores is a function of experimental conditions and the possible mechanism is the "Donnan Exclusion". At high pH, the repulsive forces rendering the molecules to enter the pores and meso porous monolith structure is no more accessible for template and its counterpart.

4.3.3. Diffusion (Dialysis) through MIP Composite Membranes

PET track etched membranes with nominal pore diameter of 0.4 and 3.0 μm were used after pore-filled functionalization *poly(MAA-co-EDMA)* with and without pre-modification step. The composite membranes based on PET membranes with nominal pore diameter of 0.4 μm

were pre-modified with 25 g/L of PEGMA. While the composite membranes based on PET membranes with nominal pore diameter of 3.0 µm were pre-modified with 25 and 50 g/L of PEGMA.

Figure 4.30 shows the effect of time on permeate-concentration of racemic mixture of Boc-D-PhA and Boc-L-PhA through the *poly(MAA-co-EDMA)* monolith PET composite membrane imprinted with and without the template Boc-D-PhA. The MIP composite membranes showed higher transport for both racemic mixtures in AN and MeOH as compared to NIP composite membranes. But in both cases no detectable enantioselectivity was observed.

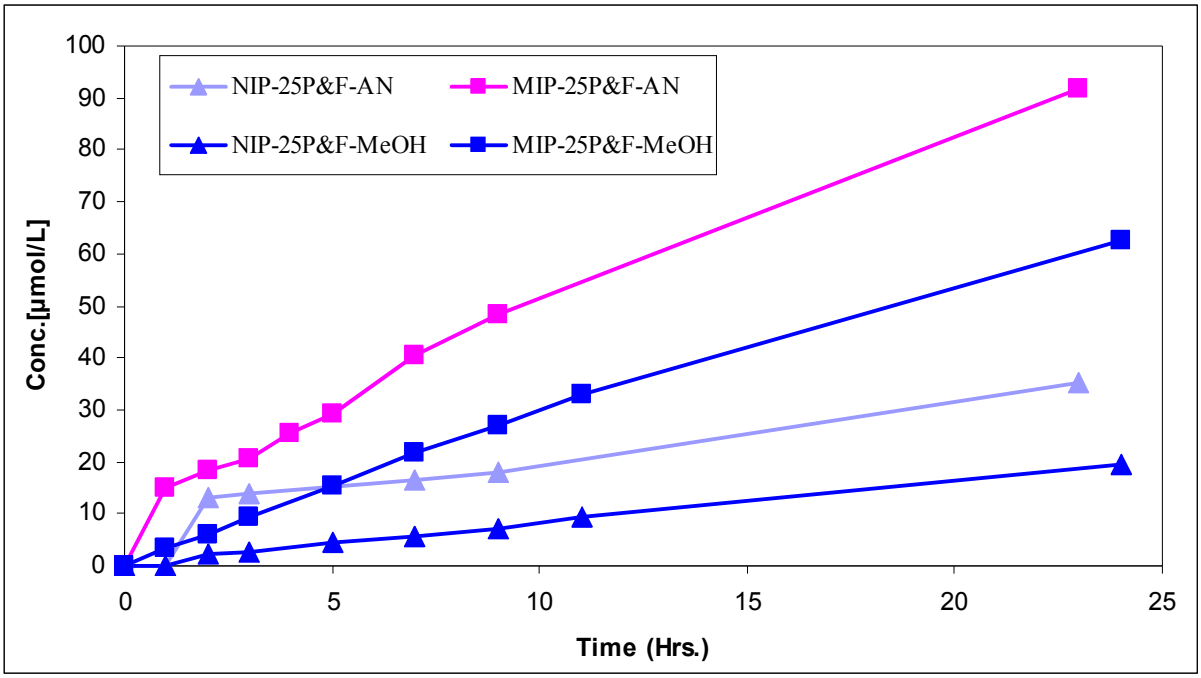

Figure 4.30. Effect of time on permeate concentration of the racemic mixture (Boc-DL-PhA) solution in AN and MeOH, through the MIP and NIP *poly(MAA-co-EDMA)* monolith-PET composite membranes prepared with pre-modification. In this case PET membranes with nominal pore diameter of 0.4 µm were used as base material.

Both MIP and NIP composite membranes had shown higher permeation of racemic mixture in AN than in MeOH (cf. Figure 4.30). The decreased concentration on the permeate side (cf. Figure 4.30) and smaller D_{eff} values (cf. Table 4.9) when MeOH was used as solvent could be due to excessive hydrogen bonding of MeOH with imprinted sites in membrane pores and with the Boc-D/L-PhA molecules in the racemic mixture. The MIP composite membrane had shown larger effective diffusion coefficient (D_{eff}) values for the racemic mixture than non-imprinted composite membrane (cf. Table 4.9).

Table 4.9. Effective diffusion coefficient values for Boc-DL-PhA in AN or MeOH through different *poly(MAA-co-EDMA)* monolith PET composite membranes.

Base Membrane	**Composite Membrane**	**Effective Diffusion Coefficient, D_{eff} (m^2/s)**
PET with Nominal Pore Diameter = 400 nm	MIP-25P&F-AN	2.44×10^{-10}
	NIP-25P&F-AN	1.46×10^{-10}
	MIP-25P&F-MeOH	1.61×10^{-10}
	NIP-25P&F-MeOH	4.71×10^{-11}
PET with Nominal Pore Diameter = 3 μm	MIP-25P&F-MeOH	1.78×10^{-10}
	NIP-25P&F-MeOH	2.97×10^{-10}
	MIP-50P&F-MeOH	1.78×10^{-10}
	NIP-50P&F-MeOH	3.48×10^{-11}
	MIP-F-MeOH	3.62×10^{-11}
	NIP-F-MeOH	4.10×10^{-11}

Incase of PET membrane with nominal pore diameter of 3.0 µm, the MIP composite membranes pre-modified with 25 g/L of PEGMA had shown less permeation of racemic mixture than the NIP composite membrane. While in case of membranes when pre-modified with 50 g/L of PEGMA, the MIP composite membranes had shown higher transport of racemic molecules than the NIP composite membrane (cf. Figure 4.31). The MIP composite membrane prepared after pre-modification with 50 g/L of PEGMA had shown higher D_{eff} value than the NIP composite membrane while the MIP composite membrane prepared after pre-modification with 25 g/L of PEGMA had shown smaller D_{eff} value than the NIP composite membrane (cf. Table 4.9). Again, no detectable enantioselectivity was observed through MIP composite membranes.

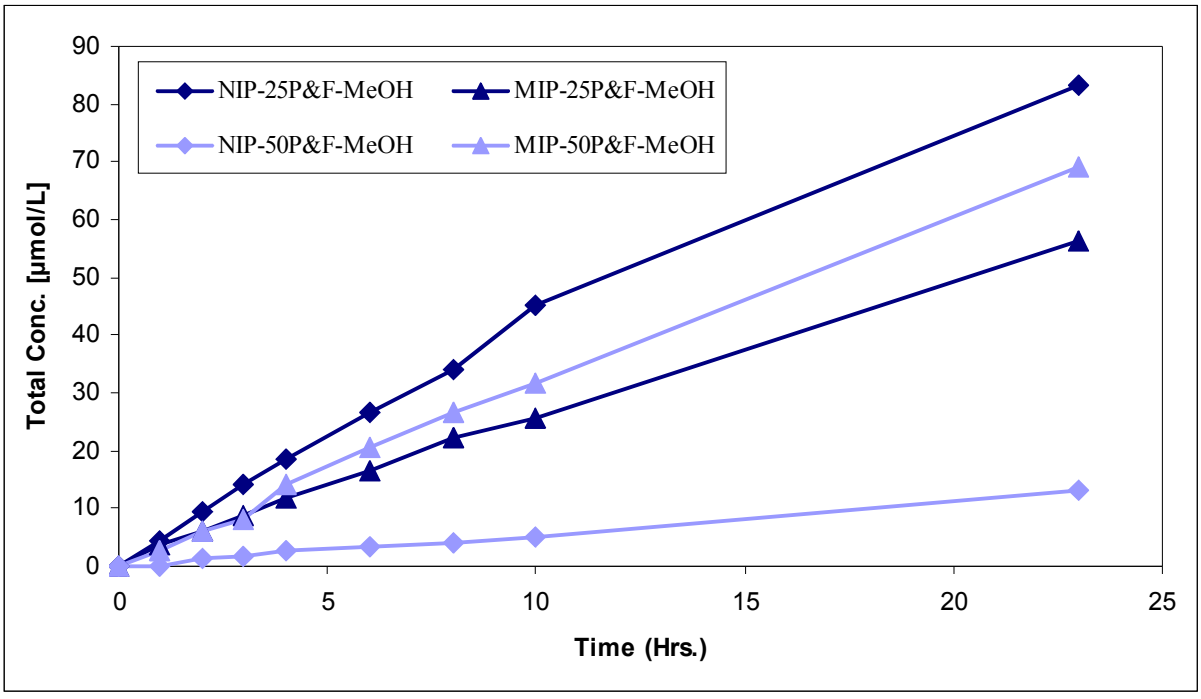

Figure 4.31. Effect of time on permeate concentration of the racemic mixture (Boc-DL-PhA) solution in MeOH through the MIP and NIP *poly(MAA-co-EDMA)* monolith-PET composite membranes prepared with pre-modification. In this case PET membranes with nominal pore diameter of 3 µm were used as base material.

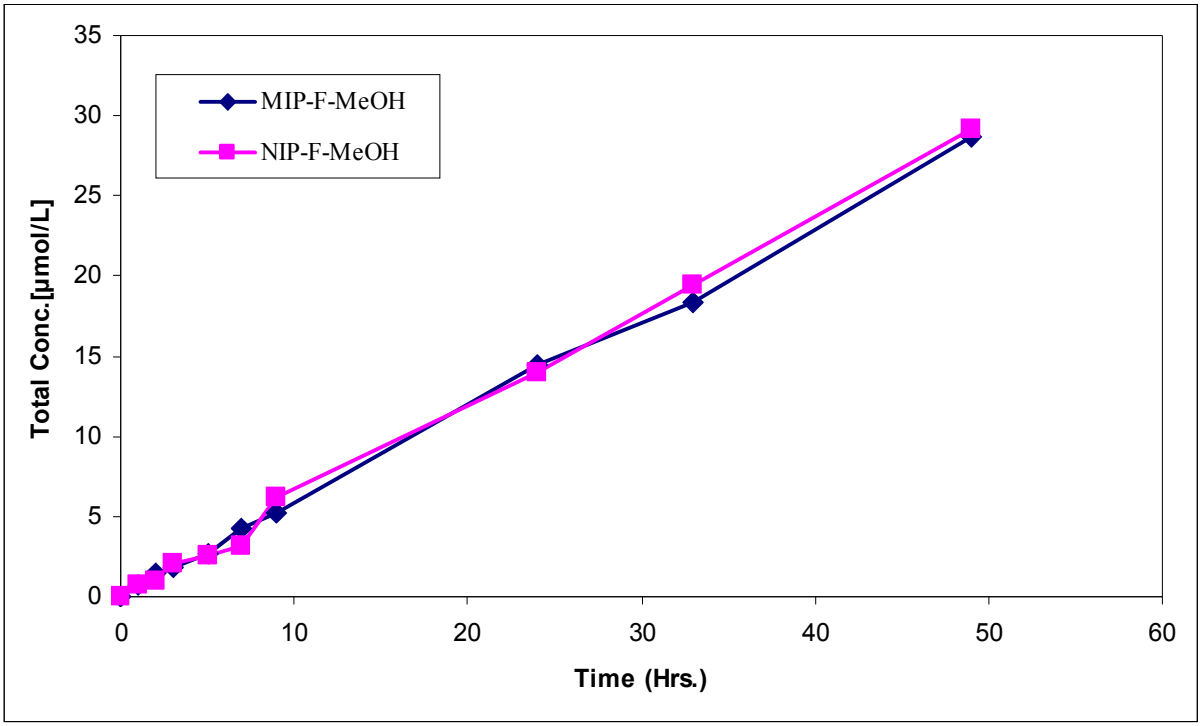

Figure 4.32. Effect of time on permeate concentration of the racemic mixture (Boc-DL-PhA) solution in MeOH through the MIP and NIP *poly(MAA-co-EDMA)* monolith-PET composite membranes prepared without pre-modification. In this case PET membranes with nominal pore diameter of 3 µm were used as base material.

In case of composite membranes which had been pore-filled functionalized (*poly(MAA-co-EDMA)*) without pre-modification, the both MIP and NIP composite membranes had shown almost same amount of Boc-DL-PhA permeated through to permeate side (cf. Figure 4.32) and The NIP composite membrane had a little larger value for the average D_{eff} than that of MIP composite membrane but the overall D_{eff} values were smaller than the composite membranes which were functionalized with pre-modification (cf. Table 4.9).

Although all the membranes were prepared under similar conditions but still there is a chance that a macroscopic change in the composite membrane structure may impart totally

different effects. The original PET membrane has a thickness of 23 μm and the composite membranes have a final thickness of 28 ± 4 μm which also include a very thin top layer (3 ± 1 μm) of polymer monolith on both sides of the membrane which could also have effects on the intended use of these membranes. To avoid these differences, the membranes of nearly equal thickness were used for all comparative studies.

By taking into consideration all these difference during the membrane preparations, from this study it can be concluded that overall the MIP *poly(MAA-co-EDMA)* monolith PET composite membranes had shown higher permeation and effective diffusion coefficient values for the Boc-DL-PhA than the NIP *poly(MAA-co-EDMA)* monolith PET composite membranes. In case of PET membranes with nominal pore diameter of 0.4 μm, the composite membranes pre-modified with 25 g/L of PEGMA had shown higher permeation and effective diffusion values than the NIP composite membranes when AN and MeOH were used as solvent. Anyhow these membranes had shown higher permeation of the racemic mixture in AN than in MeOH. The decrease in concentration on the permeate side (cf. Figure 4.30) and smaller D_{eff} values (cf. Table 4.9) when MeOH was used as solvent could be due to excessive hydrogen bonding of MeOH with imprinted sites in membrane pores and with the Boc-D/L-PhA molecules in the racemic mixture.

In case of PET membranes with nominal pore diameter of 3.0 μm, the composite membranes pre-modified with 25 g/L of PEGMA has shown overall higher permeation and effective diffusion values than the composite membranes pre-modified with 50 g/L. For both type of PET membrane, the composite membranes pre-modified with 25 g/L of PEGMA had shown over all higher transport of racemic molecules as clear from the larger effective diffusion

coefficient values (cf. Table 4.9). But in all cases, the composite membranes did not show any detectable enantioselectivity.

4.4. Correlations between Syntheses, Pore Structure, Binding and Transport Properties

The bulk monoliths and the monoliths in the pores of PP and PET membranes were synthesized under the same polymerization conditions. The pore structure of the bulk monoliths with respect to specific surface area and pore volume (cf. Table 4.6) is significantly different from the monoliths that are in the pores of PP microfiltration and PET track etched composite membranes.

Considering the membrane porosity as well as the observed slight shrinkage and related decrease in porosity during functionalization (cf. Section 4.1.2, Pre-modification and pore-filling of PP and PET membranes), the theoretical value for the specific surface area of a PP membrane where the entire pore volume is filled with polymer having the pore structure of a large bulk monolith should be ~145 m^2/g. This estimate is significantly larger than the experimental values (97.2 ± 3.2 m^2/g). These differences in pore structure between large (mm scale) and small (nm scale) monoliths could be due to different structural heterogeneity. On the one hand, it could be speculated that UV initiation of the polymerization could be more even for the very thin (~195 μm) membranes when compared with the large bulk polymer materials (diameter 7 mm, height 40 mm). On the other hand, the membranes have a wide pore size distribution, and incomplete filling of smaller membrane pores during polymerization as well as shrinkage of monolith could cause disturbed monolith morphology as compared to the large samples.

The thickness of the PET membrane (~23 μm) is significantly less than that of the PP membranes, and the PET membranes have cylindrical through-pores. The confinement effect and

restrictions offered by pore walls are even stronger because of the more regular and rigid pore-structure due to higher mechanical strength of the PET membranes, which may result in a polymeric monolith with undisturbed shape and with even more narrow pore size distribution than the bulk monolith. The effect of UV initiation of the polymerization could be more significant in case of PET membranes where more regular shaped polymer monoliths are evenly filled in the cylindrical pores of thickness of ~23 μm. From the above discussion, it can be concluded that the size and shape of the mold are very crucial to control the pore structure of the polymer monoliths with respect to specific surface area and pore volume.

The binding properties and specificity towards the template molecules in bulk monoliths are also significantly different from the composite membranes (cf. Figure 4.33). The *poly(MAA-co-EDMA)* based monoliths have smaller adsorption binding values for Boc-DL-PhA even at longer equilibration time (cf. Figure 4.16) and higher separation factor value (cf. Figure 4.15 and 4.17) than the composite membranes (cf. Figure 4.20 and 4.22).

The amounts of Boc-DL-PhA adsorbed by *poly(MAA-co-EDMA)* based polymer materials increases while the enantioselectivity decreases with the decrease in the dimensions of the monolith. Hence, the properties of monolith from "bulk" to "in the membrane pores" are changing with their dimensions, and the amount of other binding sites which are not involved in specific binding increases with the decrease in the monolith size, resulting at the same time in a polymer material with less specific area and pore volume values. The total amount of Boc-DL-PhA adsorbed by the *poly(MAA-co-EDMA)* monoliths and *poly(MAA-co-EDMA)* monolith PP and PET composite membranes are ~1.5, 2.0 and 6.0 μmol/g, at a total racemate concentration of 1 mmol/L, respectively (cf. Figure 4.33). These values are comparable with the amount of the

template adsorbed by similar polymer material (~2.5 μmol/g) at a total template concentration of 0.2 mmol/L [44].

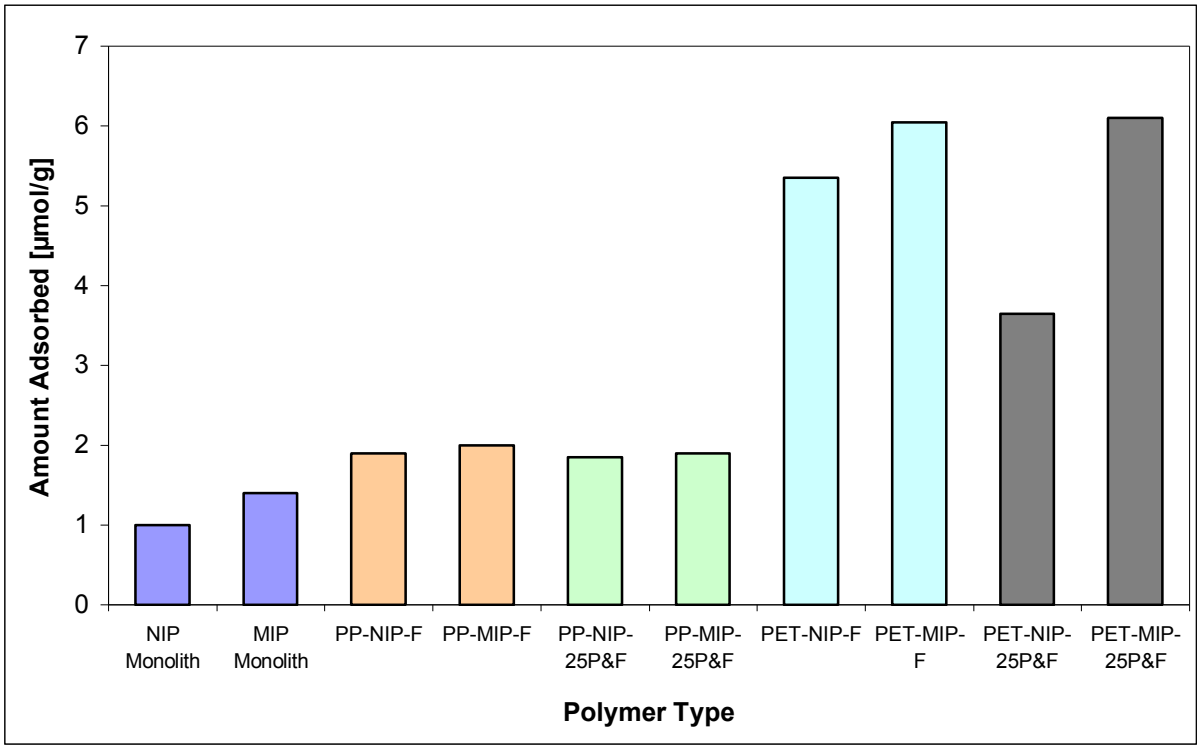

Figure 4.33. Amount of Boc-DL-PhA adsorbed (normalized to monolith mass) at the same racemate concentration in AN by the MIP and NIP *poly(MAA-co-EDMA)* based monoliths, and monoliths in the PP and PET composite membranes with and without pre-modification step.

The bulk monoliths have less outer surface area and larger inner surface area relative to total surface area while the ratio between outer and inner surface area is increasing for the PP and PET composite membranes. In general, the outer surface area relative to total surface area increases with the decrease in the thickness. As the outer surface area contains less specific sites as compared to inner surface area and also, the bulk monoliths have higher specific surface area values than the PP and PET composite membranes, the bulk monolith would exhibit more

specific binding than the PP and PET composite membranes. The extent of specific binding decreases with the increase in the outer surface area.

On the basis of above discussion, the Figure 4.34 gives a hypothetical picture about the specific cavities at the outer and inner surface of the MIP *poly(MAA-co-EDMA)* based monoliths, PP and PET composite membranes. As the PET composite membranes are much thinner than PP composite membranes and contain less inner surface and larger outer surface, they hence contain less specific cavities. PET composite membranes contain significantly large number of binding sites which are not involved in the specific binding as compared to polymer monoliths and PP composite membranes. The possible reasons for these non-specific sites could be the structure of the monoliths within the pores of membranes with non-specific binding sites, for example carboxylic groups of MAA which are not part of the ("concave") imprinted site [44] and the pore structure favoring the physical adsorption of the template and its counterpart without any discrimination.

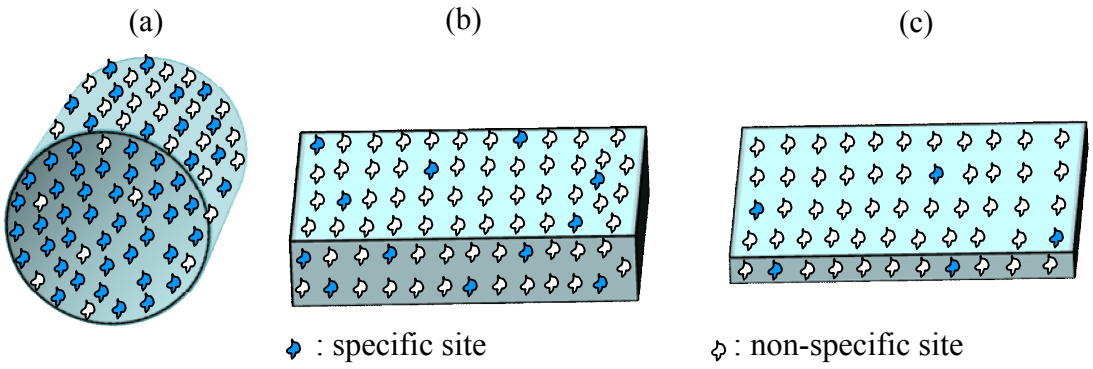

Figure 4.34. A hypothetical cross-section cum top presentation of specific binding sites on the outer and inner surfaces of *poly(MAA-co-EDMA)* based (a) bulk monolith, (b) PP composite membrane and (c) PET composite membranes.

The adsorption studies (cf. Section 4.2.2, "Equilibrium binding and enantioselectivity of MIP composite membranes") had confirmed the presence of the imprinted sites in the MIP *poly(MAA-co-EDMA)* monolith PET composite membranes. During the diffusion of different PEG's and the racemic mixture (Boc-DL-PhA), the high effective diffusion coefficient values had confirmed the presence of connected pores due to imprinting in the pore structure of these MIM. When these membranes were used for the diffusion of single enantiomer in AN/H_2O system, the MIP composite membrane did not offer any hindrance to the transport of L-enantiomer through it, while the D-enantiomer (template) was blocked. This is presumably due to increase in pore-swelling as a consequence of template binding to MIP sites and the composite membrane behaves like a "gate". These membranes behaved like a "gate": only for the amino acid used as template, no flux was detected while the other enantiomer diffused through the membrane. With mainly meso- and microporous MIM, template binding to imprinted sites can change the pore network thus altering the membrane permeability, i.e. a "gate effect" is observed [4]. From Figure 4.35, the substance A has no specific interaction with the membrane surface and will be transported by diffusion processes while the substance B has specific binding to the MIP sites and is responsible for pore-blocking due to an increase in swelling of the monolith in membrane pores. As the pore-walls in PET membrane are rigid, hence, the swelling in MIM is not a free swelling. As a consequence of this directional-swelling; the membrane-pores will be blocked and will not be available for transport of the substance B through MIM, thus behaving like a gate for the substance A.

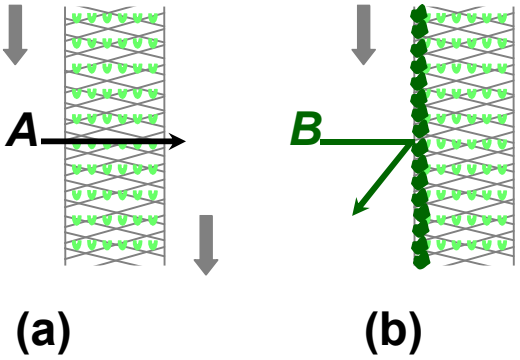

Figure 4.35. Transport mechanism for MIM as a consequence of the binding selectivity obtained by imprinting for a substance B: (a) non-specific transport of a neutral molecule A, driven by a concentration gradient across the membrane, (b) substance B is blocked due to an increase of directional-swelling as a consequence of specific binding of B to MIP sites on the surface of trans-membrane pores. In this work inter-connected micro- and mesopores in the MIP monolith filling the macropores of the base membrane.

Chapter 5

CONCLUSION

The pore structure and homogeneity of monoliths by *in situ* polymerization in bulk had been studied and reaction conditions suited for the synthesis of stable materials with high specific surface area and most pores having a diameter of <100 nm have been identified. The UV-initiated polymerization and use of DMPAP as a photo-initiator were found to be more suitable than AIBN to obtain the polymer monoliths with suited pore morphology. The identical BET surface area, before and after the exposure of monoliths to acetonitrile, had confirmed the rigid structure of the porous polymer monoliths. Molecular imprinting for a chiral amino acid derivative has been successful for porous *poly(MAA-co-EDMA)* based monoliths with high specific surface area. The MIP *poly(MAA-co-EDMA)* based monoliths showed significant binding specificity and enantioselectivity (up to ~6) for the template Boc-D-PhA from the racemic mixture dissolved in AN after 24 hours of adsorption. Under the conditions used in the binding studies (equilibrium concentrations up to ~0.35 mmol/L), the maximum binding capacities of the materials have not yet been reached and the enantioselectivity was slightly decreased with the increase in the equilibration time. In addition, as expected for affinity materials with a distribution of binding sites with different affinity, the binding selectivity was decreasing with increasing solute concentration. However, both MIP and NIP *poly(MAA-co-EDMA)* based monoliths had shown less adsorption without any binding specificity and enantioselectivity for the template Boc-D-PhA from the racemic mixture in aqueous AN solution. The ionic repulsions (Donnan exclusion) may be responsible for the low adsorption and competitive H-bonding by the solvent may be responsible for the non-enantioselective behavior.

Hence, the nature of solvent and its pH are very much important for the binding and transport of molecules within the polymer monolith.

Via *in situ* polymerization in the porous substrate, polymer monoliths were filled into the pores of PP microfiltration and PET track etched membranes. Both, SEM images and gravimetric data confirmed the complete pore filling of *poly(MAA-co-EDMA)* monolith PP and PET composite membranes. Pre-modification of PP and PET membranes with *PEGMA* had no macroscopic effect on the functionalization with polymeric monoliths. The MIP *poly(MAA-co-EDMA)* monolith PP and PET composite membranes showed significant binding specificity and enantio-selectivity for the template Boc-D-PhA from the racemic mixture, and the pre-modification of the pore walls with grafted *poly(PEGMA)* prior to the pore-filling improved the imprinting efficiency and recognition properties. A significant influence of pre-modification of the pore surface of the base polymer onto the interaction between the polymeric monolith and the base polymer, leading to an improved composite structure, had been confirmed (cf. Figure 4.11). Hence, the pre-modification was crucial for a good compatibility of the polymeric monoliths with the pore walls of PET and PP membranes, yielding more even pore-filling and less disturbed monolith morphology, and this was ultimately also important for creating defect-free barriers within the membranes. *PEGMA* and the polymers synthesized therefrom are compatible with various organic solvents and monomers. Hence by *in situ* pre-modification with *poly(PEGMA)* prior to functionalization step, numerous monomers which are soluble in organic solvents can be effectively polymerized and tightly anchored into the pores of polymer membranes or micro-fluidic channels for various industrial applications.

The diffusion of PEGs through the composite membranes was a function of imprinting and degree of pre-modification. The MIP *poly(MAA-co-EDMA)* monolith PET composite membranes

pre-modified with 25 g/L of *PEGMA* had shown larger effective diffusion coefficient values than the NIP *poly(MAA-co-EDMA)* monolith PET composite membranes. The further increase in the DG values of pre-modification resulted in a significant decrease in effective diffusion coefficient values.

During the diffusion of racemic mixture of template (Boc-D-PhA) and its counterpart (Boc-L-PhA) in AN or MeOH, overall the MIP *poly(MAA-co-EDMA)* monolith PET composite membranes had shown higher permeation and effective diffusion coefficient values than the NIP *poly(MAA-co-EDMA)* monolith PET composite membranes. Again, the further increase in the DG values of pre-modification resulted in significant decrease in effective diffusion coefficient values. The composite membranes had shown lower effective diffusion coefficient values in MeOH. The excessive H-bonding of MeOH with imprinted sites in membrane pores and with the Boc-D/L-PhA molecules in the racemic mixture could be a reason for this decrease. The larger values of effective diffusion coefficient for the diffusion of PEGs and racemic mixture through MIP composite membranes indicated that the imprinting leads to connected pores within the composite structure which are responsible for this increased flux. During the diffusion of single enantiomer in AN/H_2O, MIM allowed the transport of L-enantiomer while the transport of the D-enantiomer (template) was totally blocked. These membranes behaved like a "gate", presumably due to an increase of membrane swelling as a consequence of binding of the template to imprinted sites which resulted in the blocking of the pathways for the transport of the molecules. Further studies should be devoted to a more detailed investigation of this very interesting and potentially useful "gate effect".

During the process of electrodialysis where applied potential difference was used as driving force, the transport of template molecules (Boc-D-PhA) through the *poly(MAA-co-EDMA)*

composite membranes pre-modified with *poly(PEGMA)* had been facilitated, while there was no significant transport of the template molecules through these composite membranes during the diffusion process. However, both MIP and NIP composite membranes did not show any enantioselective transport during the process of diffusion or electrodialysis. The nature of the solvent and its pH are very much important for the binding and selective transport of molecules through the imprinted polymer materials. The influence of solute concentration onto enantio-selectivity (high for low concentrations) and onto flux through the membrane (high for high concentrations) are contradictory with respect to enantio-selective transport in the diffusion experiments. And electrodialysis was only possible in an aqueous solvent where enantio-selectivity was not detectable.

The results of this work are the basis for the preparation of macroporous membranes which are filled defect-free with micro- and mesoporous monoliths and also provide a strong base for the enantioselective and facilitated transport through composite MIM prepared by pore-filling. The more rigid and inert Anodisc alumina membranes would be suitable base material for pore-filling functionalization for the enantioselective and facilitated transport because of higher porosity (~50%) and a thinner barrier layer. Nevertheless, the limits for miniaturizing polymeric monoliths by using molds with characteristic dimensions in the nanometer scale must be also further investigated.

References

[1] E. Drioli, L. Giorno, Biocatalytic membrane reactors, Taylor & Francis, Padstow, UK, 1999.

[2] J. Caldwell, Importance of stereospecific bioanalytical monitoring in drug development, J. Chromatogr. A 719 (1996) 3.

[3] J. Wang, C. Fu, T. Lin, L. Yu, S. Zhu, Preparation of chiral selective membranes for electrodialysis separation of racemic mixture, J. Memb. Sci. 276 (2006) 193.

[4] M. Ulbricht, Membrane separations using molecularly imprinted polymers, J. Chromatogr. B 804 (2004) 113.

[5] D. W. Armstrong, H. L. Jin, Enrichment of enantiomers and other isomers with aqueous liquid membranes containing cyclodextrin carriers, Anal. Chem. 59 (1987) 2237.

[6] G. Wulff, Molecular imprinting in cross-linked materials with the aid of molecular templates-a way towards artificial anti bodies, Angew. Chem. Int. Ed. Engl. 34 (1995) 1812.

[7] S. A. Piletsky, I. Y. Dubey, D. M. Fedoryak, V. P. Kukhar, Biopolym. Kletka 6 (1990) 55.

[8] S. A. Piletsky, H. Matuschewski, U. Schedler, A. Wilpert, E. V. Piletskaya, T. A. Thiele, M. Ulbricht, Surface functionalization of porous polypropylene membranes with molecularly imprinted polymers by photograft copolymerization in water, Macromolecules 33 (2000) 3092.

[9] T. A. Sergeyeva, H. Matuschewski, S. A. Piletsky, J. Bendig, U. Schedler, M. Ulbricht, Molecularly imprinted polymer membranes for substance-selective solid-phase

extraction from water by surface photo-grafting polymerization, J. Chromatogr. A 907 (2001) 89.

[10] M. Yoshikawa, J. Izumi, T. Kitao, Enantioselective electrodialysis of N-alpha-acetyltryptophans through molecularly imprinted polymeric membranes, Chem. Lett. 8 (1996) 611.

[11] H. Y. Wang, Y. Kobayashi, T. Fukaya, N. Fujii, Molecular imprint membranes prepared by the phase inversion precipitation technique. 2. Influence of coagulation temperature in the phase inversion process on the encoding in polymeric membranes, Langmuir 13 (1997) 5396.

[12] J. Mathew-Krotz, K. J. Shea, Imprinted polymer membranes for the selective transport of targeted neutral molecules, J. Am. Chem. Soc. 118 (1996) 8154.

[13] J. M. Hong, P. E. Anderson, J. Qian, C. R. Martin, Selectively-permeable ultrathin film composite membrane based on molecularly-imprinted polymers, Chem. Mater. 10 (1998) 1029.

[14] M. Yoshikawa, J. Izumi, T. Kitao, Enantioselective electrodialysis of amino acids with charged polar side chains through molecularly imprinted polymeric membranes containing DIDE derivatives, Polym. J. 29 (1997) 205.

[15] H. Y. Wang, Y. Kobayashi, T. Fukaya, N. Fujii, Molecular imprint membranes prepared by the phase inversion precipitation technique, Langmuir 12 (1996) 4850.

[16] T. Kobayashi, H. Y. Wang, N. Fujii, Molecular imprint membranes of polyacrylonitrile copolymers with different acrylic acid segments, Anal. Chim. Acta 365 (1998) 81.

[17] F. Svec, Preparation and HPLC applications of rigid macroporous organic polymer monoliths, J. Sep. Sci. 27 (2004) 747.

[18] J. Seidl, J. Malinsky, K. Dusek, W. Heitz, Macroporous styrene-divinylbenzene copolymers and their use in chromatography and for the preparation of ion exchangers, Adv. Polym. Sci. 5 (1967) 11.

[19] K. A. Kun, R. Kunin, Macroreticular resins. III. Formation of macroreticular styrene-divinylbenyene copolymers, J. Polym. Sci. Polym. Chem. Ed. 6 (1968) 2689.

[20] W. L. Sederel, G. J. DeJong, Styrene-divinylbenzene copolymers. Construction of porosity in styrene-divinylbenzene matrixes, J. Appl. Polym. Sci. 17 (1973) 2835.

[21] F. Svec, J. M. J. Fréchet, Continuous rods of macroporous polymer as high-performance liquid chromatography separation media, Anal. Chem. 64 (1992) 820.

[22] F. Svec, J. M. J. Fréchet, New designs of macroporous polymers and supports: from separation to biocatalysis, Science 273 (1996) 205.

[23] E. C. Peters, F. Svec, J. M. J. Fréchet, Rigid macroporous polymer monoliths, Adv. Mater. 11 (1999) 1169.

[24] I. Mihelic, M. Krajnc, T. Koloini, Kinetic model of methacrylate-based monolith preparation, Ind. Eng. Chem. Res. 40 (2001) 3495.

[25] M. T. Dulay, J. P. Quirino, B. D. Bennett, M. Kato, R. N. Zare, Photopolymerized sol-gel monolith for capillary electrochromatography, Anal. Chem. 73 (2001) 3921.

[26] S. Hjertén, Standard and capillary chromatography, including electrochromatography, on continuous polymer beds (monoliths), based on water soluble monomers, Ind. Eng. Chem. Res. 38 (1999) 1205.

[27] S. Hjertén, Continuous beds: high resolving, cost effective, chromatographic matrices, Nature 356 (1992) 810.

[28] J. L. Liao, N. Chen, C. Ericson, S. Hjertén, Preparation of continuous beds derivatized with one-step alkyl and sulphonate groups for capillary electrochromatography, Anal. Chem. 68 (1996) 3468.

[29] F. Svec, J. M. J. Fréchet, Kinetic control of pore formation in macroporous polymers. The formation of "molded" porous materials with high flow characteristics for separation of catalysis, Chem. Mater. 7 (1995) 707.

[30] F. Svec, J. M. J. Fréchet, Temperature, a simple and efficient tool for the control of pore size distribution in macroporous polymers, Macromolecules 28 (1995) 7580.

[31] C. Yu, M. Xu, F. Svec, J. M. J. Fréchet, Preparation of monolithic polymers with controlled porous properties for microfluidic chip applications using photoinitiated free-radical polymerization, J. Polym. Sci. Part A: Polym. Chem. 40 (2002) 755.

[32] F. Svec, J. M. J. Fréchet, Molded rigid monolithic porous polymers: an inexpensive, efficient, and versatile alternative to beads for the design of materials for numerous applications, Ind. Eng. Chem. Res. 38 (1999) 34.

[33] C. Viklund, F. Svec, J. M. J. Fréchet, K. Irgum, Monolithic, "molded", porous materials with high flow characteristics for separation, catalysis, or solid phase chemistry: control of porous properties during polymerization, Chem. Mater. 8 (1996) 744.

[34] J. J. Brazier, M. Yan, Micromonoliths and microfabricated molecularly imprinted polymers, in M. Yan, O. Ramström, Molecularly imprinted materials, Science and Technology, Marcel Dekker, New York, 2005, p. 491.

[35] B. P. Santora, M. R. Gagne, K. G. Moloy, N. S. Radu, Porogen and cross-linking effects on the surface area, pore volume distribution and morphology of macroporous polymers obtained by bulk polymerization, Macromolecules 34 (2001) 658.

[36] A. Biffis, N. B. Graham, G. Siedlaczek, S. Stalberg, G. Wulff, The synthesis, characterization and molecular recognition properties of imprinted microgels, Macromol. Chem. Phys. 202 (2001) 163.

[37] K. Hosoza, Z. Iwakoshi, K. Zoshizako, K. Kimata, N. Tanaka, An unexpected molecular imprinting effect for a polyaromatic hydrocarbon, anthracene, using uniform size ethylene dimethacrylate particle, J. High Resol. Chromatogr. 22 (1999) 256.

[38] A. G. Mayes, K. Mosbach, Molecularly imprinted polymer beads: suspension polymerization using a liquid perfluorocarbon as the dispersing phase, Anal. Chem. 68 (1996) 3769.

[39] Z. Pelzbauer, J. Lukas, F. Svec, J. Kalal, Reactive polymers, XXV. Morphology of polymeric sorbents based on glycidyl methacrylate copolymers, J. Chromatogr. 171 (1979) 101.

[40] T. Rohr, D. F. Ogletree, F. Svec, J. M. J. Fréchet, Surface functionalization of thermoplastic polymers for the fabrication of microfluidic devices by photoinitiated grafting, Adv. Funct. Mater. 13 (2003) 4.

[41] D. J. Throckmorton, T. J. Shepodd, A. K. Singh, Electrochromatography in microchips: reversed-phase separation of peptides and amino acids using photopatterned rigid polymer monoliths, Anal. Chem. 74 (2002) 784.

[42] D. S. Peterson, T. Rohr, F. Svec, J. M. J. Fréchet, Enzymatic microreactor-on-a-chip: protein mapping using trypsin immobilized on porous polymer monoliths molded in channels of microfluidic devices, Anal. Chem. 74 (2002) 4081.

[43] Z. S. Liu, Y. L. Xu, H. Wang, C. Yan, R. Y. Gao, Chiral separation of binaphthol enantiomers on MIP monoliths by capillary electrochromatography, Analytical Sciences 20 (2004) 673.

[44] B. Sellergren, Molecular imprinting by noncovalent interactions: enantioselectivity and binding capacity of polymers prepared under conditions favoring the formation of the template complexes, Macromol. Chem. 190 (1989) 2703.

[45] A. G. Mayes, K. Mosbach, Molecularly imprinted polymers: useful materials for analytical chemistry? Trends Anal. Chem. 16 (1997) 321.

[46] I. A. Nicholls, O. Ramström, K. Mosbach, Insights into the role of the hydrogen bond and hydrophobic effect on recognition in molecularly imprinted polymer synthetic peptide receptor mimics, J. Chromatogr. A 691 (1995) 349.

[47] M. Kempe, K. Mosbach, Chiral recognition of N alpha-protected amino acids and derivatives in non-covalently molecularly imprinted polymers, Int. J. Pep. Protein Res. 44 (1994) 603.

[48] G. Wulff in Polymeric Reagents and catalysts, Ed. W. T. Ford, ACS Symp. Ser. 308 (1986) 186.

[49] G. Wulff, J. Vietmeier, H. G. Poll, Enzyme-analogue built polymers, 22. Influence of the nature of the crosslinking agent on the performance of imprinted polymers in racemic resolution, Makromol. Chem. 188 (1987) 731.

[50] B. Sellergren, K. J. Shea, Influence of polymer morphology on the ability of imprinted network polymers to resolve enantiomers, J. Chromatogr. 635 (1993) 31.

[51] M. H. Park, R. Saito, K. Ishizu, T. Fukutomi, Synthesis of microphased core-corona type microgel, Polym. Commun. 29 (1988) 230.

[52] N. Kihara, C. Kanno, T. Fukutomi, Synthesis and properties of microgel bearing a mercapto group, J. Polym. Sci. A 35 (1997) 1443.

[53] K. Ohkubo, Y. Funakoshi, T. Sagawa, Catalytic activity of a novel water-soluble cross-linked polymer imprinted by a transition-state analogue for the stereoselective hydrolysis of enantiomeric amino acid esters, Polymer 37 (1996) 3993.

[54] L. Ye, R. Weiss, K. Mosbach, Synthesis and characterization of molecularly imprinted microspheres, Macromolecules 33 (2000) 8239.

[55] B. Sellergren, Direct drug determination by selective sample enrichment on an imprinted polymer, Anal. Chem. 66 (1994) 1578.

[56] A. Molinelli, R. Weiss, B. Mizaikoff, Advanced solid phase extraction using molecularly imprinted polymers for the determination of quercetin in red wine, J. Agric. Food Chem. 50 (2002) 1804.

[57] F. L. Dickert, P. Lieberzeit, M. Tortschanoff, Molecular imprints as artificial antibodies-a new generation of chemical sensors, Sens. Actuators B 65 (2000) 186.

[58] D. Kriz, K. Mosbach, Competitive amperometric sensor based on an agarose immobilized molecularly imprinted polymer, Anal. Chim. Acta 300 (1995) 71.

[59] R. J. Ansell, A. O. Ramström, K. Mosbach, Towards artificial antibodies prepared by molecular imprinting, Clin. Chem. 69 (1996) 1506.

[60] H. V. Beach, K. J. Shea, Designed catalysts: a synthetic network polymer that catalyzes the dehydrofluorination of 4-fluoro-4-(p-nitrophenyl)butan-2-one, J. Am. Chem. Soc. 116 (1994) 379.

[61] A. Strikovsky, J. Hradil, G. Wulff, Catalytically active, molecularly imprinted polymers in bead form, React. Func. Polym. 54 (2003) 49.

[62] G. Vlatakis, I. I. Andersson, R. Müller, K. Mosbach, Drug assay using antibody mimics made by molecular imprinting, Nature 361 (1993) 645.

[63] A. G. Hadd, S. C. Jacobson, J. M. Ramsey, Microfluidic assays of acetylcholinesterase inhibitors, Anal. Chem. 71 (1999) 5206.

[64] M. Yan, A. Kapua, Fabrication of molecularly imprinted polymer microstructures, Anal. Chim. Acta 435 (2001) 163.

[65] P. G. Conrad II, P. T. Nishimura, D. Aherne, B. J. Schwartz, D. Wu, N. Fang, X. Zhang, M. J. Roberts, K. Shea, Functional molecularly imprinted polymer microstructures fabricated using microstereolithography, Adv. Mater. 15 (2003)1541.

[66] M. Ulbricht, Advanced functional polymer membranes, Polymer 47 (2006) 2217.

[67] M. Ulbricht, M. Riedel, U. Marx, Novel photochemical surface functionalization of polysulfone ultrafiltration membranes for covalent immobilization of biomolecules, J. Membr. Sci. 120 (1996) 239.

[68] M. Ulbricht, H. Matuschewski, A. Oechel, H.-G. Hicke, Photo-induced graft polymerization surface modifications for the preparation of hydrophilic and low-protein–adsorbing ultrafiltration membranes, J. Membr. Sci. 115 (1996) 31.

[69] C. Geismann, M. Ulbricht, Photoreactive functionalization of poly(ethylene terephthalate) track-etched pore surfaces with ‘‘smart’’ polymer systems, Macromol. Chem. Phys. 206 (2005) 268.

[70] M. Ulbricht, A. Oechel, C. Lehmann, G. Tomaschewski, H.-G. Hicke, Gas-phase photoinduced graft polymerization of acrylic acid onto polyacrylonitrile ultrafiltration membranes, J. Appl. Polym. Sci. 55 (1995) 1707.

[71] M. Ulbricht, Photograft–polymer–modified microporous membranes with environment–sensitive permeabilities, React. Funct. Polym. 31 (1996) 165.

[72] M. Ulbricht, M. Riedel, Ultrafiltration membrane surfaces with grafted polymer 'tentacles': preparation, characterization and application for covalent protein binding, Biomaterials 19 (1998) 1229.

[73] M. Ulbricht, H. Yang, Porous polypropylene membranes with different carboxyl polymer brush layers for reversible protein binding via surface-initiated graft copolymerization, Chem. Mater. 17 (2005) 2622.

[74] M. Lehmann, H. Brunner, G. Tovar, Selective separations and hydrodynamic studies: a new approach using molecularly imprinted nanospheres composite membranes, Desalination 149 (2002) 315.

[75] M. Lehmann, H. Brunner, G. Tovar, Molekular geprägte Nanopartikel als selektive Phase in Kompositmembranen: Hydrodynamik und Stofftrennung in nanoskaligen Schüttungen, Chem. Ing. Tech. 75 (2003) 149.

[76] S. A. Piletsky, T. L. Panasyuk, E. V. Piletskaya, I. A. Nicholls, M. Ulbricht, Receptor and transport properties of imprinted polymer membranes – a review, J. Memb. Sci. 157 (1999) 263.

[77] M. Yoshikawa, Molecularly imprinted polymeric membranes, Bioseparation 10 (2002) 277.

[78] T. A. Sergeyeva, S. A. Piletsky, A. A. Brovko, L. A. Slinchenko, L. M. Sergeeva, T. L. Panasyuk, A. V. El'Skaya, Conductimetric sensor for atrazine detection based on molecularly imprinted polymer membranes, Analyst 124 (1999) 331.

[79] T. A. Sergeyeva, S. A. Piletsky, E. V. Piletska, O. O. Brovko, L. V. Karabanova, L. M. Sergeeva, A. V. El'skaya, A. P. F. Turner, In situ formation of porous molecularly imprinted polymer membranes, Macromolecules 36 (2003) 7352.

[80] M. Yoshikawa, J. Izumi, T. Kitao, S. Koya, S. Sakamoto, Molecularly imprinted polymeric membranes for optical resolution, J. Membr. Sci. 108 (1995) 171.

[81] M. Yoshikawa, J. Izumi, T. Ooi, T. Kitao, M. D. Guiver, G. P. Robertson, Carboxylated polysulfone membranes having a chiral recognition site induced by an alternative molecular imprinting technique, Polymer Bull. 40 (1998) 517.

[82] M. Yoshikawa, J. Izumi, T. Kitao, Alternative molecular imprinting, a facile way to introduce chiral recognition sites, React. Funct. Polym. 42 (1999) 93.

[83] M. Yoshikawa, T. Ooi, J. Izumi, Alternative molecularly imprinted membranes from a derivative of natural polymer cellulose acetate, J. Appl. Polym. Sci. 72 (1999) 493.

[84] M. Yoshikawa, K. Koso, K. Yonetani, S. Kitamura, S. Kimura, Optical resolution of racemic amino acid derivatives with molecularly imprinted membranes bearing oligopeptide tweezers, J Polym. Sci. A Polym. Chem. 43 (2005) 385.

[85] M. Yoshikawa, J. Izumi, Chiral recognition sites converted from tetrapeptide derivatives adopting racemates as print molecules, J. Macromol. Biosci. 3 (2003) 487.

[86] S. A. Piletsky, E. V. Piletskaya, T. L. Panasyuk, A. V. El'skaya, R. Levi, I. Karube, G. Wulff, Imprinted membranes for sensor technology: opposite behavior of covalently and noncovalently imprinted membranes, Macromolecules 31 (1998) 2137.

[87] A. Dzgoev, K. Haupt, Enantioselective molecularly imprinted polymer membranes, Chirality 11 (1999) 465.

[88] M. Ulbricht, Molecularly imprinted polymer films and membranes, in M. Yan, O. Ramström, Molecularly imprinted materials, Science and Technology, New York, Marcel Dekker 2005, p. 455.

[89] T. B. Stachowiak, T. Rohr, E. F. Hilder, D. S. Peterson, M. Yi, F. Svec, J. M. J. Frechet, Fabrication of porous polymer monoliths covalently attached to the walls of channels in plastic microdevices, Electrophoresis 24 (2003) 3689.

[90] K. Kato, E. Uchida, E. Kang, T. Uyama, Y. Ikada, Polymer surface with graft chains, Prog. Polym. Sci. 28 (2003) 209.

[91] C. Geismann, A. Yaroshchuk, M. Ulbricht, Permeability and electrokinetic characterization of poly(ethylene terephthalate) capillary pore membranes with grafted temperature-responsive polymers, Langmuir 23 (2007) 76.

[92] B. Sellergren, B. Ekberg, K. Mosbach, Molecular imprinting of amino acid derivatives in macroporous polymers demonstration of substrate- and enantio-selectivity by chromatographic resolution of racemic mixtures of amino acid derivatives, J. Chromatogr. A 347 (1985) 1.

[93] B. Sellergren, M. Lepistö, K. Mosbach, Highly enantioselective and substrate-selective polymers obtained by molecular imprinting utilizing noncovalent interactions. NMR and chromatographic studies on the nature of recognition, J. Am. Chem. Soc. 110 (1988) 5853.

[94] B. Sellergren, Molecular imprinting by noncovalent interactions: tailor-made chiral stationary phases of high selectivity and sample load capacity, Chirality 1 (1989) 63.

[95] M. Mulder, Basic principles of membrane technology, Kluwer Academic Publishers, The Netherlands, 2nd Ed., 1997, p. 164.

[96] M. Mulder, Basic principles of membrane technology, Kluwer Academic Publishers, The Netherlands, 2nd Ed., 1997, p. 173.

[97] P. T. Kissinger, Ed., Introduction to detectors for liquid chromatography, BAS Press, Indiana (1981), Section 2.8.

[98] M. Mulder, Basic principles of membrane technology, Kluwer Academic Publishers, The Netherlands, 2nd Ed., 1997, p. 237.

[99] M. Mulder, Basic principles of membrane technology, Kluwer Academic Publishers, The Netherlands, 2nd Ed., 1997, p. 359.

[100] M. Mulder, Basic principles of membrane technology, Kluwer Academic Publishers, The Netherlands, 2nd Ed., 1997, p. 267.

[101] M. Mulder, Basic principles of membrane technology, Kluwer Academic Publishers, The Netherlands, 2nd Ed., 1997, p. 380.

[102] G. Odian, Principles of polymerization, 2nd ed., Wiley, New York, 1981, 196.

[103] J. Brandrup, E. H. Immergut, E. A. Eds. Grulke, Polymer Handbook, 4th ed., Wiley, New York, 1999, II, 3.

[104] T. Rohr, C. Yu, M. H. Davey, F. Svec, J. M. J. Fréchet, Porous polymer monoliths: Simple and efficient mixers prepared by direct polymerization in the channels of microfluidic chips, Electrophoresis 22 (2001) 3959.

[105] B. Sellergren, A. J. Hall, Fundamental aspects on the synthesis and characterization of imprinted network polymers, in Molecularly imprinted polymers: man-made mimics of antibodies and their applications in analytical chemistry, Elsevier, Amsterdam, Ed. B. Sellergren, 2001, p. 21.

[106] K. S. W. Sing, D. H. Everett, R. A. W. Haul, L. Moscou, R. A. Pierotti, J. Rouquerol, T. Siemienieswska, Reporting physisorption data for gas/solid systems with special reference to the determination of surface area and porosity, Pure Appl. Chem. 57 (1985) 603.

[107] K. Kaneko, Determination of pore size and pore size distribution 1. Adsorbents and catalysts, J. Membr. Sci. 96 (1994) 59.

[108] E. C. Peters, F. Svec, J. M. J. Fréchet, Preparation of large-diameter "molded" porous polymer monoliths and the control of pore structure homogeneity, Chem. Mater. 9 (1997) 1898.

[109] M. Yoshikawa, J. Izumi, T. Kitao, S. Sakamoto, Molecularly imprinted polymeric membranes containing DIDE derivatives for optical resolution of amino acids, Macromolecules 29 (1996) 8197.

Appendix-1

List of publications during doctoral study

Papers in Journals (peer-reviewed)

1. A. Salam, M. Ulbricht, Effect of surface modification on synthesis of pore-filling polymeric monoliths in microfiltration membranes made from polypropylene and poly(ethylene terephthalate), Macromol. Mater. Eng. 292 (**2007)** 310.
2. A. Salam, M. Ulbricht, Enantio-selective MIP nano-monolith composite membranes, Desalination 199 (**2006**) 532.

Oral Papers in International Conferences

2006 **Euromembrane 2006, Sep, 24-28, Giardini Naxos, Sicily, Italy.**

"Enantio-selective MIP "Nano-Monolith" Composite Membranes"

3rd Graduate Student Symposium on Molecular Imprinting Technology,

Feb. 22-24, University of Dortmund, Dortmund, Germany.

"Synthesis & Characterization of MIP "Nano-Monolith" Composite Membranes"

2005 **7th Network Young Membrains (NYM) Meeting, June 22-24, University of Twente, The Netherlands.**

"Synthesis of MIP Nano-monolith Composite Membranes"

Poster Papers in International Conferences

2007 **Marie Curie Workshop on "New Materials for Membranes" June 4-6, Geesthacht, Germany.**

"Enantioselective MIP "nano monolith" composite membranes"

2005 **BioNanoMat Organized by DECHEMA, Nov. 23-24, Chemiepark, Marl, Germany.**

"Synthesis of molecularly imprinted polymer "nano-monolith" composite membranes"

Appendix-2

Curriculum Vitae

Personal Details

Name	Abdus Salam
Date of birth	23/5/1970
Nationality	Pakistani
Family status	Married, 03 children
Address	Meistersingerstr. 48c,
	D-45307 Essen.
	Mobile +49 176 20336790
	abdus.salam@uni-due.de

Academic Qualifications

Jan., 2005–Feb., 2008 Doctoral studies	: Institute of Technical Chemistry (Lehrstuhl für Technische Chemie II), Department of Chemistry, Universität Duisburg-Essen, Germany, with field of the research in membrane technology
1991 – 1994	: Degree: M.Sc. Chemistry (1st division) Institute of Chemistry, University of the Punjab, Lahore, Pakistan
1988 – 1991	: Degree: B.Sc. (1st division) Govt. College Asghar Mall, Rawalpindi, Pakistan

Research and Work Experience

1.2005 – present	University Duisburg-Essen, Germany, Institute of Technical Chemistry Responsibilities: Scientific Co-worker Research project, dissertation thesis "Towards molecularly imprinted polymer (MIP) "nano-monolith" composite membranes for enantio-selective separations"
1.1997 – 9.2003	Metal Paint Products (Pvt.) Limited, Islamabad, Pakistan Responsibilities: Head Quality Control in chemical (paint, metal, in-organic and polymer) industries
11.1994 – 5.1995	Construction Machinery Training Institute, Islamabad, Pakistan Responsibilities: Instructor Chemistry